



**SAARLAND  
UNIVERSITY**

Department of Cellular Neurophysiology,  
Center for Integrative Physiology and Molecular Medicine,  
Faculty of Medicine, Saarland University,  
Homburg / Saar, Germany.

**Biogenesis of large dense core vesicles and  
molecular mechanisms of dead-end docking  
in mouse chromaffin cells**

A thesis submitted to the Faculty of Medicine, University of  
Saarland in fulfillment of the requirement for the degree of

**Doctor of Philosophy (Ph.D.)  
Germany 2017**

Name: Ekta Mayur Dembla  
Date of birth: 2<sup>nd</sup> October 1985  
Place of birth: Valsad, Gujarat, India

## **Anlage I**

### **Erklärung gemäß § 7 Abs. 1 Nr. 4**

Ich erkläre hiermit an Eides statt, dass ich die vorliegende Arbeit ohne unzulässige Hilfe Dritter und ohne Benutzung anderer als der angegebenen Hilfsmittel angefertigt habe. Die aus anderen Quellen direkt oder indirekt übernommenen Daten und Konzepte sind unter Angabe der Quelle gekennzeichnet.

Bei der Auswahl und Auswertung folgenden Materials haben mir die nachstehend aufgeführten Personen in der jeweils beschriebenen Weise unentgeltlich/entgeltlich geholfen:

1. Dr. Ralf Mohrmann: Er hat mir das Syt7 Konstrukt gegeben welches ich für Überexpression Experimente eingesetzt habe.
2. Prof. Dieter Bruns: Er hat mir alle Genmodifizierte maüse zur Verfügung gestellt.
3. Dr. Yvonne Schwarz/Patrick Schmidt: Sie habe die Genotypisierung der Synaptobrevin-2 maüse durchgeführt.

Weitere Personen waren an der inhaltlich-materiellen Erstellung der vorliegenden Arbeit nicht beteiligt. Insbesondere habe ich nicht die entgeltliche Hilfe von Vermittlungs- bzw. Beratungsdiensten (Promotionsberater/innen oder anderer Personen) in Anspruch genommen. Außer den Angegebenen hat niemand von mir unmittelbar oder mittelbar geldwerte Leistungen für Arbeiten erhalten, die im Zusammenhang mit dem Inhalt der vorgelegten Dissertation stehen.

Die Arbeit wurde bisher weder im Inland noch im Ausland in gleicher oder ähnlicher Form in einem anderen Verfahren zur Erlangung des Doktorgrades einer anderen Prüfungsbehörde vorgelegt.

Ich versichere an Eides statt, dass ich nach bestem Wissen die Wahrheit gesagt und nichts verschwiegen habe.

Vor Aufnahme der vorstehenden Versicherung an Eides Statt wurde ich über die Bedeutung einer eidesstattlichen Versicherung und die strafrechtlichen Folgen einer unrichtigen oder unvollständigen eidesstattlichen Versicherung belehrt.

Ort, Datum

Unterschrift der/des Promovierenden

Unterschrift der die Versicherung an Eides statt aufnehmenden Beamtin bzw. des aufnehmenden Beamten

**SUPERVISOR:**

**CO-SUPERVISOR:**

## **ACKNOWLEDGEMENTS**

It is an immense pleasure to mention the people who helped me directly or indirectly in my thesis work.

First and foremost, I would like to express my highest thankfulness to my supervisor PD. Dr. Ute Becherer, who gave me an opportunity for initiating my project work under her guidance. She was always open to my ideas and also always ready for discussing my results. I would also thank for her support during my initial time in her group.

I thank Prof. Dr. Jens Rettig for his guidance during lab meetings as well as bump meetings.

I convey my special thanks to Prof. Dr. Dieter Bruns, Dr. Yvonne Schwarz, Dr. Madhurima Dhara, Dr. Soumyajit Dutta, and Marina Wirth for the knock out mouse models used in my work as well as for their co-operation. I would like to mention a special thanks to Dr. Ralf Mohrmann for providing the Syt7 construct.

I would like to thank Dr. Claudia Schirra for the electron microscopy experiment to support my work, Dr. David Stevens for discussing my difficulties in patch clamp technique, and PD. Dr. Elmar Krause for helping me with SIM.

I would like to thank Margarete Klose, Anja Ludes, Anne Weinland, Kathrin Sandmeier, and Manuela Schneider for their excellent technical support during my thesis work. I would also like to thank Bernadette Schwarz and Josephine Kretschmer for their help in administrative matters.

I would like to acknowledge Praneeth Chitirala and Keerthana Ravichandran for their discussions professionally as well as for being my friends.

I would also like to thank my previous colleagues, Dr. Sandra Hugo and Dr. Anneka Bost for their contribution in teaching me some important scientific techniques.

The financial support from SFB894 is greatly appreciated.

Last but not the least, my heartfelt thanks go to my parents, my sister, and my husband Dr. Mayur Dembla who always supported me in all my decisions and provided a loving atmosphere to focus on my professional and personal matters.

**DEDICATED TO MY BELOVED  
HUSBAND, MY PARENTS, AND MY  
SISTER**

## **SUMMARY**

Ca<sup>2+</sup>-dependent regulated exocytosis is major form of exocytosis in neurons and neuroendocrine cells. These cells release neurotransmitters and hormones through exocytosis of secretory vesicles upon external stimuli. Regulated exocytosis occurs in different stages: biogenesis of the secretory vesicles, translocation of these vesicles, that are targeted and docked to the plasma membrane (PM). Ultimately when the Ca<sup>2+</sup> concentration strongly increases, fusion of secretory vesicles with the PM occurs inducing release of the neurotransmitter cargo outside the cells. In the last 30 years, adrenal medullary chromaffin cells have emerged as a model system to study regulated secretory pathway because they are round, rendering them easy to patch and because they can be used for membrane capacitance measurements. Furthermore, due to their common origin with the sympathetic neurons their molecular machinery for regulated secretion is very similar to that found in neurons. Even though chromaffin cells are extensively used to study the regulated secretory pathway, biogenesis and recycling of the chromaffin secretory granules which are called large dense core vesicles (LDCVs) still remains unresolved.

In order to get more insights into these processes, I used adrenal chromaffin cells from newborn mice and successfully electroporated them with Neuropeptide Y (NPY)-mCherry fusion protein construct to specifically label the newly generated LDCVs. I followed them by fixing the chromaffin cells at different time intervals from 2 h to 24 h post transfection. Immunostaining of the cis-Golgi compartment and the cortical actin network was used to analyze the distribution of the newly formed vesicles over time. I could show that initial expression of NPY-mCherry was already visible after 2 h post transfection but it was localized near Golgi and that few vesicles were formed. Over the time LDCVs moved away from the Golgi and distributed in the cytoplasm. LDCVs accumulated in the cortical actin ring but not directly adjacent to the PM. Furthermore, there was only partial colocalization between NPY and the cis- or trans-Golgi markers irrespective of the time used to study colocalization. With the help of correlative fluorescence electron microscopy (CLEM), we could show that the non-overlapping area near the Golgi, which was neither cis- nor trans-Golgi, was indeed another Golgi compartment. The identification of this compartment remains to be elucidated. I was also able to show that the vesicular proteins Synaptobrevin-2 (Syb-2), Cellubrevin (Ceb), and Synaptotagmin1 (Syt1) gets associated with the newly generated LDCVs at a later stage in the biogenesis because their colocalization with NPY-mCherry increased over time and was highest at 24 h post transfection. Moreover, I also studied the endocytosis of Syt1 in NPY-mCherry transfected chromaffin cells by inducing

exocytosis followed by endocytosis with application of 60mM KCl, allowing the uptake of luminal domain anti-Syt1 antibody, and fixing the cells at increasing time of recovery. I also used anti-TGN38 and anti-Rab11A antibodies to study the fate of the endocytosed Syt1. I counted the number of Syt1 punctae overlapping with NPY-mCherry after stimulation and the number of Syt1 punctae remaining at the cell periphery. We observed that Syt1 required a minimum of 2 h for recycling, and this recycling was not mediated by Rab11A positive endosomes because the number of punctae positive for endocytosed Syt1 and Rab11A were scarce. The three major conclusions from this study were:

1. Generation of vesicles needs at least 2 h and a new Golgi compartment devoid of GM130 and TGN38 retains the expression of NPY-mCherry probably for loading of vesicles with neuropeptides and Granins.
2. Association of vesicular membrane proteins with the newly formed vesicles happens at late stage in biogenesis.
3. Recycling of Syt1 needs a minimum of 2 h after first round of exo/endocytosis and it is not dependent on Rab11A positive endosomes.

Our group previously showed that dead-end vesicles which remain attached at the PM for a long time without fusing exist in bovine chromaffin cells. We demonstrated that target-Soluble NSF Attachment Protein Receptors (t-SNAREs) mediates dead-end docking via formation of unproductive t-SNARE acceptor complexes that hinders the fusion of docked vesicles with the PM. However, the vesicular component interacting with the unproductive t-SNARE acceptor complexes remained unknown. We used knock out mouse models for different vesicular proteins like Syb-2, Ceb, Syt1, and Syt7. I perfused the mouse chromaffin cells with high free  $Ca^{2+}$  and used the combination of membrane capacitance measurement through patch-clamp technique and total internal reflection fluorescence microscopy (TIRFM) allowing the analysis of single vesicle fusion and of their behavior during the recording period. First I was able to show that dead-end vesicles also existed in mouse chromaffin cells. Then I analyzed the effect of the absence of the above cited vesicular proteins on dead-end docking. Syb-2 KO induced significant reduction in global secretion but no effect on the number of dead-end vesicles. Also, there was no docking defect in Syb-2 KO cells. Ceb KO showed no effect on any of the TIRFM parameters and no effect on overall secretion. Syt1 KO cells showed strong docking defect and a high reduction in single vesicle secretion in comparison to control. However, no influence on overall exocytosis or number of dead-end vesicles was found. Syt7 KO cells also showed mild but significant docking defect and strong decrease in number of vesicles that were secreted in TIRF in comparison to WT control. Surprisingly, there was also a massive decline in the

number of dead-end vesicles. The specificity of the effect of Syt7 on dead-end docking was further tested by overexpressing Syt7 in Syt7 KO, which rescued the number of dead-end vesicles. From this study, I concluded that:

1. Dead-end vesicles also exist in mouse chromaffin cells.
2. v-SNAREs have no role in dead-end docking.
3. Syt1 has an important role in productive docking but not in dead-end docking.
4. Syt7 is the only vesicular protein to be involved in unproductive docking.

## ZUSAMMENFASSUNG

Ca<sup>2+</sup>-abhängige regulierte Exozytose ist die Hauptform der Exozytose in Neuronen und neuroendokrinen Zellen. Diese Zellen setzen Neurotransmitter und Hormone durch Exozytose von sekretorischen Vesikeln auf entsprechende Stimuli hin frei. Die regulierte Exozytose erfolgt in verschiedenen Stadien: Biogenese der sekretorischen Vesikel, Translokation dieser Vesikel, zur Plasmamembran (PM) und "Andocken" dieser Vesikel mit der PM. Nach einem Anstieg der intrazellulären Ca<sup>2+</sup>-Konzentration erfolgt die Fusion von sekretorischen Vesikeln mit der PM ein, die zur Freisetzung der Neurotransmitter-Ladung führt. In den letzten 30 Jahren sind Chromaffin-Zellen des Nebennierenmarks als Modellsystem etabliert worden, um den regulierten sekretorischen Weg zu untersuchen. Dies hat verschiedene Gründe: zum einen sind Chromaffine Zellen rund, was sie leicht zu patchen und was für Membrankapazitätsmessungen sehr nützlich macht. Darüber hinaus ist aufgrund ihrer gemeinsamen Herkunft mit den sympathischen Neuronen aus der Neuralleiste ihre molekulare Maschinerie für regulierte Sekretion sehr ähnlich wie bei Neuronen. Obwohl Chromaffin-Zellen weitgehend verwendet werden, um den regulierten sekretorischen Weg zu untersuchen, bleibt die Biogenese und das Recycling der chromaffinen Sekretionsgranula, die hier als große dichte Kern-Vesikel (large dense core vesicles, LDCVs) bezeichnet werden, noch ungelöst.

Um mehr Einblicke in diese Prozesse zu erhalten, benutzte ich adrenale Chromaffin-Zellen der Nebenniere von neugeborenen Mäusen und transfizierte sie erfolgreich mit einem Neuropeptid Y (NPY)-mCherry-Fusionsprotein-Konstrukt, um die neu erzeugten LDCVs spezifisch zu markieren. Ich untersuchte die Biogenese der chromaffinen Granula, indem ich die Chromaffinzellen in verschiedenen Zeitintervallen von 2 h bis 24 h nach der Transfektion fixierte. Die Immunfärbung des cis-Golgi-Kompartiments und des kortikalen Aktin-Netzwerks wurde verwendet, um die Verteilung der neu gebildeten Vesikel im Laufe der Zeit zu analysieren. Ich konnte zeigen, dass eine erste Expression von NPY-mCherry bereits 2 h nach der Transfektion sichtbar war. Die Expression 2 h nach der Transfektion war aber in der Nähe von Golgi beschränkt und es wurden nur wenige Vesikel zu diesem Zeitpunkt gebildet. Im Laufe der Zeit entfernten sich die LDCVs vom Golgi und verteilten sich im Zytoplasma. LDCVs sammelten sich im kortikalen Aktinring an, aber nicht direkt neben der PM. Darüber hinaus gab es nur eine partielle Kollokalisierung zwischen NPY und den cis- oder trans-Golgi-Markern. Mit Hilfe der korrelativen Fluoreszenz-Elektronenmikroskopie (CLEM) konnten wir zeigen, dass die nicht überlappende Fläche in der Nähe des Golgi, die weder cis- noch trans-Golgi war, tatsächlich ein weiteres Golgi-Kompartiment

darstellte. Die Identifizierung dieses unbekanntes Golgi-Kompartimentes bleibt abzuklären. Ich konnte auch zeigen, dass die vesikulären Proteine Synaptobrevin-2 (Syb-2), Cellubrevin (Ceb) und Synaptotagmin1 (Syt1) mit den neu erzeugten LDCVs in einem späteren Stadium der Biogenese assoziiert werden, weil ihre Kolokalisation mit NPY-mCherry erst im Laufe der Zeit sich erhöhte und am höchsten 24 h nach der Transfektion war. Darüber hinaus habe ich auch die Endozytose von Syt1 in NPY-mCherry-transfizierten Chromaffin-Zellen untersucht. Dazu habe ich zunächst mittels einer Applikation von 60 mM KCl eine Exozytose induziert, gefolgt von einer Endozytose, was die Aufnahme von luminalen Domänen-Anti-Syt1-Antikörpern ermöglicht und die Zellen nach unterschiedlichen Zeitpunkten fixiert. Ich habe u.a. Anti-TGN38 und Anti-Rab11A-Antikörper verwendet, um das Schicksal des endozytisierten Syt1 zu untersuchen. Ich zählte die Anzahl der Syt1 Punkte, die mit NPY-mCherry nach der Stimulation überlappten, und die Anzahl der Syt1 Punkte, die an der Zellperipherie verbleiben. Wir beobachteten, dass Syt1 mindestens 2 h für das Recycling benötigte, und dieses Recycling nicht durch Rab11A positive Endosomen vermittelt wurde, da die Anzahl der Punkte, die sowohl für endozytierte Syt1 als auch für Rab11A positive waren, gering war. Die drei wichtigsten Schlussfolgerungen aus dieser Studie waren:

1. Die Erzeugung von Vesikeln (LDCVs) benötigt mindestens 2 h und benötigt ein neues Golgi-Kompartiment, das weder GM130 noch TGN38 aufweist, und wahrscheinlich für die Beladung von Vesikeln mit Neuropeptiden und Graninen zuständig ist.
2. Die Verknüpfung von vesikulären Membranproteinen mit den neu gebildeten Vesikeln erfolgt im späten Stadium der Biogenese.
3. Recycling von Syt1 braucht mindestens 2 Stunden nach der ersten Runde der Exo / Endozytose und ist nicht abhängig von Rab11A positiven Endosomen.

Unsere Gruppe zeigte zuvor, dass sogenannte "dead-end" Vesikel, die an der PM lange haften bleiben, ohne zu fusionieren, auch in Rinder-Chromaffin-Zellen vorhanden sind. Wir haben gezeigt, dass sogenannte target-Soluble NSF Attachment Protein Receptors (t-SNAREs) das dead-end Docking durch Bildung von unproduktiven t-SNARE-Akzeptorkomplexen vermitteln, die die Verschmelzung von angedockten Vesikeln mit der PM behindern. Die vesikuläre Komponente, die mit den unproduktiven t-SNARE-Akzeptorkomplexen interagiert, blieb jedoch unbekannt. Wir verwendeten Knock out Maus Modelle für verschiedene vesikuläre Proteine wie Syb-2, Ceb, Syt1 und Syt7. Ich habe die Maus-Chromaffin-Zellen mit hohen Konzentrationen von freiem  $Ca^{2+}$  perfundiert und die Kombination der Membrankapazitätsmessung durch Patch-Clamp-Technik und Total-Reflexions-Fluoreszenzmikroskopie (TIRFM) verwendet, um

die Analyse der Einzelvesikelfusion und ihres Verhaltens während der Aufzeichnungsperiode zu ermöglichen. Zuerst konnte ich zeigen, dass dead-end Vesikel auch in Maus-Chromaffin-Zellen existierten. Dann analysierte ich die Wirkung der Abwesenheit der oben genannten vesikulären Proteine auf dead-end Docking. Syb-2 KO induzierte eine signifikante Reduktion der globalen Sekretion, aber keine Wirkung auf die Anzahl der dead-end Vesikel. Auch gab es keinen Docking-Defekt in Syb-2 KO-Zellen. Ceb KO zeigte keine Wirkung auf einen der TIRFM-Parameter und keine Auswirkung auf die Gesamtsekretion. Syt1-KO-Zellen zeigten einen starken Docking-Defekt und eine hohe Reduktion der Einzel-Vesikel-Sekretion im Vergleich zur Kontrolle. Es wurde jedoch kein Einfluss auf die Gesamt-Exozytose oder die Anzahl der dead-end Vesikel festgestellt. Syt7-KO-Zellen zeigten auch einen leichten, aber signifikanten Docking-Defekt und eine starke Abnahme der Anzahl von Vesikeln, die im Vergleich zur WT-Kontrolle in TIRF sezerniert wurden. Überraschenderweise gab es auch einen massiven Rückgang der Anzahl der dead-end Vesikel. Die Spezifität der Wirkung von Syt7 auf dead-end Docking wurde weiter durch Überexpression von Syt7 in Syt7 KO, die die Anzahl der dead-end Vesikel wieder herstellt getestet. Aus dieser Studie kam ich zu folgenden Schlussfolgerungen:

1. Dead-End-Vesikel gibt es auch in Maus-Chromaffin-Zellen.
2. v-SNAREs haben keine Rolle im dead-end Docking.
3. Syt1 hat eine wichtige Rolle bei der produktiven Andockung, aber nicht bei dead-end Docking.
4. Syt7 ist das einzige vesikuläre Protein, das sowohl in unproduktives Docking involviert ist.

# **CONTENTS**

<b>No.</b>	<b>Title</b>	<b>Page no.</b>
1.	Introduction	15
	1.1 Secretory granule exocytosis	15
	1.2 Biogenesis of large dense-core secretory granules	15
	• 1.2.1 Role of Golgi Complex	15
	• 1.2.2 Maturation of secretory granules	16
	1.3 Chromaffin cells as model system to study regulated exocytosis	17
	• 1.3.1 Large dense core vesicles: chromaffin vesicle	18
	➤ NPY – a marker of LDCV	19
	1.4 Regulated secretory pathway	19
	• SNAREs and other accessory proteins involved in priming	21
	• 1.4.1 Vesicle docking and proteins involved	22
	1.5 Endocytosis and recycling of proteins involved in exocytosis	24
2.	AIM	26
3.	Materials and Methods	27
	3.1 Materials	27
	• 3.1.1 Reagents	27
	• 3.1.2 Enzymes	27
	• 3.1.3 Antibodies	27
	• 3.1.4 Solutions	28
	➤ 3.1.4.1 General solutions	28
	➤ 3.1.4.2 Solutions for chromaffin cell preparation	28
	➤ 3.1.4.3 Solutions for immunocytochemistry	29
	➤ 3.1.4.4 Solutions for electrophysiology	30
	3.2 Methods	30
	• 3.2.1 Mouse chromaffin cell preparation	30
	• 3.2.2 Electroporation of mouse chromaffin cells	31
	• 3.2.3 Immunocytochemistry	31
	• 3.2.4 Structured Illumination Microscopy (SIM)	32
	• 3.2.5 Correlative Fluorescence Electron microscopy (CLEM)	33
	• 3.2.6 Electrophysiological measurements by patch	34

	clamp technique	
	• 3.2.7 Measurement of single vesicle exocytosis by TIRFM	35
	• 3.2.8 Genotyping	36
4.	Results	39
	• 4.1 Biogenesis of large dense core vesicles in chromaffin cells of newborn mice.	39
	➤ 4.1.1 NPY-mCherry labeled vesicles are LDCVs.	39
	➤ 4.1.2 Chromaffin cells require a minimum of 2 h to generate new LDCVs.	40
	➤ 4.1.3 LDCVs pause at or near Golgi for about an hour before moving towards the PM.	41
	➤ 4.1.4 The primary NPY-mCherry expression ascertains a discrete cellular compartment that does not correspond to cis/trans-Golgi.	43
	➤ 4.1.5 Syb-2, Ceb, and Syt1 are sorted at later stage in the LDCV biogenesis.	46
	➤ 4.1.6 Syt1 merges with NPY-mCherry within 2 h after endocytosis and only a small subset of endocytosed Syt1 is transported via Rab11A vesicles.	50
	• 4.2 Molecular mechanisms of dead-end docking in mouse chromaffin cells.	53
	➤ 4.2.1 Dead-end vesicles exist in mouse chromaffin cells.	53
	➤ 4.2.2 v-SNAREs are not involved in dead-end docking.	56
	➤ 4.2.3 Syt1 has a role in functional docking but not dead-end docking.	60
	➤ 4.2.4 Syt7 is involved in unproductive or dead-end docking.	63
5.	Discussion	67
	• 5.1 Biogenesis of large dense core vesicles in chromaffin cells of newborn mice	67
	• 5.2 Molecular mechanisms of dead-end docking in mouse chromaffin cells	70
6.	References	75
7.	Annexure	89
8.	Abbreviations	90
9.	List of figures	92
10.	List of tables	94

<b>11.</b>	<b>Curriculum vitae</b>	<b>95</b>
<b>12.</b>	<b>Posters and Publications</b>	<b>96</b>

## **1. INTRODUCTION**

### **1.1 SECRETORY GRANULE EXOCYTOSIS**

Regulated exocytosis of secretory granules has been extensively studied in different cell types depending on their physiological significance and experimental benefits. George Palade (1975) described the pathway of secretory process in pancreatic exocrine cells. Recently, one of the most studied cells in that context have been the adrenal chromaffin cells and it became a model to investigate the biochemical and electrophysiological aspects of exocytosis. Nevertheless, secretory granule exocytosis also exists in many different neuroendocrine and endocrine cells for secretion of peptides and hormones, and also in exocrine cells for release of digestive enzymes (Burgoyne and Morgan, 2003). Subsequent to the discovery of secretory granules by electron microscopy, they have been studied comprehensively because they are involved in important phenomenon such as the release of hormones and neuropeptides via regulated secretory pathway (Borgonovo, Ouwendijk, and Solimena, 2006).

### **1.2 BIOGENESIS OF DENSE – CORE SECRETORY GRANULES**

In eukaryotic cells, the newly formed proteins that are intended for secretion are first transported from the cytoplasm to the ER-lumen. Then they advance through the Golgi-apparatus from the cis-Golgi to the trans-Golgi network (TGN) where they are packaged in various secretory pathway depending on the function of these proteins. One pathway is the constitutive pathway which exists in all cells. Secretion occurring via constitutive pathway is not tightly controlled by the extracellular activity. This type of secretion takes place through vesicle budding from the TGN, transport to the PM, and fusion with the PM. It is used by cells for their growth, and to renew the protein content of the PM. On the other hand, many cells have another secretory pathway called “the regulated secretory pathway”, that is used for instance for neurotransmitter release in response to extracellular stimuli (Kim et al., 2006, Bowman et al., 2009). In neuroendocrine and endocrine cells regulated exocytosis occurs for release of hormones, and in other cell types such as immune cells it occurs for the release of cytokines and other products (Becherer et al., 2012). Both the pathways are depicted in fig. 1.

#### **1.2.1 ROLE OF GOLGI COMPLEX**

The Golgi complex is considered a fundamental part of the secretory pathway where cargo proteins and lipids are modified, categorized, filled into specific transporters and sent to their final destinations. Golgi stacks have been classified into cis, medial, and trans stacks. The newly manufactured proteins are transported to cis-Golgi from the ER while the cargo leaves from trans-Golgi by travelling across the stack in approximately 10-20 min (Ladinsky et al., 1999; Martinez – Menarguez JA, 2013; Martínez-Alonso et al., 2013). Large number of transport vesicles are generated at the TGN that are specialized for the transport of their contents to different cellular compartments and to

the PM for secretion. The TGN is also considered to be a sorting station for soluble proteins. Different mechanisms have been proposed for the sorting of proteins, namely sorting by selective aggregation, and receptor-mediated luminal protein sorting (Kienzle and von Blume, 2014). Chromogranin A (CgA) has been proposed to be involved in the sorting mechanisms at the TGN (Kim et al., 2001; Kim et al., 2005; Gerdes and Glombik, 2000).

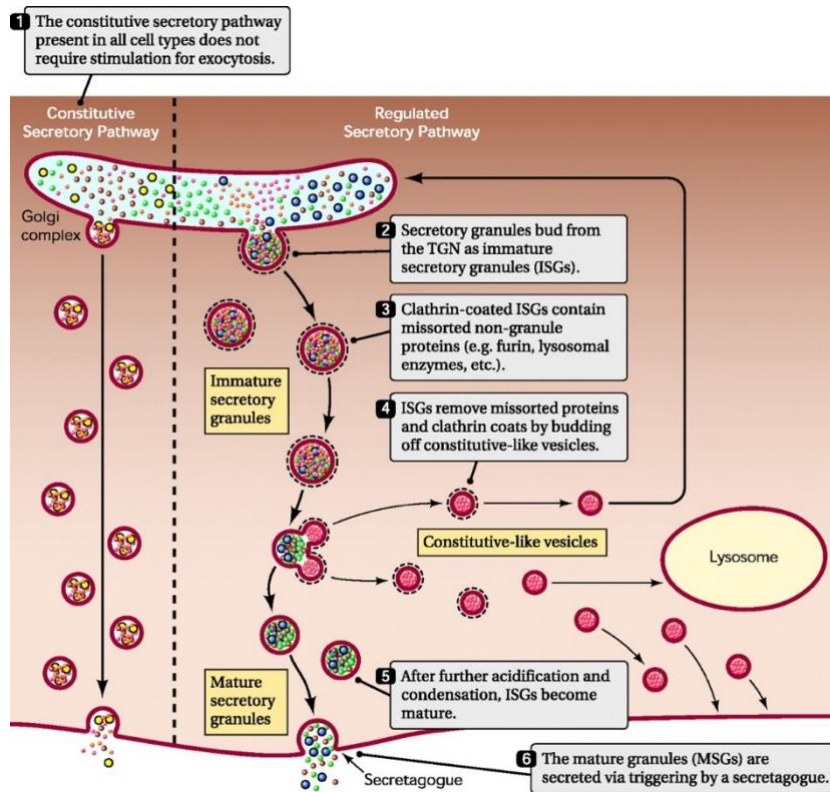


**Figure 1: Steps involved in LDCV biogenesis:** Two distinctive secretory pathways are present in neuroendocrine and endocrine cells to mediate constitutive or regulated secretion of proteins. From Kim et al., 2006.

## 1.2.2 MATURATION OF SECRETORY GRANULES

After the formation of immature secretory granule (ISG) from budding of TGN, they apparently undertake a maturation process in order to gain the ability to respond to stimulations. Newly formed ISGs possess less electron-dense core than the mature granules (Klumperman et al., 1998). It has been proposed that vesicle maturation involves reduction in lumen pH, vesicle fusion, and membrane restoration (Bonnemaison et al., 2013, fig. 1). In insulin secretory granules and PC12 cells it has been shown that the lumen of TGN and the lumen of ISGs have pH 6.3, whereas pH of mature secretory granules (MSGs) is more acidic pH 5.5 (luminal) (Hutton, 1982; Orci et al., 1986; Urbé et al., 1997). The proteolytic processing of some prohormones and Granins starts in ISGs, not in TGN. pH reduction during the granule maturation is an essential step for total processing of granins and prohormones (Husten and Eipper, 1994). This reduction in pH from TGN to mature granule is facilitated by steady rise in the active H<sup>+</sup> pump density and decrease in H<sup>+</sup> permeability of organelle membranes (Wu et al., 2001). On the other hand, increase in Ca<sup>2+</sup> concentration in the vesicle lumen occurs along with other cations, which is essential to neutralize the charge of the largely acidic core proteins (Mahapatra et al., 2004; Steinberg et al., 2010).

### 1.3 CHROMAFFIN CELLS AS MODEL SYSTEM TO STUDY REGULATED EXOCYTOSIS

The adrenal glands are made of two main parts, both have their own function and are from different embryological origin. The outer part, which is the major portion of the adrenal gland is formed from the mesoderm. It is important for mediating the stress response through the production and secretion of mineralocorticoids (e.g. aldosterone) and glucocorticoids (e.g. cortisol). The adrenal medulla is the inner part, and it is responsible for the crucial “fight or flight” response of the body to an attack. The adrenal medulla is derived from the neural crest and consists of chromaffin cells that secrete epinephrine (adrenaline), norepinephrine (noradrenaline), and also small amount of dopamine under stressful conditions (fig. 2, Berridge, 2012). Chromaffin cells receive stimulation from preganglionic fibers of the sympathetic nervous system that originates from the thoracic spinal cord T5-T11. As it is innervated by the preganglionic nerve fibers, the adrenal medulla can be considered as specialized ganglia. In contrast to other sympathetic ganglia, adrenal medulla does not form distinct synapses, but release their secretions directly into the blood stream for systemic effects (García et al., 2006).

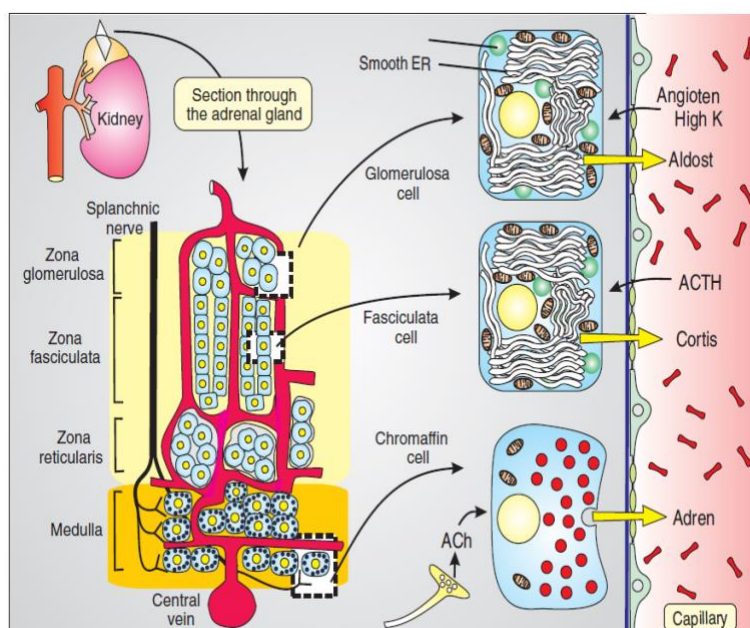


**Figure 2: Adrenal gland structure and function.** A section through the gland illustrates the outer cortex, which is divided into three zones and an inner medulla that has the chromaffin cells. The latter are innervated by the splanchnic nerve. Shown on the right are the functions of the cells specialized to synthesize and secrete hormones (yellow arrows). Angiotensin II and high K<sup>+</sup> stimulate aldosterone release, corticotrophin (ACTH) stimulates the release or cortisol, while release of acetylcholine (ACh) from the splanchnic nerve endings activates the chromaffin cells to release adrenaline. From Berridge 2012.

Chromaffin cells are easily available from cows, share a common origin with sympathetic neurons, are easily isolated and prepared for cultures. These advantages make them a very good candidate for electrophysiological, neuropharmacological, and biochemical studies. Their physiological function, the stress induced release of catecholamines in the blood circulation, is a Ca<sup>2+</sup> -dependent process. Hence, chromaffin cells are widely used as model system to study regulated exocytosis (García et al., 2006).

### 1.3.1 LARGE DENSE CORE VESICLES

Secretory granules that exist in chromaffin cells are called chromaffin vesicles. They are so-called because they are positive for “chromaffin reaction” i.e. these structures exhibit histochemical affinity to chromate salts (Crivellato et al, 2008). Catecholamines were found in the cytoplasmic fraction upon differential centrifugation of chromaffin cells (Blaschko and Welch, 1953; Hillarp et al., 1953). Electron microscopy analysis showed that this cytoplasmic fraction was formed of specialized membrane-bound organelles called “chromaffin granules” (Hillarp et al., 1954). These vesicles are 150 to 350 nm large and they are strongly electron-dense in electron micrographs. Therefore, chromaffin granules are also known as LDCVs. Coupland (1965) has shown the presence of two types of LDCVs: adrenaline containing vesicles, which are less electron-dense and the noradrenaline containing vesicles which are highly electron-dense. They account for about 13.5% of the cytoplasmic volume of chromaffin cell and a typical bovine chromaffin cell contains approximately 10,000 vesicles (Kryvi et al., 1979, Crivellato et al., 2008). Fig. 3 depicts the structural organization of a chromaffin cell.

Chromaffin granules are structurally complex organelles. Not only they contain catecholamines, but also contain and secrete CgA, CgB, and Sgs which are a group of acidic, soluble proteins. These proteins are ubiquitously dispersed in neuroendocrine and nervous system. They also function as valued markers for sympathoadrenal activity as well as secretion from normal and neoplastic neuroendocrine cells (Taupenot et al., 2003). CgA has been shown to be involved in the formation of dense-core granules and segregation of hormones in neuroendocrine cells (Kim et al., 2001).

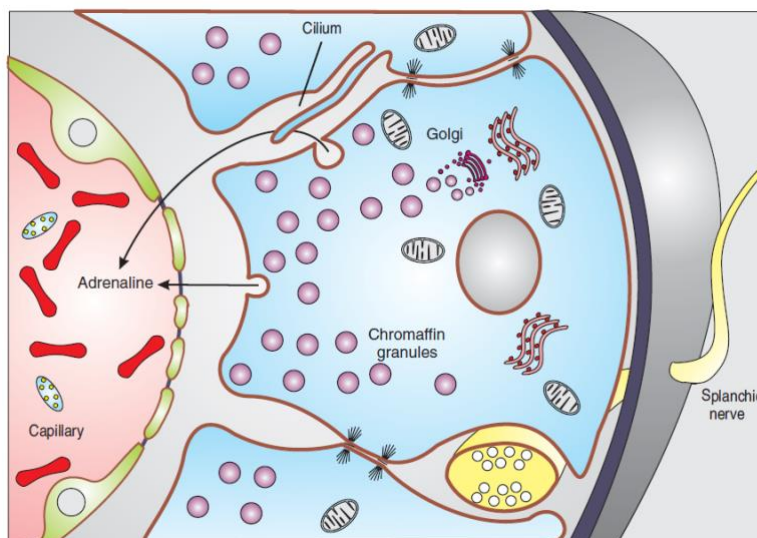


**Figure 3: Structural organization of the chromaffin cells.** Chromaffin cells located in the adrenal medulla are specialized to secrete catecholamines into the neighboring capillaries. Secretion is stimulated by acetylcholine released from splanchnic nerve endings that often insinuate themselves in between the chromaffin cells. Many of the chromaffin cells contain a single primary cilium that extends into the intercellular space facing the capillaries. From Berridge 2012.

LDCVs release their components in the extracellular space by fusion with the PM in response to splanchnic nerve stimulation. LDCVs serve as prototype for regulated secretory vesicles. The mechanism of LDCV exocytosis from adrenal chromaffin cells

resembles that of synaptic vesicle exocytosis in classical CNS synapses (Crivellato et al., 2008).

## NPY – a marker of LDCV

LDCV also contain other biogenic peptides such as NPY. Tatemoto (1982) deciphered the amino acid sequence of NPY and showed that it has 70% sequence homology with peptide YY (porcine intestinal peptide) and 50% homology with pancreatic polypeptide. It was proposed that NPY, peptide YY, and pancreatic polypeptide belonged to the same family. In the following year, NPY was found in high concentrations in adrenal gland of dog, mouse, and rat (Allen et al., 1983). NPY is a small 36 amino acid peptide that is highly conserved. It is ubiquitously present in central and peripheral nervous system (Nussdorfer and Gottardo, 1998). NPY plays an important part in regulation of appetite, blood pressure, learning, and memory (Colmers and Wahlestedt, 1993). Majane et al., (1985) showed that NPY concentration was considerably higher in adrenal medulla than in adrenal cortex, indicating that chromaffin cells contain the highest concentration of NPY. Schalling et al., (1988) showed that the adrenaline as well as noradrenaline secreting cells from rat adrenal medulla were positive for NPY, indicating that NPY can be used as a marker for LDCVs.

## 1.4 REGULATED SECRETORY PATHWAY

The synchronized pathway of vesicle exocytosis is also called “stimulus-secretion coupling” (Lin and Salton, 2013). This process of stimulus-secretion coupling in adrenal chromaffin cells occurs in different steps: first, extracellular  $\text{Na}^+$  and  $\text{Ca}^{2+}$  enters the cell when their acetylcholine receptors are stimulated; second, the ensuing short depolarization that opens voltage dependent  $\text{Na}^+$  channels; third, opening of  $\text{Na}^+$  channels results in large depolarization that opens various voltage-sensitive  $\text{Ca}^{2+}$  channels; lastly, the increase in the intracellular  $\text{Ca}^{2+}$  activates secretory vesicles fusion with the PM (Aunis and Langley, 1999; fig. 4).

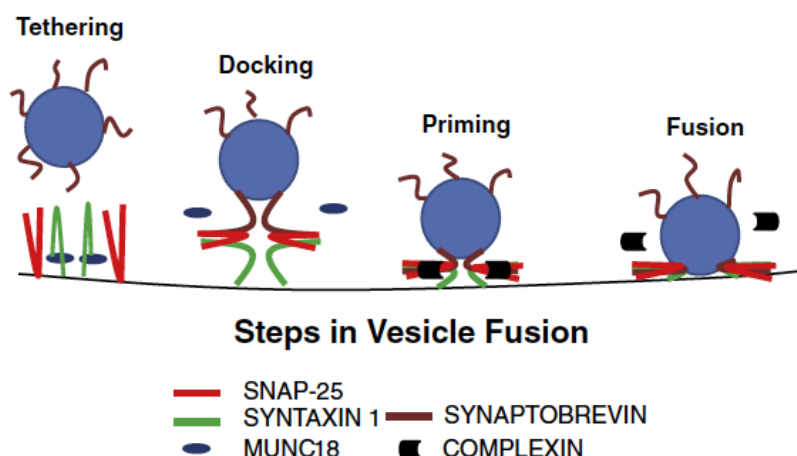


**Figure 4: Steps in synaptic vesicle fusion.** Steps in vesicle fusion include vesicle tethering, docking, priming and finally, fusion. These events are driven by high-affinity interaction between v-SNARE and t-SNARE proteins, regulated by calcium and calcium-binding proteins through their interaction with the SNARE complexes. From Ramakrishnan et al., 2012.

Before LDCVs gain fusion capability, they pass different functional stages. Vesicles are tethered, then docked to the PM, then they become primed, and finally they can release their contents upon fusing with the PM. To ensure that neuroendocrine

secretion operates correctly, all these steps are tightly regulated and coordinated both spatially and temporally by a large number of proteins.

**Tethering:** Tethering refers to a process, in which vesicles are transported to the release sites so as to enable the contact between the vesicular (v)-SNARE and the target (t)-SNARE proteins located in the PM (Whyte and Munro, 2002; Ramakrishnan et al., 2012). This process is accompanied by a multitude of proteins among which Munc18 is the most prominent as will be described later (Smyth et al., 2010). It is followed by the process of docking during which SNARE proteins approach each other via SNARE motifs in a  $\text{Ca}^{2+}$ - independent manner.

**Docking:** Docking is the first step in regulated secretory pathway in which the vesicles comes in close contact with the adjacent PM. This process is being explained in detail later.

**Priming:** Priming is the step that makes the vesicles ready for exocytosis when  $\text{Ca}^{2+}$  enters through the voltage dependent  $\text{Ca}^{2+}$  channels in response to an action potential (Rizo and Südhof, 2002). Essentially, in this priming step the t-SNAREs, SNAP25 and Stx1, and the v-SNAREs, Syb-2 or Ceb, interact to form the fully zippered SNARE complex bringing the vesicular membrane in close contact with the PM. It is regulated by different cytosolic, vesicular, and PM proteins that interact with each other. It is also a  $\text{Ca}^{2+}$  dependent process in a range of 150 nM to 600 nM (Voets, 2000).

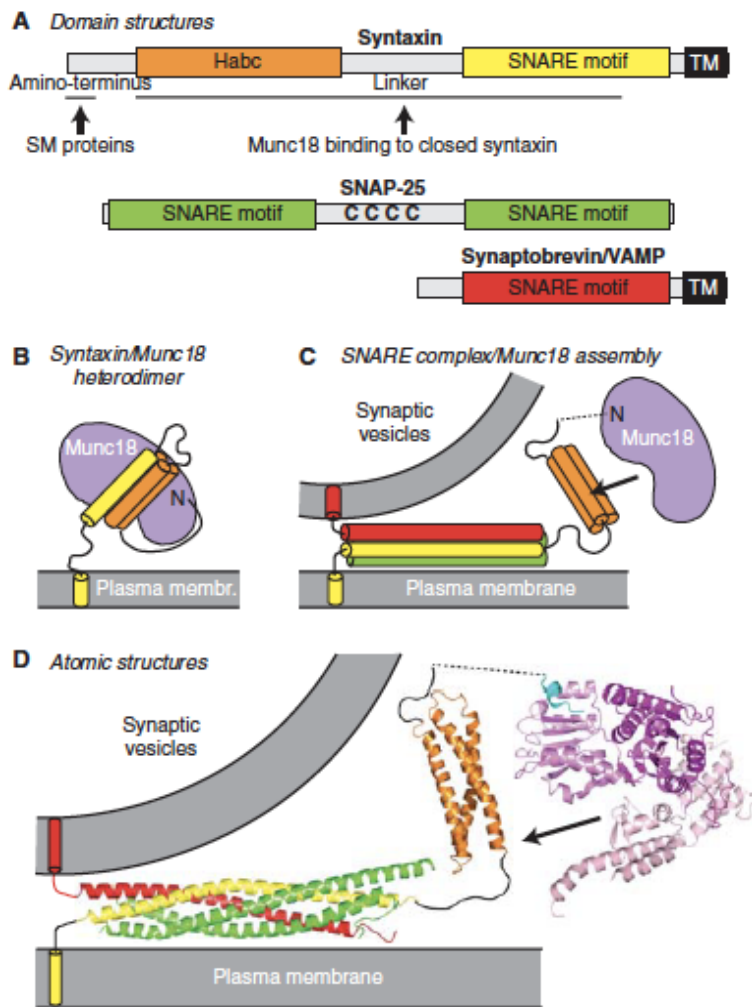


**Figure 5: Structures of synaptic SNARE and SM proteins.** (A) Schematic diagram of the domain structures of syntaxin, SNAP-25, and synaptobrevin/VAMP (Habc, Habc-domain; TM, transmembrane region). (B, C) Cartoon of the two modes of interaction of the SM protein Munc18 with SNARE proteins during synaptic exocytosis: Binding of Munc18 to the closed conformation of syntaxin-1 that occludes the SNARE motif (B), and binding of Munc18 to assembling SNARE trans-complexes that depends on the syntaxin-1 amino terminus (C). Note that the precise mode of Munc18 binding to assembling SNARE complexes is unknown, apart from the fact that it is anchored by interaction of the syntaxin amino terminus (indicated by an N) with the N-lobe of Munc18; the arrow indicates the uncertain atomic nature of this binding, which may involve wrapping of Munc18 around the SNARE helical bundle analogous to the binding of Munc18 to the closed conformation of syntaxin (Südhof and Rothman 2009). (i) Atomic structures of the fully assembled SNARE complex, the syntaxin-1A Habc domain, and Munc18 containing a bound syntaxin amino-terminal peptide (blue), drawn to scale. Modified from Südhof and Rizo, 2011.

## SNAREs and other accessory proteins involved in priming

The major molecular players of membrane fusion process are the SNAREs. SNAREs are comprised of large family of proteins that are recognized by 60 amino acid residues called the SNARE motif. This motif forms a coiled coil domain that is highly conserved (Rizo and Südhof, 2002). There is formation of a heterotrimeric SNARE complex between t-SNAREs SNAP25 and Stx1 with v-SNARE Syb-2 (Ashery et al., 2009; fig. 5). SNARE complex is formed in two stages; first there is formation of heterodimeric complex between t-SNAREs Stx1 and SNAP25 and second the v-SNARE Syb-2 is inserted to form heterotrimeric trans SNARE complex (Chen et al., 2001; Borisovska et al., 2005; Walter et al., 2010; Borisovska et al., 2012; Jahn and Fasshauer, 2012; James and Martin, 2013). Various studies have shown that the SNARE complex is made of very stable four helices that are arranged in a parallel fashion in the core complex (Südhof et al., 1993; Fasshauer et al., 1998; Sutton et al., 1998; Dulubova et al., 1999). Other accessory proteins like Munc13, Munc18, and CAPS also play a role in priming of vesicles. Dulubova et al., (1999) have shown that when Stx1 is in isolation, it is in a closed conformation that is incompatible with the formation of SNARE core complex. This closed state of Stx1 prevents unrequired interactions with

SNARE proteins before priming and is favored by Munc18. Furthermore, Munc18 has a chaperone role because in its absence, the transport of Stx1 to PM is reduced resulting in the abolishment of exocytosis (Verhage et al., 2000). Also, Schollmeier et al., (2011) have shown using liposome assays that Munc18-1 enhances the formation of trans-SNARE complex thereby accelerating priming when incubated with t-/v-SNAREs. The switching of Munc18-1 from inhibitory mode in which it interacts with the closed Stx1 to stimulatory mode to enhance priming has been proposed to be accomplished by Munc13-1 (Rizo and Südhof, 2012). In hippocampal and cortical neurons Munc13-1 and Munc18-1 play a role in stabilizing the fusion competent vesicles by inhibiting de-priming which is mediated by NSF (He et al., 2017). In bovine chromaffin cells the overexpression of Munc13-1 resulted in high increase in the fusion of release ready vesicles as well as in the sustained component without affecting the number of docked vesicles, thereby suggesting a role of Munc13-1 in priming of LDCVs (Ashery et al., 2000). CAPS has also been implicated to play a role in priming. Deletion of CAPS in mouse chromaffin cells resulted in reduction in the amount of exocytosis (Speese et al., 2007; Liu et al., 2010). Finally, there are other proteins like PKA and PKC that helps in the process of priming. High levels of PKA enhances the secretion in neurons as well as in chromaffin cells as it phosphorylates SNAP25 that in turn helps to maintain the size of SRP and RRP (Trudeau et al., 1996; Nagy et al., 2004). Also, PKC has been shown in chromaffin cells to play a role in replenishment of the releasable pools thereby making the vesicles available for priming (Gillis et al., 1996, Smith et al., 1998).

**Fusion:** Fusion is the final step in regulated secretory pathway. As soon as the intracellular  $Ca^{2+}$  level increases due to the entry of  $Ca^{2+}$  through voltage dependent  $Ca^{2+}$  channels, primed vesicles fuse with the PM. The major molecular determinants for fusion are Syts. Syt1 and Syt7 are the two  $Ca^{2+}$  sensors known to exist in chromaffin cells. Syt1 is present on the vesicle membrane and possess two C2 domains, C2A and C2B that bind three and two  $Ca^{2+}$  ions respectively (Sutton et al., 1995; Fernandez et al., 2001). Studies have shown that mutants of Syt1 that either lack or gain the affinity for  $Ca^{2+}$  resulted in changes in the release of vesicles, which suggested that Syt1 is a  $Ca^{2+}$  sensor for release (Fernández-Chacón et al., 2001; Rhee et al., 2005). Schonn et al., (2008) have shown that Syt1 and Syt7 share the function of  $Ca^{2+}$  sensing in mouse chromaffin cells suggesting Syt1 as a fast  $Ca^{2+}$  sensor responsible for the release of RRP whereas Syt7 as a slow  $Ca^{2+}$  sensor responsible for the sustained component. Recently, Complexins have also been implicated in enhancing the synchronous release by increasing the affinity for  $Ca^{2+}$  in mouse chromaffin cells (Dhara et al., 2014). They have shown that the N-terminal domain of Complexin II decreases the secretory delay and enhances the kinetics of  $Ca^{2+}$  dependent exocytosis by interacting with Syt1.

### 1.4.1 VESICLE DOCKING AND PROTEINS INVOLVED

Docking is considered the first transitional maturation step before LDCVs gain fusion-competence and release their neurotransmitters. It is the step, which is the least understood in comparison to priming and fusion and is subject of some controversies.

“Docked vesicle”, this term has been defined originally using electron microscopy, as those vesicles been in close contact with the PM. Currently, there are different criteria used to define docked vesicles; vesicles lying close to the PM at a distance <30 nm or vesicles having a “contact patch” with the PM are considered docked (Verhage and Sorensen, 2008). Several studies using evanescent-wave fluorescence microscopy suggest that there is a dramatic reduction in LDCV mobility upon reaching the PM, presumably reflecting a docking interaction (Robinson and Martin, 1998; Nofal et al., 2007; Pasche et al., 2012). Vesicles docking can be explained in two ways. Morphological docking occurs when vesicles visualized by electron microscopy appear to interact with the plasma membrane (Plattner et al., 1997; Steyer et al., 1997). Alternatively, a vesicle is defined as biochemically docked when a protein connection is established between the two merging membranes (Martin and Kowalchuk, 1997).

Several proteins like Munc18, t-SNAREs, Syt1, and other regulatory proteins have been shown to regulate targeting and docking of vesicles in chromaffin cells. Voets et al., (2001) revealed that Munc18-1 deficient chromaffin cells had a tenfold reduction of “morphologically” docked LDCVs through the ultrastructural analysis of LDCV distribution. Also, Munc18-1 expression level was proportional to the degree of LDCV docking in a gene-dose dependent manner (Toonen et al., 2006; Gulyás-Kovács et al., 2007). t-SNARE proteins like Stx1 and SNAP25 have also been shown to play a role in docking, since their deletion resulted in reduced number of morphologically docked vesicles (de Wit et al., 2006). N-terminal part of Syb-2 has been proposed to be involved in LDCV docking in PC12 cells as well as in synaptic vesicle docking in hippocampal neurons (Wu et al., 2012, Imig et al., 2014). More recently, Syt1 has been identified as a docking factor in chromaffin cells as deficiency of Syt1 resulted in a decrease of docked vesicle number. In addition, several other proteins have also been associated in docking in different secretory cells, such as Rab27, Rabphilin 3A, Granuphilin, and Exophilin4/Slp2a. But these proteins are not essential for LDCV docking in chromaffin cells (Ashery et al., 2000; van Weering et al., 2007).

### **Productive (functional) and unproductive (non-functional or “dead-end”) docking**

One molecule of SNAP25 interacts with one molecule of Stx1 to form 1:1 t-SNARE acceptor complexes (fig. 6), to which one molecule of Syb-2 binds resulting in a functional or productive priming complex ultimately allowing fusion of the bound vesicle. Additionally, in-vitro experiments performed to study the interaction between different SNARE proteins revealed the formation of usual as well as an unusual t-SNARE complexes between Stx1 and SNAP25 (Bajohrs et al., 2004).

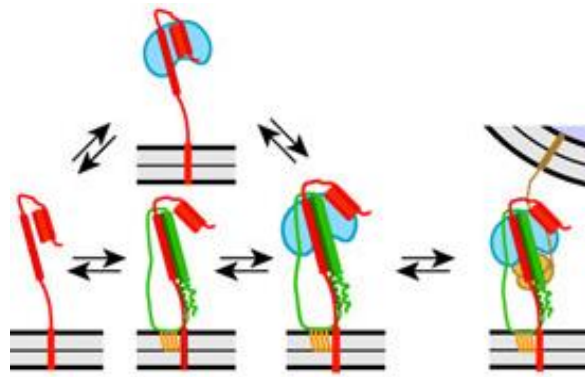


**Figure 6: Docking proteins and their interaction steps leading to priming and fusion.** Model shows potential subsequent steps in the exocytosis pathway, starting with several initial protein complexes consisting of Stx1 (red), SNAP25 (green), Syt1 (yellow), and/or Munc18-1 (blue). This model illustrates a functional mechanism leading to fusion of vesicle. From de Wit et al., 2009.

The usual binary complex is formed in 1:1 stoichiometry whereas the unusual tertiary complex is formed in a 2:1 stoichiometry between 2 Stx1 molecules binding 1 SNAP25 molecule. The binding of an additional Stx1 molecule to SNAP25 molecule results in the unavailability of the binding site for Syb-2 on SNAP25, ultimately leading to a so called dead-end interaction or unproductive SNARE acceptor complex. It was hypothesized that in live cells it produces a dead-end docking which is not followed by priming and fusion (fig. 7, Verhage and Sørensen, 2008). These dead-end complexes are not as stable as the ternary SNARE complexes but these dead-end complexes dissociate very slowly, hence they represent kinetically trapped dead-end vesicles or liposomes that might require special chaperones for their disassembly, if formed in vivo (Weninger et al., 2008).

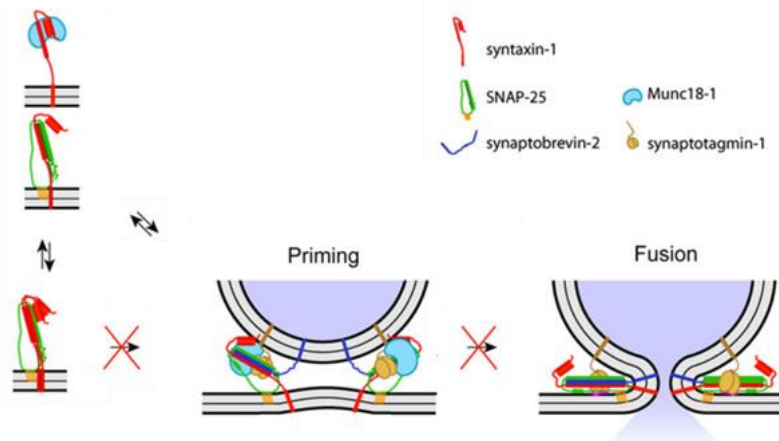


**Figure 7: Model for dead-end docking.** Two Stx-1 molecules interact with one SNAP-25 molecule. This complex has a relatively slow dissociating stoichiometry resulting in the inhibition of priming and fusion of the vesicle. Modified from de Wit et al., 2009.

Previously the existence of dead-end complex was only shown by in-vitro experiments, but our group showed in bovine chromaffin cells (Hugo et al., 2013) that the 2:1 unproductive SNARE acceptor complex is formed in living cells, and that it leads dead-end docking.

## 1.5 ENDOCYTOSIS AND RECYCLING OF PROTEINS INVOLVED IN EXOCYTOSIS

In neuroendocrine cells and neurons, the transmitter release results in an increase in the surface area of PM, aggregation of vesicular proteins at the site of fusion as well as

exhaustion of the availability of release ready vesicles. To compensate these changes, vesicle membrane and proteins are removed from the PM by endocytosis (fig. 8).

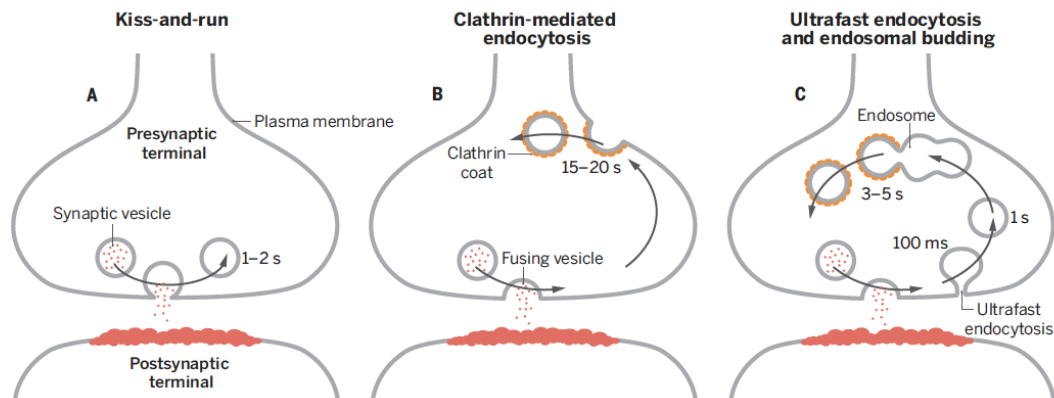


**Figure 8: Models of synaptic vesicle recycling:** (A) The kiss-and-run model. Vesicles transiently fuse with the plasma membrane. After the neurotransmitter release, the fusion pore is closed and the vesicles are recovered. (B) The clathrin-mediated endocytosis model. A synaptic vesicle fuses and collapses into the membrane. A new vesicle is formed in a region distant from the fusion site. (C) A new model of synaptic vesicle recycling. After a rapid internalization of the membrane via ultrafast endocytosis, the vesicle membrane is delivered to an endosome. Clathrin-mediated regeneration of synaptic vesicles occurs at the endosome. From Watanabe, 2017.

Ceccarelli et al (1972) showed that in frog neuromuscular junction within 4 h of stimulation, almost 45% of fused vesicles were already endocytosed for the next round of exocytosis. Characterization studies from Philips et al., (1983) and Murthy and De Camilli, (2003) have shown that endocytosis seems to be a clathrin-mediated phenomenon. Similarly, it was also shown previously that clathrin-mediated endocytosis is the process undertaken by synaptic vesicles to recycle in nerve terminals as well as neuroendocrine cells (Heuser and Reese, 1973; Gad et al., 1998; Teng and Wilkinson, 2005, Bittner et al., 2013). Clathrin and other accessory proteins play a major role in internalization of different proteins. They also provide a driving force for invagination of membrane, after which the GTPase dependent protein Dynamin comes into play. It forms a ring surrounding the neck of the invagination, and catalyze the fission of clathrin-coated vesicles (Murthy and De Camilli, 2003). This process is then followed by uncoating of clathrin and the resulting vesicles fuse with early endosomes, ultimately leading to the beginning of a new synaptic vesicle cycle (Murthy and De Camilli, 2003). Another mode of endocytosis is “kiss-and-run”. In this process vesicles are temporarily attached to the PM but vesicle membrane proteins do not mix with the PM components. In its place, the vesicle is recaptured by a rapid endocytic process and then again it is refilled with the neurotransmitters for next round of exocytosis. This process had a big advantage over the clathrin-mediated endocytosis because it does not require the total uptake of the vesicle membrane. This process is very rapid in comparison to clathrin-mediated endocytosis because it does not involve coating, fusion, and budding of vesicles from the endosomes (Palfrey and Artalejo, 1998). However, the “kiss-and-run” and ultrafast endocytosis are not advantageous for neuroendocrine cells because in neuroendocrine cells the LDCVs not only contain hormones but also neuropeptides and these neuropeptides are filled in

LDCVs at the Golgi apparatus. So, for the next round of exocytosis vesicle has to reach the Golgi to refill its cargo.

Previous studies have also shown that two independent modes of endocytosis exist in bovine adrenal chromaffin cells, compensatory and excess retrieval which are  $\text{Ca}^{2+}$  regulated (Smith and Neher, 1997; Engisch and Nowycky, 1998; Chan and Smith, 2001). Other than these two mechanisms, there is also another relatively rapid process of endocytosis that retrieves large portion of membrane within seconds and accounts for the retrieval of 60% of exocytosed membrane (Smith and Neher, 1997). Also, many proteins have been implicated to play a role in the process of endocytosis in neurons and neuroendocrine cells namely; Calcineurin (CaN), Calmodulin (CaM), Synaprotagmin1 (Syt1), Synaptophysin1 (Syp1) as well as L-type  $\text{Ca}^{2+}$  channels (Mahapatra et al., 2012; Rosa et al., 2012; Wu et al., 2014; Wu et al., 2014; Rajappa et al., 2016).

Despite the numerous studies on endocytosis and related mechanisms, exactly how the recycling pathway works in neuroendocrine cells and which endosomal compartments are involved in this phenomenon is still not well investigated.

## **2. AIM**

LDCVs in chromaffin cells share features of its life cycle with synaptic vesicles. They contain epinephrine and norepinephrine, peptides like NPY, other natriuretic peptides, as well as core proteins like Chromogranin A (CgA), Chromogranin B (CgB), and Secretogranins (Sgs). When chromaffin cells receive stimulation from splanchnic nerve, LDCVs are released through regulated exocytosis. However, before the LDCVs become release ready, they have to reach the PM. Biogenesis of LDCVs involves different steps. First the secretory proteins, peptidergic hormones, and neuropeptides are made and are condensed in the TGN where the immature secretory vesicles containing the manufactured cargo are generated. While travelling towards the PM, these immature vesicles are filled with catecholamines and further gain maturity. This pathway of LDCV biogenesis has been studied by several groups in PC12 cells and to some extent in bovine chromaffin cells. However, biogenesis of LDCVs in mouse chromaffin cells has not been investigated in detail. To gain more insights into this aspect of LDCVs, the objective of my work was to study their biogenesis, when and where the content is packed in LDCVs, when they get associated with the vesicular membrane proteins and how these are recycled in mouse chromaffin cells.

Regulated exocytosis has been studied widely using chromaffin cells. It includes several steps like tethering, docking, priming, and finally the release of LDCVs upon elevation in the  $Ca^{2+}$  concentration. Docking is the least understood step. It occurs when t-SNAREs, SNAP25 and Stx1 form a 1:1 productive t-SNARE complex and interact with vesicular protein Syt1 (de Wit et al., 2009). Munc18 stabilizes this complex allowing priming and fusion of the LDCVs. However, another docking mechanism called “dead-end” docking occurs in bovine chromaffin cells (Hugo et al., 2013) involving the unproductive t-SNARE complex formed by interaction of 2 molecules of Stx1 and 1 molecule of SNAP25 that renders fusion incompetent vesicles docked at this complex. They showed that 15% of LDCVs at the PM are dead-end vesicles and their number is modulated by the overexpression of t-SNAREs as well as Munc18. However, the identity of the vesicular protein that interacts with the unproductive t-SNARE complex and mediate dead-end docking is unknown. Hence, another important aim of my work was to study the mechanisms of dead-end docking in mouse chromaffin cells to identify the vesicular protein that interacts with the unproductive t-SNARE acceptor complex and mediate dead-end docking.

### 3. Materials and methods

#### 3.1 Materials

##### 3.1.1 Reagents

Name	Company
Agarose	Carl Roth GmbH
Albumin	Sigma
Calcium chloride dihydrate	Merck KGaA
Collagen	BD Biosciences
Disodium hydrogen phosphate dihydrate	Merck KGaA
DMEM	Gibco by Life Technologies
DMSO	Sigma
DPBS	Gibco by Life Technologies
EDTA	Sigma
Ethanol	Roth
FCS	Invitrogen
Glucose monohydrate	Merck KGaA
Glycin	Roth
HEPES	Sigma
HPLC water	Sigma
HCl	Roth
ITS – X	Gibco by Life Technologies
KCl	Merck KGaA
L – cysteine	Sigma
Magnesium chloride hexahydrate	Merck KGaA
Neural goat serum	Invitrogen
Paraformaldehyde	Merck KGaA
Pen/Strep	Invitrogen
Sapphire discs	Leica
Sodium chloride	Merck KGaA
Sodium dihydrogen phosphate monohydrate	Merck KGaA
Sodium hydroxide	Sigma-Aldrich
Tris	Roth
Triton-X-100	Roth
Trypsin inhibitor	Sigma
Uranyl acetate	Science Services

##### 3.1.2 Enzymes

Name	Company
Papain	Worthington Biochemical Corp.

##### 3.1.3 Antibodies

Name	Company	Dilution used
Anti-CgA (goat anti – rabbit)	Abcam	1:1000
Anti-Ceb (goat anti – rabbit)	Synaptic Systems	1:1000
Anti-GM130 (rat anti – mouse)	BD Biosciences	1:100
Anti-Syb-2 (monoclonal anti – mouse)	Synaptic Systems	1:100
Anti-Syt1 (rabbit anti – mouse)	Synaptic Systems	1:2000
Anti-Rab11A (rabbit monoclonal anti - human)	Abcam	1:100
Anti-LAMP1 (monoclonal anti - mouse)	Developmental studies hybridoma bank	1:500

Anti-TGN38 (rabbit anti – rat)	AbD Serotec	1:200
Anti-SNAP25 (rabbit anti - human)	GenScript	1:500
Anti-Stx1 (monoclonal anti-mouse)	HPC/1 mouse ascites, from Prof. Jahn, Max-Planck-Institut für biophysikalische Chemie, Göttingen, Germany	1:500
Affinity Fab fragments	Biomol	1:50
Alexa 647 Phalloidin	Life Technologies	2.5%
Alexa 488 Phalloidin	Life Technologies	2.5%
Alexa Fluor 488 goat anti–mouse IgG (H+L)	Life Technologies	1:2000
Alexa Fluor 488 goat anti–rabbit IgG (H+L)	Life Technologies	1:2000
Alexa Fluor 647 goat anti–rabbit IgG (H+L)	Life Technologies	1:2000
Alexa Fluor 647 goat anti–mouse IgG (H+L)	Life Technologies	1:2000

### 3.1. 4 Solutions

#### 3.1.4.1 General solutions

##### 1. PBS

Composition	Amount
Na <sub>2</sub> HPO <sub>4</sub> . H <sub>2</sub> O	58 mM
NaH <sub>2</sub> PO <sub>4</sub> . 2H <sub>2</sub> O	17 mM
NaCl	83 mM
pH	7.4
Osmolarity	310 – 320 mOsm
Dissolve the contents in 500 mL of distilled water. Adjust the pH to 7.4 with 1N NaOH. Make up the volume to 1000 mL and measure the osmolarity.	

#### 3.1.4.2 Solutions for Chromaffin cell preparation

##### 1. Locke's solution

Composition	Amount
NaCl	154 mM
KCl	5.6 mM
Na <sub>2</sub> HPO <sub>4</sub> . H <sub>2</sub> O	2.15 mM
NaH <sub>2</sub> PO <sub>4</sub> . 2H <sub>2</sub> O	0.85 mM
Glucose	10 mM
pH	7.4
Osmolarity	312 mOsm

##### 2. Papain solution

Composition	Amount
DMEM	50 mL
L – Cysteine	10 mg (to activate papain)
100 mM CaCl <sub>2</sub>	0.5 mL
50 mM EDTA	0.5 mL (to activate papain)
Frozen in the form of 2 and 3 mL aliquots. After thawing: 20 Units of papain to be added per mL of this solution and bubbled with carbogen for 20 min.	

### 3. Inactivation solution

Composition	Amount
DMEM	50 mL
FCS	5 mL
Albumin	125 mg
Trypsin inhibitor	125 mg
Frozen in the form of 2 and 3 mL aliquots.	

### 4. Cell culture medium

Composition	Amount
DMEM	40 mL
ITS – X	400 µL
Pen/Strep	160 µL
After mixing all the components incubate at 37°C with 13% CO <sub>2</sub> .	

#### 3.1.4.3 Solutions for Immunocytochemistry

##### 1. Fixation solution: 15% PFA

Composition	Amount
Paraformaldehyde	3 g
Distilled H <sub>2</sub> O	20 mL
1N NaOH	20 µL
pH	7.4
Heat the distilled water to 60°C and add paraformaldehyde to it. Mix immediately well. Add NaOH and mix well. Keep the solution on magnetic stirrer at 60°C and allow the solution to become clear. Filter the solution and check the pH. When required dilute the solution to 4% and use.	

##### 2. Quenching solution

Composition	Amount
Glycin	50 mM
PBS	50 mL
1M MgCl <sub>2</sub>	100 µL
1M CaCl <sub>2</sub>	25 µL

##### 3. Permeabilization solution

Composition	Amount
PBS	50 mL
NGS	1.25 mL (2.5%)
Triton – X – 100	50 µL (0.1%)
1M MgCl <sub>2</sub>	100 µL
1M CaCl <sub>2</sub>	25 µL

##### 4. Blocking solution

Composition	Amount
PBS	50 mL
NGS	1.25 mL (2.5%)
1M MgCl <sub>2</sub>	100 µL
1M CaCl <sub>2</sub>	25 µL

## 5. Mounting medium

Composition	Amount
Mowiol 4 – 88	2.4 g
Glycerol	6.0 g
Tris – buffer	12 mL
Distilled H <sub>2</sub> O	6.0 mL

### 3.1.4.4 Solutions for Electrophysiology

#### 1. Intracellular solution: 6 $\mu$ M Ca<sup>2+</sup> solution

Composition	Amount
L-Glutamic acid	110 mM
H-EDTA	9 mM
CaCl <sub>2</sub>	5 mM
HEPES	40 mM
Mg-ATP	2 mM
Na <sub>2</sub> -GTP	0.3 mM
HPLC-H <sub>2</sub> O	20 mL
pH	7.2
Osmolarity	297 mOsm

Dissolve components from 1 to 4 in 14 mL HPLC-H<sub>2</sub>O and adjust the pH to 7.2 with 50% CsOH. Then add nucleotides and adjust pH to 7.2 with 10% CsOH and make up the total volume to 20 L with HPLC-H<sub>2</sub>O. Measure the osmolarity.

#### 2. Extracellular solution (10X)

Composition	Amount
NaCl	1520 mM
KCl	24 mM
HEPES	100 mM
MgCl <sub>2</sub> . 6H <sub>2</sub> O	12 mM
CaCl <sub>2</sub> . 2H <sub>2</sub> O	25 mM
pH	7.4
Osmolarity	310 (1:10)

Dissolve all the components in 1000 mL of distilled water. Adjust the pH to 7.4 with 1N NaOH and measure the osmolarity. When required to use, add 10 mM Glucose monohydrate to the solution. Measure the osmolarity of the solution.

## 3.2 Methods

### 3.2.1 Mouse chromaffin cell preparation

In the case of WT, Syt7 KO, and Ceb KO newborn pups age p3 were used, but due to the lethal phenotype of Syt1 KO and Syb-2 KO, E18 pups were used. The head of the pup was decapitated with a scissor. The pup was dissected under the microscope and adrenal glands were carefully removed with forceps and placed in cold Locke's solution. The adrenal glands were cleaned to eliminate the fat with the forceps and small scissor. To prepare one 6 well plate adrenal gland from two pups were pooled. Adrenal glands were placed in a falcon tube containing 500  $\mu$ L of papain solution (20 U/mL) and digested in shaking water bath at 37°C for 21 min (E18 – 18 min.). The enzyme solution was removed after digestion and 500  $\mu$ L of inactivation solution was

added to the glands and incubated in shaking water bath at 37°C for 4 min. The inactivation solution was removed and 500 µL of culture medium was added to the glands. They were then triturated with 200 µL pipette tip until the tissue was completely dissociated. Then the cells were subjected to the electroporation procedure.

### **3.2.2 Electroporation of mouse chromaffin cells**

In our experiments, the transfection efficiency of chromaffin cells was ≈18-20% with reasonable cell viability. After the tissue was completely dissociated, the cells were transferred to an eppendorf tube and centrifuged at 4000 rpm for 5 min. After centrifugation, the culture medium was removed and 500 µL of DPBS was added. Cells were again centrifuged at 4000 rpm for 5 min. Neon transfection system was used for electroporation of mouse chromaffin cells. 20 µL of R buffer was added and 4 µg of plasmid (pmax-NPY-mCherry) was added to the cells. Solution was mixed well and 10 µL cell solution was used in electroporation (1 pulse of 1400 V with 30 ms pulse width). In the overexpression experiments, cells were double transfected with pmax-NPY-mCherry and Lenti-pSyn-pH-Syt7 constructs. 4 µg total of both plasmids was used and procedure was same as before.

### **3.2.3 Immunocytochemistry**

Mouse chromaffin cells were cultured 2 DIV or the indicated time before experiments. The culture medium was removed and the cells were washed twice with PBS containing Mg<sup>2+</sup> and Ca<sup>2+</sup>. Cells were fixed with 4% PFA for 20 min at room temperature. After fixation cells were washed thrice with PBS every 3 min. Then quenching was done with 50 mM Glycine for 10 min, and washed thrice with PBS. Cells were permeabilized with 0.1 % Triton X-100 solution for 30 min, after which they were subjected to blocking by washing twice with 2.5% NGS solution. During the incubation time of permeabilization step, primary antibodies were diluted with blocking solution as required (Table 1). After blocking, 100 µL of primary antibody solution was placed on a parafilm and covered by the coverslips placed upside down. The incubation time was 1 h at room temperature in a wet chamber so as to prevent the drying of antibody solution. During this incubation, the secondary antibody was diluted with blocking solution, typically with a factor 1:2000. The secondary antibody solution was subjected to centrifugation for 10 min at 13000 rpm at 4°C to spin down the highly fluorescent particles in secondary antibody solution that creates background problems during imaging. After incubation, the cells were washed thrice with Triton-X-100 solution. Then cells were incubated with secondary antibody for 45 min in dark at room temperature in wet chamber. Subsequently, the cells were washed 5 times with Triton-X-100 solution and 2 times with PBS solution. The coverslips were then mounted upside down on the microscopic slides with 20 µL mounting medium per coverslip and allowed to dry at 37°C for 15 min. Lastly, the edges of coverslips were sealed with nail polish to avoid further drying. Dilutions of the antibodies are mentioned previously.

In the case of double immunolabeling with antibodies raised in the same species, first the above-mentioned protocol was followed upto the step of washing with PBS. Then cells were incubated in 2.5% NGS/PBS for 1 h at room temperature. Cells were washed thrice for 5 min each with PBS and then incubated with Fab fragments raised against immunoglobulins of the same type and species as the primary antibody for 1 h at room temperature followed by washing thrice for 10 minutes each with PBS. Cells were then immunolabeled for the second protein using the previously mentioned protocol with a secondary antibody tagged to a different fluorophore. Then coverslips were mounted as mentioned previously. Imaging was done by high resolution microscopic technique “Structured Illumination Microscopy”.

### **3.2.4 Structured Illumination Microscopy (SIM)**

SIM is based on laser-wide-field microscopy. It contains a movable grating in the excitation beam path. When laser passes through this grating, it generates a stripe like pattern which is applied to the sample. The diffraction-limited borders of this so called Moiré pattern, contain structural information about the sample that cannot be resolved by conventional light microscopy. By shifting and rotating the grating, one generate a raw image stack, that is then processed via Fourier transformation, allowing the extraction of diffraction-limited structural information. The result is a highly-resolved image, with a resolution limit of 100 nm in XY axis and 200-250 nm in Z axis (<http://www.andor.com/learning-academy/super-resolution-imaging-structured-illumination-microscopy-application-note>; Bost et al., 2013).

In this study, the SIM setup used was from Carl Zeiss Microscopy GmbH. The objective used was plan – apochromat 63X/1.4 NA oil (DIC), the laser lines used were 488 nm, 561 nm and 647 nm and the images were acquired through Andor iXon EM-CCD camera at 100 ms of exposure time. Zen (black edition) software with SIM module was used for acquiring and processing the images.

### **Analysis of SIM Images**

The analysis of the distribution of LDCVs in reference to plasma membrane and Golgi apparatus was done by using an in-house written software based of Labview (developed by Detlef Hof, Hugo et al 2013), called EasyCell. The plasma membrane, Golgi apparatus and the LDCVs were marked manually using EasyCell and then this software calculated the shortest possible distance between the center of the LDCVs to the plasma membrane and Golgi apparatus (fig. 9). The numbers were then transferred to IgorPro software to generate the histograms. All the images displayed were processed by ImageJ 1.47f software. The colocalization analysis was done by using Pearson’s and Mander’s colocalization coefficients from the JACoP plugin in ImageJ 1.47f software (<http://imagej.nih.gov/ij/>) and the numbers were then transferred to IgorPro to generate the graphs. Pearson’s coefficient is based on the linear relationship between the intensities in two channels and is estimated by linear regression. Pearson’s coefficient value ranges from -1 to +1, where -1 shows complete negative

correlation and +1 shows complete positive correlation. Mander's coefficients measures the co-existence of structures independent of the signal intensities. It requires the thresholding of the images so as to differentiate signal from noise (Bolte and Cordelières, 2006; Dunn et al., 2011).

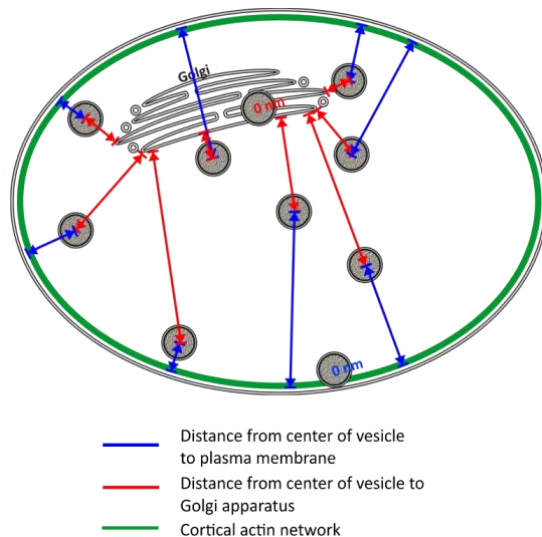


**Figure 9: Method of analysis.** Graphical representation of the method used to analyse the distance from vesicles to the PM and the Golgi apparatus.

### 3.2.5 Correlative fluorescence electron microscopy (CLEM)

This experiment was done in collaboration with Dr. Claudia Schirra in our lab. For the sample preparation, acutely dissociated chromaffin cells transfected with NPY-mCherry were plated on collagen coated sapphire discs (Leica) in 4-well plates. They remained 48 h in culture before fixation to allow good adhesion to the substrate. Then the sapphire discs with cultured cells were transferred into flat specimen carriers and frozen at high pressure after addition of DMEM-medium with 30% FCS (Leica; EM PACT2). Freeze substitution and embedding in Lowicryl was done as described previously (Matti et al., 2013). Briefly, all samples were processed in an automatic freeze-substitution apparatus (Leica; AFS2). The temperature was increased from -130 to -90°C for 2 h. Cryosubstitution was performed at -90 to -70 °C for 20 h in anhydrous acetone and at -70 to -60°C for 20 h with 0.3% (w/v) uranyl acetate in anhydrous acetone. At -60 °C the samples were infiltrated with increased concentrations (30, 60 and 100%; 1 h each) of Lowicryl (3:1 K11M/HM20 mixture with 0.3% uranyl acetate). After 5 h of 100% Lowicryl infiltration, samples were UV polymerized at -60°C for 24 h and for an additional 15 h while raising the temperature linearly to 5°C. Until further processing the samples were kept in the dark at 4°C. After removing the sapphire discs, 100 nm ultrathin sections were cut parallel to the surface using a Leica EM UC7. The sections were collected on carbon-coated 200 mesh copper grids (Plano). Fluorescence analysis of EM grids was done within 1 day after sectioning, to avoid loss of fluorescence in the sections. Prior to SIM imaging, 100 nm resin sections were stained in a drop of CellMask deep red (Invitrogen) (1/500 in PBS) for 10 min, and washed in a drop of water for 1 min. Grids were then placed in a drop of water between two coverslips which were sealed with vacuum grease (Kukulski et al., 2012). Sections were imaged using SIM (Elyra PS.1 Zeiss, Göttingen, Germany) with excitation light of

561 nm and 642 nm. Nearly one entire field of view of a 200 mesh grid (around  $90 \mu\text{m}^2$ ) can be observed with a 63X objective, allowing a perfect orientation of the sample relative to the grid bars in bright field mode. Then the probe was screened using the CellMask deep red (642 nm) staining because it allows to find good chromaffin cells and to focus on the perfect image plane without bleaching the probes. Then a z-stack of 3-8 images (561 nm) was recorded with a step interval of 100 nm. Zen 2010 software was used for data acquisition and processing of the images for higher resolution. The very same grids were stained with uranyl acetate and lead citrate and analyzed with a Philips Tecnai12 Biotwin electron microscope. Only chromaffin cells with well conserved membranes, LDCVs and nuclei were analyzed and used for correlation. For data interpretation, it is important to perfectly align the mCherry SIM image within the electron micrograph. CellMask deep red stains the membranes of the cells in the resin section, the 642 nm image was used to find the perfect overlay on the electron micrograph image. The final alignment with the 561 nm image defines the position of the fluorescent signal within the cells of interest. Images were overlaid in Corel Draw.

### 3.2.6 Electrophysiological measurements by Patch-clamp technique

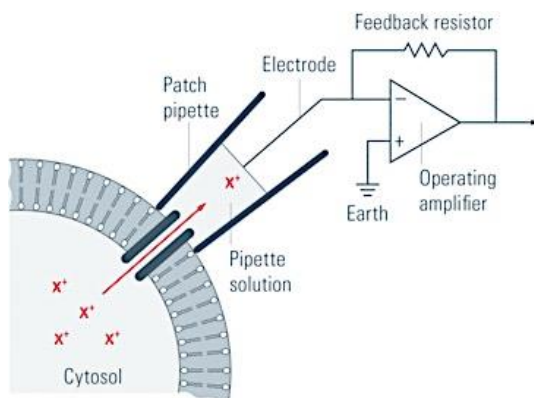


**Figure 10: General principle of patch-clamp recordings.** A glass pipette containing electrolyte solution is tightly sealed onto the cell membrane and thus isolates a membrane patch electrically. Currents fluxing through the channels in this patch flow into the pipette and can be recorded by an electrode that is connected to a highly sensitive differential amplifier. In the voltage-clamp configuration, a current is injected into the cell via a negative feedback loop to compensate changes in membrane potential. Recording this current allows conclusions about the membrane conductance. From: <http://www.leica-microsystems.com/science-lab/the-patch-clamp-technique/>.

Patch-clamp technique (fig. 10) has been extensively used to study the secretion from neuroendocrine cells via membrane capacitance measurements (Lindau and Neher, 1988; Penner and Neher, 1989). The method is based on the principle that the relation between plasma membrane capacitance and membrane area is directly proportional to each other ( $10 \text{ fF}/\mu\text{m}^2$ ). Therefore, when exocytosis occurs, leading to an increase in membrane area, we can measure the changes in the capacitance (Kilic G., 2002).

In my work, I performed conventional whole cell recordings using 3-5 M $\Omega$  borosilicate pipettes (GB150F-8P, Science products, Germany) filled with 3  $\mu\text{L}$  of intracellular solution containing 6  $\mu\text{M}$  free

Calcium. Capacitance measurements were performed using EPC-9 patch-clamp amplifier. The Lindau-Neher technique was implemented as "sine+dc" mode of the "software lock-in" extension of Pulse software. 1 kHz, 70 mV peak-to-peak sinusoid command potential stimulus was applied to at a DC holding potential of -70 mV. Cells were stimulated by perfusing 6  $\mu\text{M}$  free Calcium for 5 min. Simultaneously to the whole cell capacitance measurements, TIRF measurements were also performed.

### 3.2.7 Measurement of single vesicle exocytosis by TIRFM

TIRFM involves the generation of an electromagnetic field, called the “evanescent wave”, that is produced in a confined specimen region immediately adjacent to the interface between two media with different refractive indices. The evanescent wave is capable of selectively exciting the fluorescent molecules in the liquid near the interface within  $\leq 100$  nm (Axelrod, 2001). Contact area between the specimen and a glass coverslip is the most commonly used interface in TIRFM. Total internal reflection happens when light is travelling through two clear media with different refractive indices. Light is partially diffracted and partially reflected. At one angle the light gets completely reflected. This angle is called a critical angle. Total internal reflection takes place at that time. The evanescent wave intensity decreases exponentially as the distance from the interface increases. Therefore, the field of evanescent wave extends to only few hundred nanometers in the z-axis into the specimen. This property of evanescent wave allows the analysis of single vesicle secretion at the PM. (<https://www.microscopyu.com/techniques/fluorescence/total-internal-reflection-fluorescence-tirf-microscopy/>).

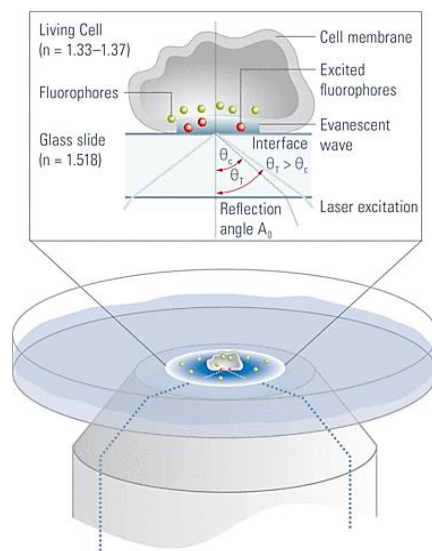


**Figure 11: Principle of TIRFM.** Total internal reflection occurs when the light travels from a medium with a higher refractive index ( $n$ ) (e.g. glass coverslip,  $n = 1.52$ ) to a medium with a lower refractive index (e.g. aqueous medium,  $n = 1.33$ ). The critical angle ( $\Theta_c$ ) of incident light, can be determined by Snell's law:  $\Theta_c = \sin^{-1}(n_1/n_2)$  where,  $n_1$  and  $n_2$  are the refractive indices of the specimen and the coverslip, respectively. (from <http://www.leica-microsystems.com/science-lab/total-internal-reflection-fluorescence-tirf-microscopy/>)

In my study, the experiments were done using a TIRF setup based on inverted Zeiss Axiovert 200 with a Zeiss TIRF-slider and a solid-state laser system emitting at 561 nm. The setup was equipped with an Andor iXon EMCCD camera and controlled by in-house software based on Lab View. Final pixel size was 160 nm. The acquisition rate was 10 Hz with an exposure time of 75 ms.

#### **Analysis and normalization of TIRF data:**

Analysis and normalization was as mentioned in Hugo et al., (2013). For normalization values were first normalized to the individual footprint area of the cell which showed the density of vesicles per  $\mu\text{m}^2$ . The resulting values were then multiplied by the average footprint area to get better understanding of the data.

### 3.2.8 Genotyping

In this study, genotyping of different mice was determined using KAPA Mouse Genotyping Hot Start Kit from Peqlab. KAPA mouse genotyping kits include KAPA Express Extract, a novel thermostable protease and buffer system that allows for the extraction of PCR-ready DNA from mouse tissue in as little as 15 min, and KAPA2G Fast Genotyping Mix with dye, containing a DNA polymerase engineered via directed evolution of high processivity and extreme speed. The combination of KAPA Express Extract and KAPA2G Fast Genotyping Mix allows for the reliable extraction and amplification of DNA fragments from mouse tissue in as little as 1 hour, as compared to  $\geq 1$  day with conventional protocols.

#### 1. Digestion of tail sample

100  $\mu$ L of Kapa lysis buffer (mixture of Kapa express extract enzyme, Kapa express extract buffer, and sigma water) was added to each sample. Eppendorfs were placed in a thermo mixer at 75°C and 1100 rpm for 15 min. Then eppendorfs were continuously placed in thermo mixer at 95°C for 12 min at 1000 rpm.

#### Mastermix

For Syb-2;

For wildtype		For knockout	
DNA	6.0 $\mu$ L	DNA	6.0 $\mu$ L
H <sub>2</sub> O	19.0 $\mu$ L	H <sub>2</sub> O	19.0 $\mu$ L
10x PCR Buffer	3.0 $\mu$ L	10x PCR buffer	3.0 $\mu$ L
MgCl <sub>2</sub>	0.5 $\mu$ L	MgCl <sub>2</sub>	0.5 $\mu$ L
Primer1 (forward 1:1)	0.5 $\mu$ L	Primer1 (forward 1:1)	0.5 $\mu$ L
Primer2 (reverse 1:1)	0.5 $\mu$ L	Primer2 (reverse 1:1)	0.5 $\mu$ L
dNTP's	0.5 $\mu$ L	dNTP's	0.5 $\mu$ L
RedTag polymerase	3.0 $\mu$ L	RedTag polymerase	3.0 $\mu$ L

For Syt1 and Syt7;

For wildtype		For knockout	
DNA	1.0 $\mu$ L	DNA	1.0 $\mu$ L
Primer1 (forward)	0.5 $\mu$ L	Primer1 (forward)	0.5 $\mu$ L
Primer2 (reverse)	0.5 $\mu$ L	Primer2 (reverse)	0.5 $\mu$ L
H <sub>2</sub> O	10.5 $\mu$ L	H <sub>2</sub> O	10.5 $\mu$ L
Kapa mix	12.5 $\mu$ L	Kapa mix	12.5 $\mu$ L

For Ceb;

For wildtype		For knockout	
DNA	2.0 $\mu$ L	DNA	2.0 $\mu$ L
H <sub>2</sub> O	13.25 $\mu$ L	H <sub>2</sub> O	13.25 $\mu$ L
MgCl <sub>2</sub>	0.5 $\mu$ L	MgCl <sub>2</sub>	0.5 $\mu$ L
DMSO	1.25 $\mu$ L	DMSO	1.25 $\mu$ L
Primer1 (forward)	1.25 $\mu$ L	Primer1 (forward)	1.25 $\mu$ L
Primer2 (reverse)	1.25 $\mu$ L	Primer2 (reverse)	1.25 $\mu$ L
Kapa mix	6.25 $\mu$ L	Kapa mix	6.25 $\mu$ L

## 2. PCR protocol for Syt1, Syt7, Syb-2, and Ceb mice

PCR protocol for Syt1 and Syt7 were identical:

### For Wildtype:

- Lid 99°C
1. T = 95°C for 3 min
  2. T = 95°C for 15 s
  3. T = 59°C for 11 s
  4. T = 72°C for 11 s
  5. Go to 2 and repeat 31 times
  6. T = 72°C for 2 min
  7. Hold at 4°C

### For Knockout:

- Lid 99°C
1. T = 95°C for 3 min
  2. T = 95°C for 15 s
  3. T = 59°C for 13 s
  4. T = 72°C for 13 s
  5. Go to 2 and repeat 31 times
  6. T = 72°C for 2 min
  7. Hold at 4°C

PCR protocol for Syb-2:

### For Wildtype:

- Lid 99°C
1. T = 95°C for 5 min
  2. T = 95°C for 50 s
  3. T = 55°C for 45 s
  4. T = 65°C for 90 s
  5. Go to 2 and repeat 35 times
  6. T = 65°C for 10 min
  7. Hold at 4°C

### For Knockout:

- Lid 99°C
1. T = 95°C for 5 min
  2. T = 95°C for 30 s
  3. T = 60°C for 30 s
  4. T = 72°C for 120 s
  5. Go to 2 and repeat 40 times
  6. T = 72°C for 10 min
  7. Hold at 4°C

PCR protocol for Ceb:

### For Wildtype:

- Lid 99°C
1. T = 95°C for 4 min
  2. T = 95°C for 30 s
  3. T = 60°C for 30 s
  4. T = 72°C for 2 min
  5. Go to 2 and repeat 40 times
  6. T = 72°C for 10 min
  7. Hold at 4°C

### For Knockout:

- Lid 99°C
1. T = 95°C for 4 min
  2. T = 95°C for 30 s
  3. T = 60°C for 30 s
  4. T = 72°C for 2 min
  5. Go to 2 and repeat 40 times
  6. T = 72°C for 10 min
  7. Hold at 4°C

### Primers:

<b>Syt1:</b>
<b>WT-300 bp</b>
Syt1_WT forward: 5' - GTA TTC AGT GCG TCT CAG AGA C - 3'
Syt1_WT reverse: 5' - AAC TAT AAT TTG TCA CAG GCA TTG CCT TTC A - 3'
<b>KO-750 bp</b>
Syt1_KO forward: 5' - GAG CGC GCG CGG CGG AGT TGT TGA C - 3'
Syt1_KO reverse: 5' - AAC TAT AAT TTG TCA CAG GCA TTG CCT TTC A - 3'
<b>Syt7:</b>
<b>WT - 400 bp</b>
Syt7_WT forward: 5' - CAT CCT CCA CTG GCC ATG AAT G - 3'
Syt7_WT reverse: 5' - GCT TCA CCT TGG TCT CCA G - 3'
<b>KO - 800 bp</b>
Syt7_KO forward: 5' - CCT ACC TGA AGC CTG TGT TCA C - 3'
Syt7_KO reverse: 5' - CAG CTG TGC TCG ACG TTG TCA CTG - 3'
<b>Syb-2:</b>
<b>WT - 500 bp</b>
Syb-2_WT forward: 5' - GCC CAC GCC GCA GTA CCC GGA TG - 3'

Syb-2_WT reverse: 5' - GCG AGA AGG CCA CCC GAT GGG AG - 3'
<b>KO – 350 bp</b>
Syb-2_KO forward: 5' - CAC CCT CAT GAT GTC CAC CAC - 3'
Syb-2_KO reverse: 5' - CAG CAG ACC CAG GCC CAG CG - 3'
<b>Ceb:</b>
<b>WT – 500 bp</b>
Ceb_WT forward: 5' - CAG ACT CAC TGA ACC TAT GAG AG - 3'
Ceb_WT reverse: 5' - CTC ACC TGA TAC ATG CAG CAC - 3'
<b>KO – 350 bp</b>
Ceb_WT forward: 5' - CAG ACT CAC TGA ACC TAT GAG AG - 3'
Ceb_WT reverse: 5' - CAG CGC ATC GCC TTC TAT CGC - 3'

### 3. Agarose gel electrophoresis for detection of DNA

In this study, 2% agarose gels were used in TAE electrophoresis buffer. Quantity of agarose used was according to the number of samples to be analyzed. For 5 to 7 samples: 0.6 g of agarose was dissolved in 30 mL TAE buffer by boiling. After the agarose was cooled up to 37°C, 1.5 µL of EtBr was added, mixed carefully and poured into the gel cassette, avoiding air bubbles. The gel was allowed to solidify at room temperature. The solidified gel was placed in the electrophoresis chamber containing TAE buffer. 10 µL of DNA samples obtained after PCR were then added into the gel pockets. 5 µL of EasyLadder I (Bioline GmbH) marker was used as standard control. EasyLadder I is a ready-to-use DNA molecular weight marker, specially designed for DNA analysis in standard and high-throughput agarose gels. The ladder is pre-mixed with red loading buffer. It contains 5 even intensity bands ranging from 100 to 2000 bp for easy identification of the DNA samples analyzed. Electrophoresis was performed at 80V for 40 min. The results were visualized by UV light illumination (fig. 12). For >10 samples: 1.8 g of agarose was dissolved in 90 mL of TAE buffer and 4.5 µL of EtBr was added. Electrophoresis was performed at 115V for 40 min. Rest of the steps were same as described for 5 to 7 samples.

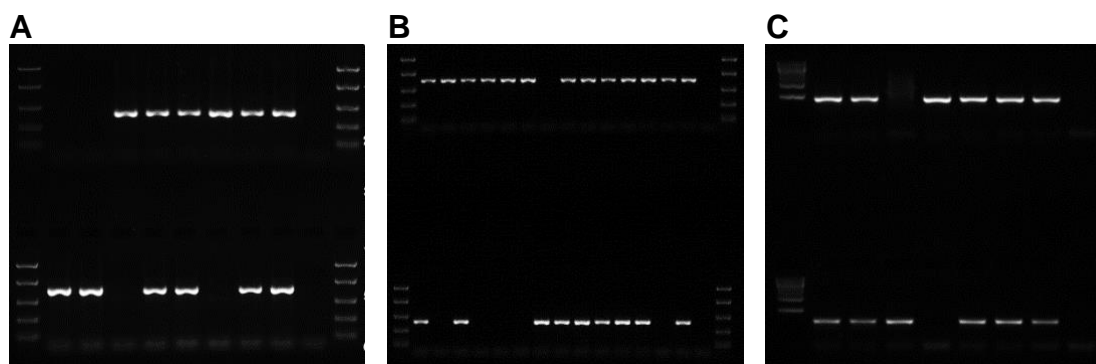


**Figure 12: Illustration of genotyping results:** (A) Exemplary DNA gel for Syt7, (B) Exemplary DNA gel for Syt1, and (C) Exemplary DNA gel for Ceb. Upper lane is always WT primers and lower lane is always knock out primers. First and last lanes are always EasyLadder I marker. If a band is observed at only upper lane then it is a WT. If a band is observed only in the lower lane then it is a KO. If bands are observed in both the lanes then it is HZ. Positive control was checked in the initial genotyping to validate the genotyping procedure and negative control was loaded every time.

## 4. Results

### 4.1 Biogenesis of LDCVs in adrenal chromaffin cells of newborn mice

#### 4.1.1 NPY-mCherry labeled vesicles are LDCVs

In order to study the biogenesis and trafficking of newly generated LDCVs in mouse chromaffin cells, I used overexpression of a specific marker protein as a primary tool. I took advantage of the fact that LDCVs not only contains catecholamines but also contains various peptides, such as Neuropeptide Y (NPY), which I used to label the newly synthesized LDCVs. It is a general thought that overexpression of a protein might lead to a false packaging of protein. So, it was critical to check whether NPY-mCherry containing vesicles were in fact true LDCVs. To check this, I used mouse chromaffin cells from adrenal glands of newborn pups (p3), transfected them with NPY-mCherry, and performed immunolabelling for CgA protein that is widely used as a marker for LDCVs in chromaffin cells.

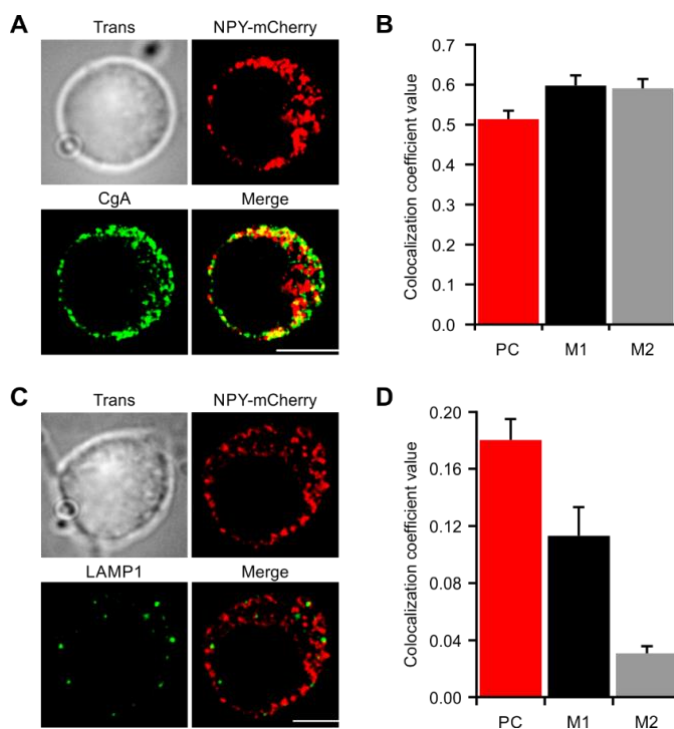


**Figure 13: NPY-mCherry containing vesicles are LDCVs.** (A) Single plane images of chromaffin cell transfected with NPY-mCherry (red) and maintained in culture for 24 h before immunolabeling with anti-CgA antibody (green). (B) Co-localization analysis between NPY-mCherry and CgA shown as Pearson's coefficient (PC), Mander's coefficient for CgA overlapping NPY-mCherry (M1), and Mander's coefficient for NPY-mCherry overlapping CgA (M2). Average co-localization coefficients  $\pm$  s.e.m. were calculated from two different experiments (n=15 cells). (C) Chromaffin cells transfected with NPY-mCherry (red) and maintained in culture for 24 h before immunolabeling with anti-LAMP1 antibody (green). (D) Co-localization analysis between NPY-mCherry and LAMP1 shown as Pearson's coefficient (PC), Mander's coefficient for LAMP1 overlapping NPY-mCherry (M1), and Mander's coefficient for NPY-mCherry overlapping LAMP1 (M2). Average co-localization coefficients  $\pm$  s.e.m. were calculated from one experiment (n=5 cells). Note the difference of scale between B and D. Images were acquired by SIM for both experiments. Scale bars: 5  $\mu$ m.

The colocalization analysis between CgA and NPY revealed a Pearson's correlation coefficient of  $0.51 \pm 0.02$  while Mander's coefficient for CgA overlapping with NPY-mCherry was  $0.6 \pm 0.03$  and for NPY-mCherry overlapping with CgA was  $0.6 \pm 0.02$ , which indicated a good colocalization between CgA and NPY (Fig. 13B). Some CgA punctae did not colocalized with NPY-mCherry because vesicles generated before NPY-mCherry transfection were not labelled red. Moreover, NPY-mCherry fluorescence did not entirely overlapped with CgA because a substantial portion of NPY-mCherry was localized in the Golgi apparatus (Fig. 13A).

As apparent from the result of NPY-mCherry and CgA colocalization study, perfect colocalization was not observed. Hence, it was necessary to confirm that the NPY-mCherry labeled vesicles were not lysosomes. I performed another immunolabelling experiment between NPY-mCherry transfected chromaffin cells and LAMP1 which is commonly used as a marker for lysosomes (Fig. 13C). Pearson's correlation coefficient was  $0.18 \pm 0.01$ . Mander's coefficient for LAMP1 overlapping to NPY-mCherry was  $0.1 \pm 0.02$  and for NPY-mCherry overlapping to LAMP1 was  $0.03 \pm 0.01$ . These values signified that there was no correlation between LAMP1 and NPY. These results clearly showed that NPY-mCherry containing vesicles were indeed LDCVs and not lysosomes.

#### 4.1.2 Chromaffin cells require a minimum of 2 h to generate new LDCVs

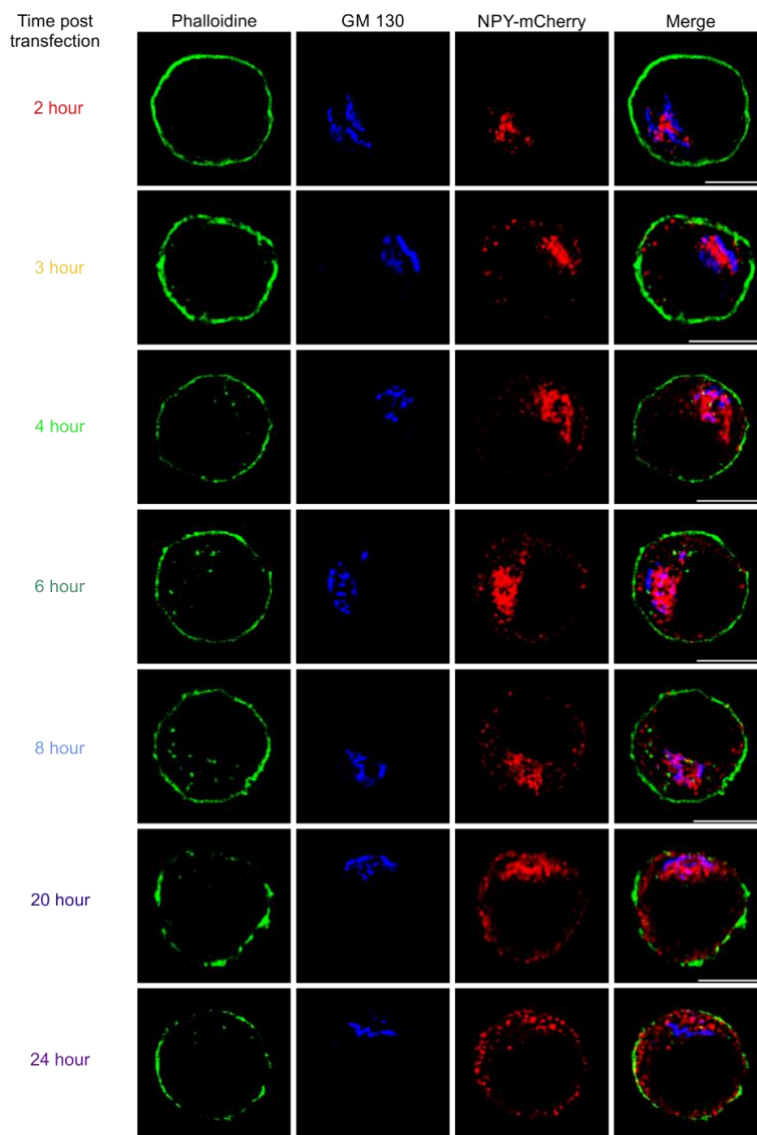


**Figure 14: First expression of NPY-mCherry is visible at 2 h post transfection.** Mouse chromaffin cells were transfected with NPY-mCherry (red) and were maintained in culture for increasing time as shown on the left side of the images. After fixation, the cortical actin network was labeled with Phalloidine Alexa-488 (green) and the cis-Golgi network was immunolabeled with the antibody against the marker GM130 (blue). Images shown are single plane SIM images of the exemplary cell for each timepoint. Scale bar is 5  $\mu$ m.

To investigate how the newly formed LDCVs were distributed, I transfected mouse chromaffin cells with NPY-mCherry to label the newly synthesized LDCVs. To follow their fate, cells were fixed at increasing time after transfection and immunocytochemistry was performed. As it is known that vesicles are synthesized in

Golgi compartments, we used cis-Golgi marker GM130 to label Golgi and used the cortical actin network marker Phalloidin Alexa- 488 to delineate the cell border.

The initial NPY-mCherry fluorescence was visible 2 h after transfection and it was primarily localized to the immediate vicinity of the cis-Golgi (fig.14, first row). The NPY-mCherry visible at 2 h only partially colocalized with GM130. Moreover, few vesicles (individual puncta) were formed by this time, which suggested that cells need the minimum time of 2 h to generate new LDCVs. One hour later, LDCVs were observed in the cytoplasm, and few already reached the cortical actin network beneath the PM (fig. 14, row 2). At later time points, the number of vesicles increased, they were distributed throughout the cytoplasm, and started to accumulate next to the PM.

#### **4.1.3 LDCVs pause at or near Golgi for about an hour before moving towards the PM**

To analyse the distribution of LDCVs over time, the distance between the vesicle and the Golgi apparatus or the PM was measured. An inhouse software was used to mark the PM, the Golgi apparatus, and vesicles manually in sequential order. Subsequently, the software measured the shortest possible distance between the centre of the vesicle to the PM/ Golgi apparatus. Fig. 9 shows schematically the method of analysis used to measure the distribution of LDCVs over time.

The distribution of newly generated LDCVs was analysed after their first visualization at 2 h up to 24 h post transfection and is displayed as distance distribution histograms (fig. 15). In the initial 2 h, most vesicles were located adjacent to the cis-Golgi compartment. Although a majority of vesicles were at/near the cis-Golgi, in some cells the Golgi was near the PM which resulted in an apparent vicinity of LDCVs to the PM. At 2 h,  $34.9 \pm 3.2$  vesicles were located at a distance of 250 nm of the cis-Golgi. Although within 250 nm of the cis-Golgi compartment, there was a reduction in the vesicle number to  $18.0 \pm 3.2$  after 3 h, their number increased again to  $23.9 \pm 7.4$  at 4 h, and it reached maximum of  $46.1 \pm 7.0$  at 8 h. Their number near the cis-Golgi stayed comparatively constant after 8 h (fig. 15H). The dual LDCV generation was possibly due to the fact that cells were stressed by cell isolation procedure and electroporation, resulting into lessened protein production at initial time points. Over the same time period, the number of vesicles localized near the PM augmented slowly over time.

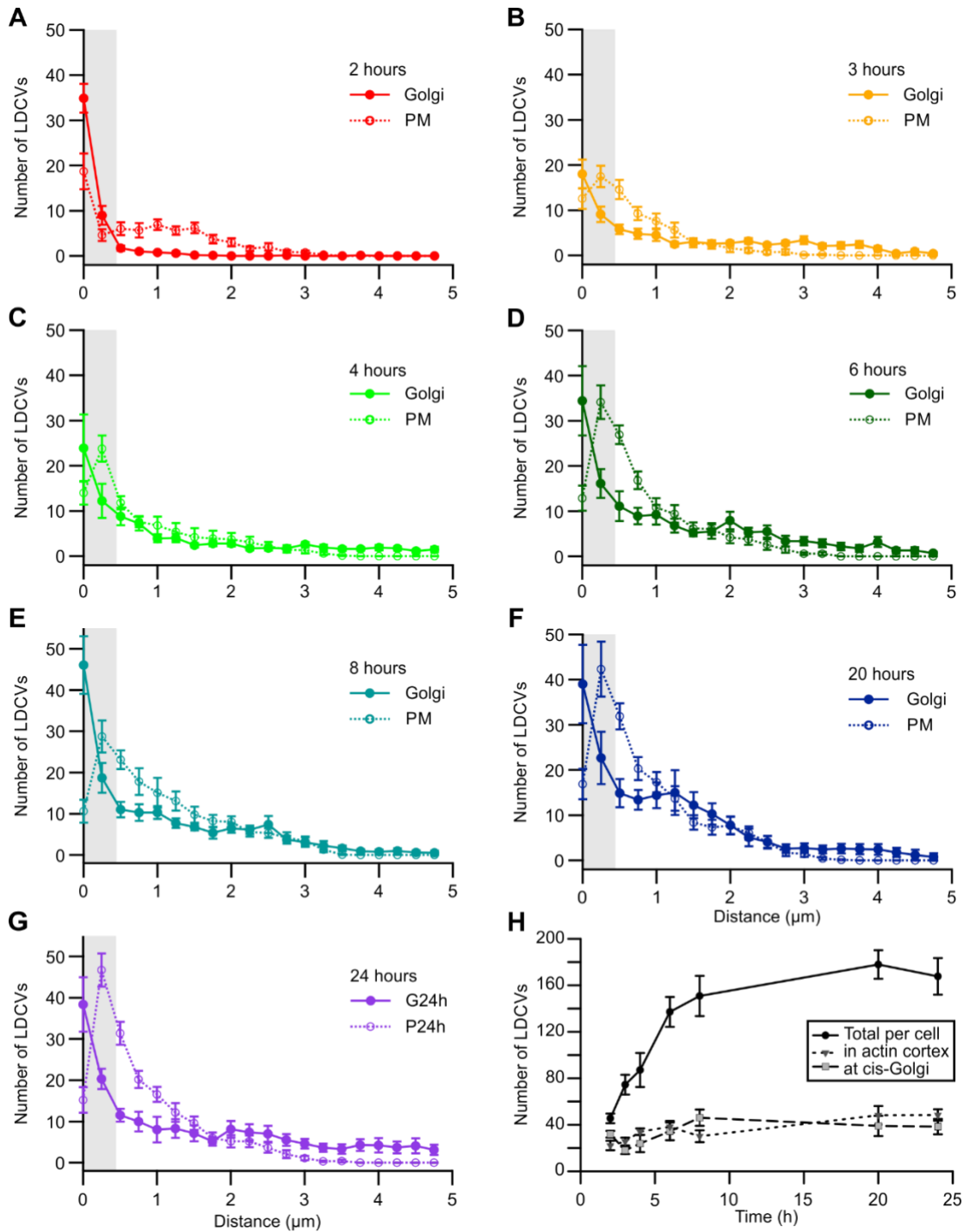


**Figure 15: LDCVs exit the Golgi only one hour after first expression of NPY-mCherry.** Localization of LDCVs in cells shown in Fig. 1 was analyzed. Their distance to the cis-Golgi (solid line with filled circle) and the PM (PM, dotted line with empty circle) is displayed as an average histogram for various time points after transfection (2h(A), 3h(B), 4h(C), 6h(D), 8h(E), 12h(F), 20h(G), and 24h(H)). Plotted are average LDCVs  $\pm$  s.e.m. (n=10 cells for each time point).

Furthermore, we counted the number of vesicles located in the cortical actin ring. The thickness of the actin ring was about 430 nm, which correspond to the full width half maximum of an intensity profile plot measured perpendicular to the Phalloidine staining on the SIM images. Fig. 15A-G shows the vesicles in the actin network adjacent to the PM in the gray highlight. The newly formed vesicles were accumulating in the cortical actin network but were not permanently staying in the actin cortex because within 6 h

of transfection these vesicles make up <30% of the red-labeled LDCVs (fig. 15H). Hence, most red-labeled LDCVs return to the cytoplasm where they are equally distributed. The number of vesicles directly at the PM were stable over time whereas vesicle number in the actin cortex increased from  $4.6 \pm 1.3$  after 2h to  $46.7 \pm 4.0$  after 24 h. This showed that most LDCVs are retained close to the PM by getting trapped in the actin cortex and not by either docking or tethering. Also, there was a strong red staining and extended structure close to the Golgi apparatus all through the experiment. It only partially colocalized with cis-Golgi marker GM130 (fig. 14). Moreover, it did not correspond to LDCVs as revealed from the CgA staining (fig. 13). This led me to look for another marker that might label this elongated structure as seen near the cis-Golgi compartment.

#### **4.1.4 The primary NPY-mCherry expression ascertains a discrete cellular compartment that does not correspond to cis/trans-Golgi**

To know whether the elongated structures labeled by NPY-mCherry belongs to any compartment of the Golgi, I performed a double immunolabelling experiment. I used the NPY-mCherry transfected chromaffin cells and labelled them with cis-Golgi marker GM130 (blue) and trans-Golgi network marker TGN38 (green) antibodies at three different time points 2 h, 3 h, and 24 h (fig. 16A). I chose these time points as the previous experiment showed that 2 h is the minimum time required for the generation of vesicles, 3 h is the time point when the newly formed vesicles already started leaving the Golgi and approaching the PM, and 24 h is the time point when sufficient amount of vesicles were produced, to form a reserve pool for exocytosis. The anti-TGN38 stained cisternal structures and vesicle like structured that were distributed all over the cytoplasm (fig. 16A). However, these vesicular structures did not overlap with NPY-mCherry arguing that these organelles were not LDCVs. There was a partial overlap between TGN38 and NPY-mCherry during its initial expression. I quantified the colocalization of GM130 and TGN38 with NPY-mCherry by using the method of Pearson's and Mander's coefficients. The analysis was done in two ways: one analysis was performed on the whole cell (fig. 6A and 6B) and the second analysis was performed on the marked area of the Golgi in order to prevent the interference of the vesicle like structures of TGN38 labelling (fig. 5B and 5C).

Pearson's and Mander's correlation coefficient values are given in table no. 1 and 2 respectively. Pearson's values showed a very low colocalization between NPY and GM130/TGN38 at all three time points. Mander's colocalization analysis also showed low values for analysis of whole cell in comparison to the analysis of only Golgi area (fig. 16C and 17).

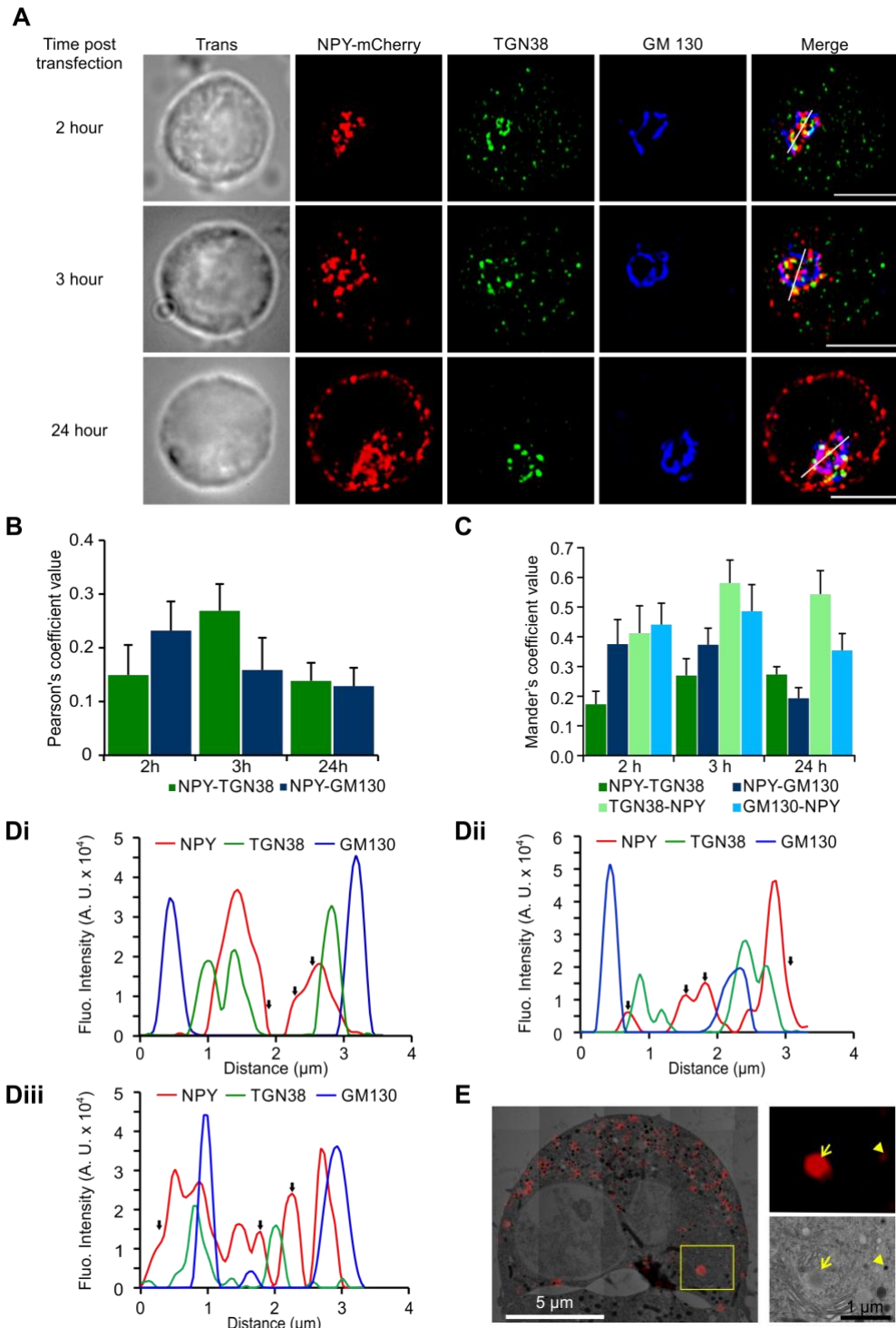


**Figure 16: NPY-mCherry expression partially overlaps with cis- and trans-Golgi network recognizing a discrete cellular compartment.** (A) Single plane SIM images of NPY-mCherry (red) transfected chromaffin cells maintained in culture for varying times indicated on the left of the images. After fixation, the cells were immunolabelled with Golgi markers; TGN38 (green) for trans-Golgi, and GM130 (blue) for cis-Golgi network. (B) Co-localization between NPY, TGN38, and GM130 was analyzed with Pearson's coefficients. (C) Mander's colocalization coefficients between NPY, TGN38, and GM130 measured on an area close to the Golgi. (D) Intensity profiles of NPY (red), TGN38 (green), and GM130 (blue) analyzed across the white line shown in the merge images in A, (i) 2 h, (ii) 3 h, and (iii) 24 h. Intensity profiles of NPY, TGN38, and GM130 signals across the white line shown in the merge images in A. Average colocalization coefficients are shown  $\pm$  s.e.m. ( $n=7$  cells for each time point). (E) Correlative light electron microscopy image of a representative NPY-mCherry (red) transfected chromaffin cell that was maintained for 2 days in culture. NPY-mCherry signal was acquired with SIM and overlaid on the electron micrograph. The Golgi area is shown enlarged on the right panels. Red fluorescent spots correspond to dense core granules (arrowhead). Arrow indicate a red fluorescent area near Golgi corresponding to a semi-dense structure in the electron micrograph. Scale bars: 5  $\mu$ m.

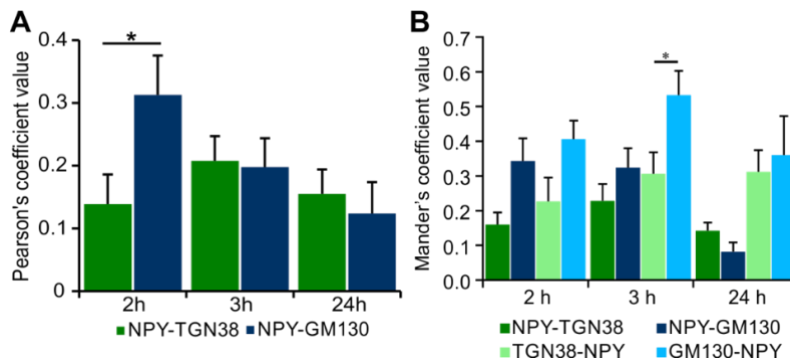


**Figure 17: Colocalization analysis between NPY, TGN38, and GM130 over the entire cell.** (A) Pearson's coefficients (B) Mander's coefficients.  $p^* = >0.05$ .

**Table 1: Pearson's correlation coefficients between NPY, GM130, and TGN38.**

Time (h)	NPY to GM130		NPY to TGN38	
	At Golgi	Whole cell	At Golgi	Whole cell
2	0.23 ± 0.05	0.31 ± 0.06	0.15 ± 0.06	0.14 ± 0.05
3	0.16 ± 0.06	0.2 ± 0.05	0.27 ± 0.05	0.21 ± 0.04
24	0.13 ± 0.03	0.12 ± 0.05	0.14 ± 0.03	0.15 ± 0.04

**Table 2: Mander's correlation coefficients between NPY, GM130, and TGN38.**

Time (h)	NPY to GM130		GM130 to NPY		NPY to TGN38		TGN38 to NPY	
	Golgi	Whole cell						
2	0.38 ± 0.08	0.34 ± 0.07	0.44 ± 0.07	0.41 ± 0.05	0.17 ± 0.04	0.16 ± 0.03	0.41 ± 0.09	0.23 ± 0.07
3	0.37 ± 0.06	0.32 ± 0.06	0.49 ± 0.09	0.53 ± 0.07	0.27 ± 0.06	0.23 ± 0.05	0.58 ± 0.08	0.31 ± 0.06
24	0.19 ± 0.04	0.08 ± 0.03	0.35 ± 0.06	0.36 ± 0.11	0.27 ± 0.03	0.14 ± 0.02	0.54 ± 0.08	0.31 ± 0.06

The overlap of cis- and trans-Golgi to NPY showed higher values than the overlap of NPY to Golgi markers. This indicated that a large portion of NPY-mCherry localized near Golgi area, was not localized to cis- and trans-Golgi, and directed us to plot the intensity profiles of NPY-mCherry (red), trans-Golgi (green), and cis-Golgi (blue) across the white line shown in the merge images of cells in fig. 16 (fig. 516Di to 16Diii). At all three time points, NPY-mCherry showed high fluorescence at the areas where cis- and trans-Golgi signals were almost zero (fig. 16Di to Diii areas marked with black arrows). To recognize the compartment that contained the NPY-mCherry fluorescence, we performed CLEM experiment in collaboration with Dr. Claudia Schirra (fig. 16E). We correlated the red NPY-mCherry fluorescent signal with the dense core LDCVs in the electron micrographs (fig. 16E inset). Both overlap well, and we also observed a large semi-dense structure close to the Golgi area that was stained red. This area could be the compartment devoid of cis- and trans-Golgi marker that harbors the vesicles before their journey towards the PM.

#### 4.1.5 Syb-2, Ceb, and Syt1 are sorted at later stage in the LDCV biogenesis

To understand the biogenesis of LDCVs it is important to know at what stage the newly generated LDCVs are associated with the vesicular membrane proteins. In theory, the cargo (proteins or peptides) should bud off the trans-Golgi network with a membrane containing all proteins necessary for the vesicle's function. Our previous experimental findings suggest that apart from staying in cis- and trans-Golgi network, the newly expressed NPY-mCherry also stays at an unknown Golgi compartment. It is possible that this compartment might serve as a station where the vesicular proteins gets sorted to the new synthesizing vesicles. If this is true then all newly formed NPY-mCherry vesicles should contain the vesicular SNARE proteins Syb-2 and Ceb, the  $Ca^{2+}$ -sensor for exocytosis Syt1, vesicular monoamine transporter to load the vesicle with catecholamines, etc.

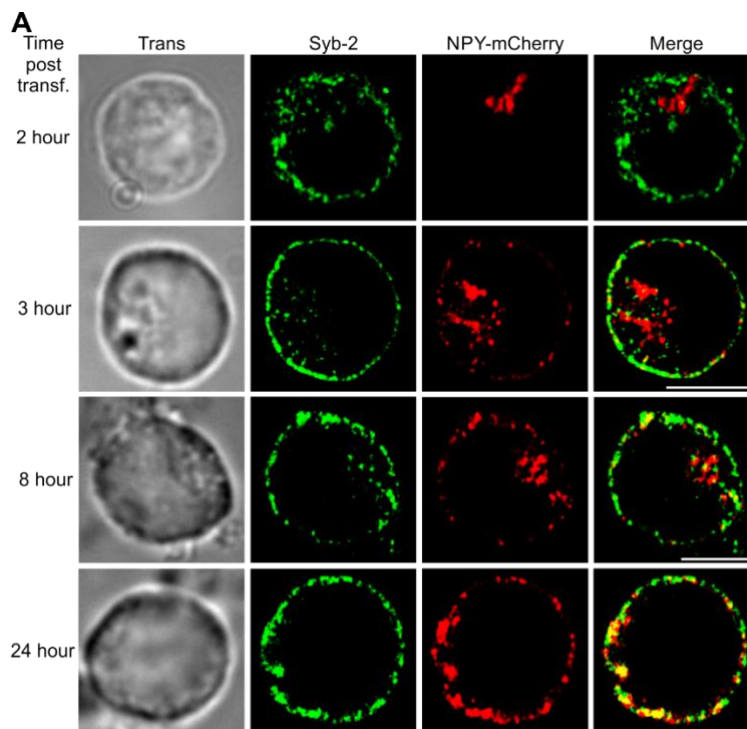
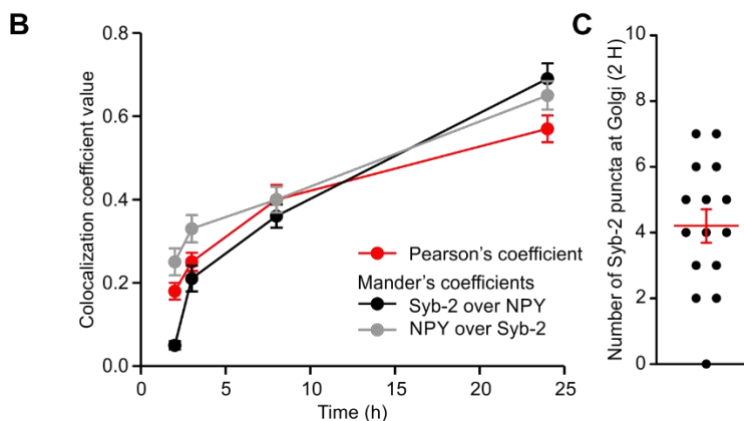


**Figure 18: Syb-2 is associated with LDCVs at later stage in biogenesis.** (A) Chromaffin cells transfected with NPY-mCherry (red) and maintained in culture for varying times as indicated on the left of the images. After fixation, cells were immuno labelled with anti-Syb-2 antibody (Syb-2, green). Representative images were acquired by SIM. (B) Colocalization between NPY-mCherry and Syb-2 over time. Pearson's coefficient and Mander's coefficients were analyzed for each time point from two different experiments. (C) Average number of Syb-2 punctae that colocalized with NPY-mCherry at 2 h quantified over the entire stack. N = 15 cells for each time point. Plotted are average colocalization coefficients  $\pm$  s.e.m. Scale bars: 5  $\mu$ m.



However, it is also possible that the vesicular membrane proteins are associated with an LDCV precursor containing the protaneous cargo at a later stage by intracellular

fusion of two vesicles. To verify this hypothesis, we performed time point experiments. We fixed the chromaffin cells transfected with NPY-mCherry (red) at different time points after transfection as described in the left panel in the figure 18A, 19A, and 21A; then immunolabeled them with anti-Syb-2 (fig. 18, green), anti-Ceb (fig. 19, green), or anti-Syt1 (fig. 21, green) antibodies. As can be seen from the images, all three proteins are localized to discrete spots in the cytoplasm although a large proportion of them can be seen in direct vicinity of the PM (figure 18A, 19A, and 21A). At 2 h, very few spots of Syb-2, Ceb, and Syt1 can be seen overlapping with the NPY-mCherry expression. The colocalization analysis performed by analyzing Pearson's (tab. 3) and Mander's coefficients (tab. 4) for all the three vesicular proteins with NPY-mCherry indicated a negligible colocalization between NPY and the three vesicular proteins at the initial hour of NPY-mCherry expression. If the vesicular proteins are boarded on the newly generated vesicles directly from the Golgi then the colocalization value should be high.

**Table 3: Pearson's correlation coefficients between NPY and vesicular proteins.**

Time (h)	NPY to Syb-2	NPY to Ceb	NPY to Syt1
2	0.18 ± 0.02	0.15 ± 0.01	0.07 ± 0.01
3	0.25 ± 0.02	0.18 ± 0.01	0.1 ± 0.02
8	0.4 ± 0.04	0.24 ± 0.01	0.24 ± 0.02
24	0.57 ± 0.03	0.33 ± 0.01	0.51 ± 0.03

**Table 4: Mander's correlation coefficients between NPY and vesicular proteins.**

Time (h)	NPY to Syb-2	Syb-2 to NPY	NPY to Ceb	Ceb to NPY	NPY to Syt1	Syt1 to NPY
2	0.25 ± 0.03	0.05 ± 0.01	0.21 ± 0.02	0.08 ± 0.01	0.09 ± 0.02	0.05 ± 0.01
3	0.33 ± 0.03	0.21 ± 0.03	0.16 ± 0.02	0.18 ± 0.01	0.09 ± 0.02	0.14 ± 0.02
8	0.41 ± 0.03	0.36 ± 0.03	0.25 ± 0.02	0.29 ± 0.01	0.16 ± 0.02	0.33 ± 0.03
24	0.65 ± 0.03	0.69 ± 0.04	0.30 ± 0.02	0.43 ± 0.01	0.52 ± 0.03	0.64 ± 0.01

In order to get more information, we counted the number of puncta over the Z-stack of all the three vesicular proteins that were overlapping with the NPY at 2 h. The values are shown in the figure 7C (average number of puncta =  $4.2 \pm 0.5$ ), 8C (average number of puncta =  $5.1 \pm 0.6$ ), and 10C (average number of puncta =  $3.9 \pm 0.6$ ) for Syb-2, Ceb, and Syt1 respectively. Since the average number of NPY-mCherry labeled vesicles is  $45.5 \pm 4.1$  (fig. 15H) these values clearly suggest that the vesicular proteins are not loaded on the newly synthesized vesicles as they exit the Golgi. Further at 3 h, more individual spots of vesicular proteins overlapped with NPY-mCherry. The colocalization analysis revealed values higher than at 2 h (fig. 18B, 19B, and 21B). After 8 h a further increase in the colocalization can be seen on the merged images in which more yellow spots are visible for all the three vesicular proteins. Colocalization analysis showed higher values in comparison to 3 h.

Colocalization of Syb-2 and Syt1 with NPY-mCherry was higher than that of Ceb as can be seen from the values depicted in table 3 and 4. I also performed double immunolabeling with anti-Syb-2 (fig. 20A, green) and anti-Ceb (fig. 20A, blue) in NPY-mCherry (red) overexpressing chromaffin cells maintained in culture for 24 h to know whether LDCVs lacking Syb-2 contained Ceb and if all NPY-mCherry labelled vesicles were positive for v-SNAREs. The colocalization between both v-SNAREs was  $0.58 \pm 0.03$  (fig. 20B, Pearson's coefficients). The colocalization coefficients of NPY-mCherry with both v-SNAREs was measured by combining the blue and green channels and comparing this merged image with the red channel of NPY-mCherry. Mander's coefficients of NPY-mCherry localized to both v-SNAREs was  $0.68 \pm 0.03$  (fig. 20C) which is similar to Mander's coefficient for NPY-mCherry localized to Syb-2 alone. This indicated that some red labelled vesicles were lacking the v-SNAREs.

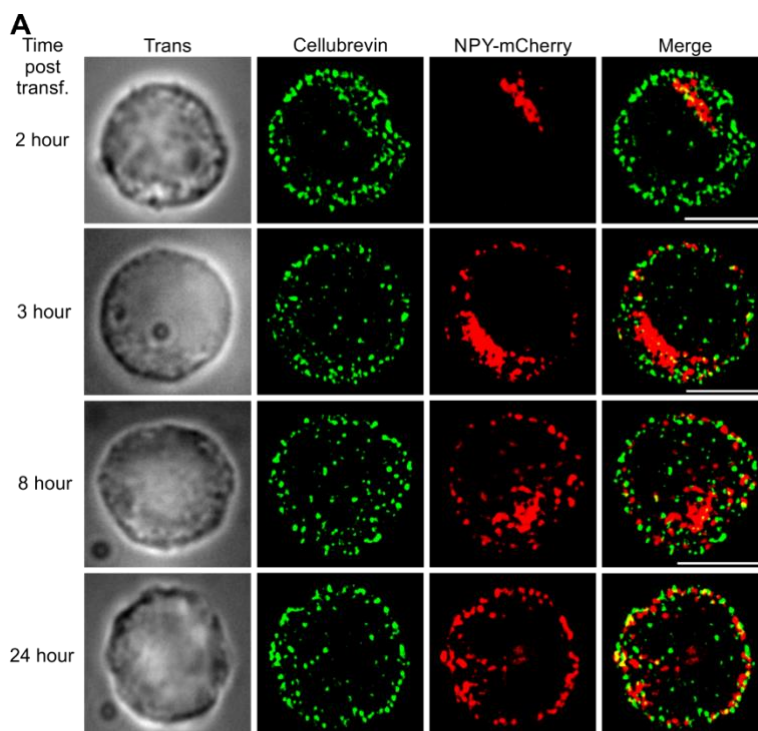
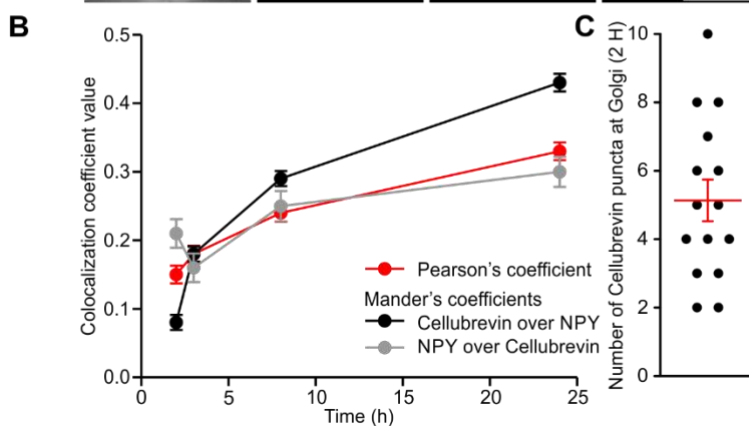


**Figure 19: Ceb is localized to a relatively small population of LDCVs.** (A) Single plane SIM images of chromaffin cells transfected with NPY-mCherry (red) and maintained in culture for varying times as described on the left-hand side of the images. After fixation, cells were labelled with anti-Ceb antibody (green). (B) Colocalization between NPY-mCherry and Ceb over time. Pearson's coefficient and Mander's coefficients were analyzed for each time point from two different experiments. (C) Average number of Ceb punctae that colocalized with NPY-mCherry at 2 h quantified over the entire stack. N = 15 cells for each time point. Plotted are average colocalization coefficients  $\pm$  s.e.m. Scale bars: 5  $\mu$ m.



Highest colocalization between NPY-mCherry and the vesicular proteins was observed at 24 h after transfection. Sequential increase of colocalization indicated that the vesicular proteins are getting associated with the NPY-mCherry positive vesicles at a late stage in the trafficking pathway and not directly from the Golgi.

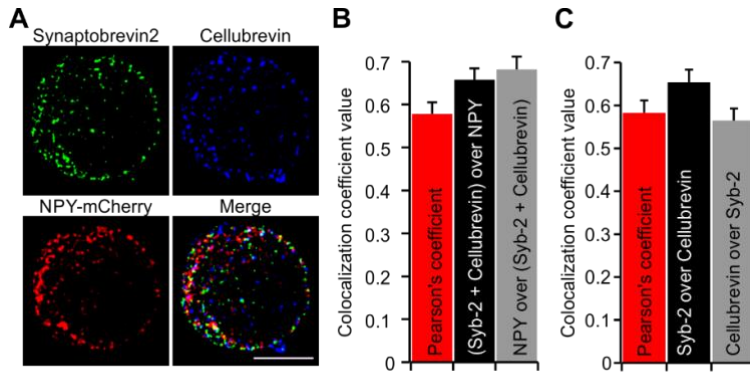


**Figure 20: Co-immunolabelling of Syb-2 and Ceb.** (A) Single plane SIM images of chromaffin cells transfected with NPY-mCherry (red) and maintained in culture for 24 h. After fixation, cells were labelled with anti-Syb-2 (green) and anti-Ceb antibodies (blue). (B) Colocalization between NPY-mCherry and combined v-SNAREs. Pearson's coefficient and Mander's coefficients from two different experiments. (C) Colocalization between v-SNAREs. N = 15 cells. Plotted are average colocalization coefficients  $\pm$  s.e.m. Scale bars: 5  $\mu$ m.

According to our findings, carrier vesicle or transport vesicle serves as a precursor vesicle or a recycling vesicle and carry the vesicular membrane proteins to fuse with NPY-mCherry containing vesicle when the NPY-mCherry containing vesicle approaches the PM.

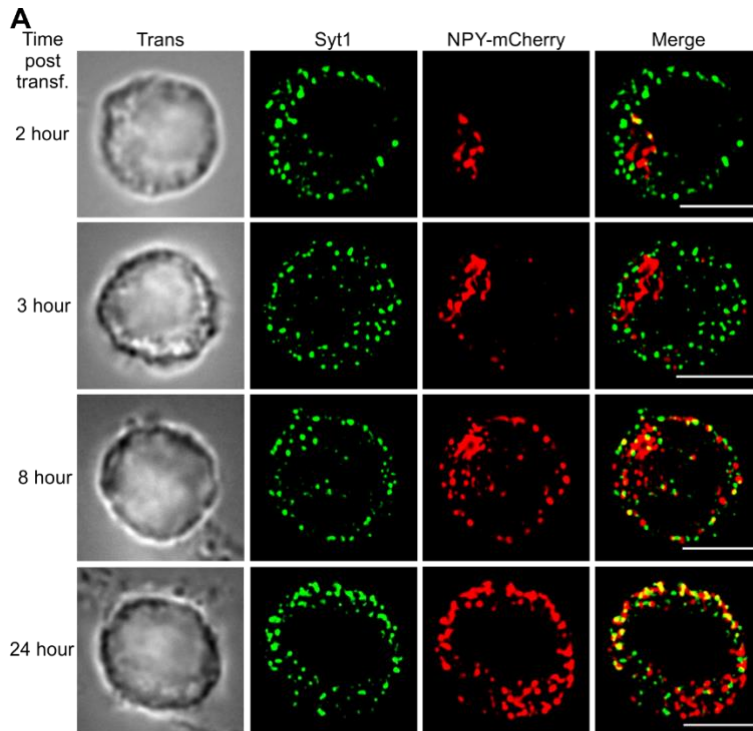


**Figure 21: Like v-SNAREs, Syt1 is sorted to LDCVs at a late stage of their biogenesis.** (A) NPY-mCherry (red) transfected chromaffin cells were maintained in culture for varying times as shown on the left of the images. After fixation, cells were immunolabelled with anti-Syt1 antibody (Syt1, green). Representative single plane images were acquired by SIM. (B) Colocalization between NPY-mCherry and Syt1 over time. Pearson's coefficient and Mander's coefficients were analyzed for each time point from two different experiments. (C) Average number of Syt1 punctae that colocalized with NPY-mCherry at 2 h quantified over the entire stack. N = 15 cells for each time point. Plotted are average colocalization coefficients  $\pm$  s.e.m. Scale bars: 5  $\mu$ m.

#### **4.1.6 Recycled Syt1 associated with NPY-mCherry labeled vesicles within 2 h after endocytosis and only a small subset of endocytosed Syt1 is transported via Rab11A vesicles**

We showed that vesicular proteins get associated to NPY-mCherry stained vesicles at later stage in the biogenesis of LDCV. There are two possibilities; one it is possible that it happens via recycling directly close to the PM and second it is possible that the vesicular protein is taken back to the Golgi and is boarded on to the precursor vesicles to associate with the newly formed LDCVs. Hence, we decided to study the endocytosis of a vesicular membrane protein. We chose Syt1 as a candidate because it is a well-known marker for vesicles and a luminal domain antibody is available for Syt1 which favors endocytosis study. Cells were depolarized with 60 mM KCl to induce exocytosis. We incubated the cells that were going through exocytosis with a luminal domain antibody of Syt1. Control group cells were subjected to stimulation with normal extracellular solution in the presence of the antibody. This was followed by the recovery phase for increasing time (shown in left of the images fig. 22A) at 37°C with 13% CO<sub>2</sub> before fixing and permeabilizing them. They were then processed for secondary antibody application.

Fixation after 0 min showed the antibody staining at the surface of the cell (fig. 22A). As the cells recovered, retrieval of the Syt1 was visible from 30 min to 6h. Number of endocytosed punctae increased with time. Colocalization of endocytosed Syt1 with NPY-mCherry was visible at 2 h and remained visible at 3 h and 6 h. At 6 h the number of Syt1 punctae associating with NPY-mCherry increased. We also analyzed the number of Syt1 punctae at the membrane over time (fig. 22B). Highest number of punctae were visible in stimulated cells that were fixed after 5 min recovery. Progression of time resulted in decreasing number of punctae from the PM due to endocytosis. Nevertheless, some Syt1 punctae were always visible at the cell periphery.

Further, we wanted to know which transport vesicles play a role in this trafficking. Different markers are known for different endosomal compartments like Rab5 for early endosomes, Rab7 for late endosomes, and Rab11 for recycling endosomes. We wanted to know through which endosomal compartment endocytosed Syt1 is recycled, so we decided to use Rab11 as a likely candidate. We stimulated the chromaffin cells with 60 mM KCl in presence of anti-Syt1 antibody and allowed the cells to recover for 2h and 3h at 37°C with 13% CO<sub>2</sub> (fig. 23). Recovery was followed by fixation of the cells at respective time points and co-immunolabeling was performed for either trans-Golgi network protein TGN38, Rab11A, or resting Syt1 pool (fig. 23A, 23B, and 23C). The resting Syt1 pool was labeled with the same luminal domain antibody after treatment with the affinity Fab fragments to differentiate it from the endocytosed Syt1 (see materials and methods). We observed that endocytosed Syt1 was found in TGN38 positive compartment at 2 h and 3 h (fig. 23A). This shows that some endocytosed Syt1 is indeed recycled to trans-Golgi network. On the contrary, only few

Rab11A vesicles were positive for endocytosed Syt1 (fig. 23E). This indicated that the recycling of Syt1 is probably independent of Rab11A. Further, we counted the number of punctae containing endocytosed Syt1 that were overlapping with any of the markers. We found that some of the endocytosed Syt1 is transported to NPY-mCherry positive vesicles, resting Syt1 carrying vesicles, and was also found on the vesicles containing NPY-mCherry and resting Syt1 both (fig. 23D).

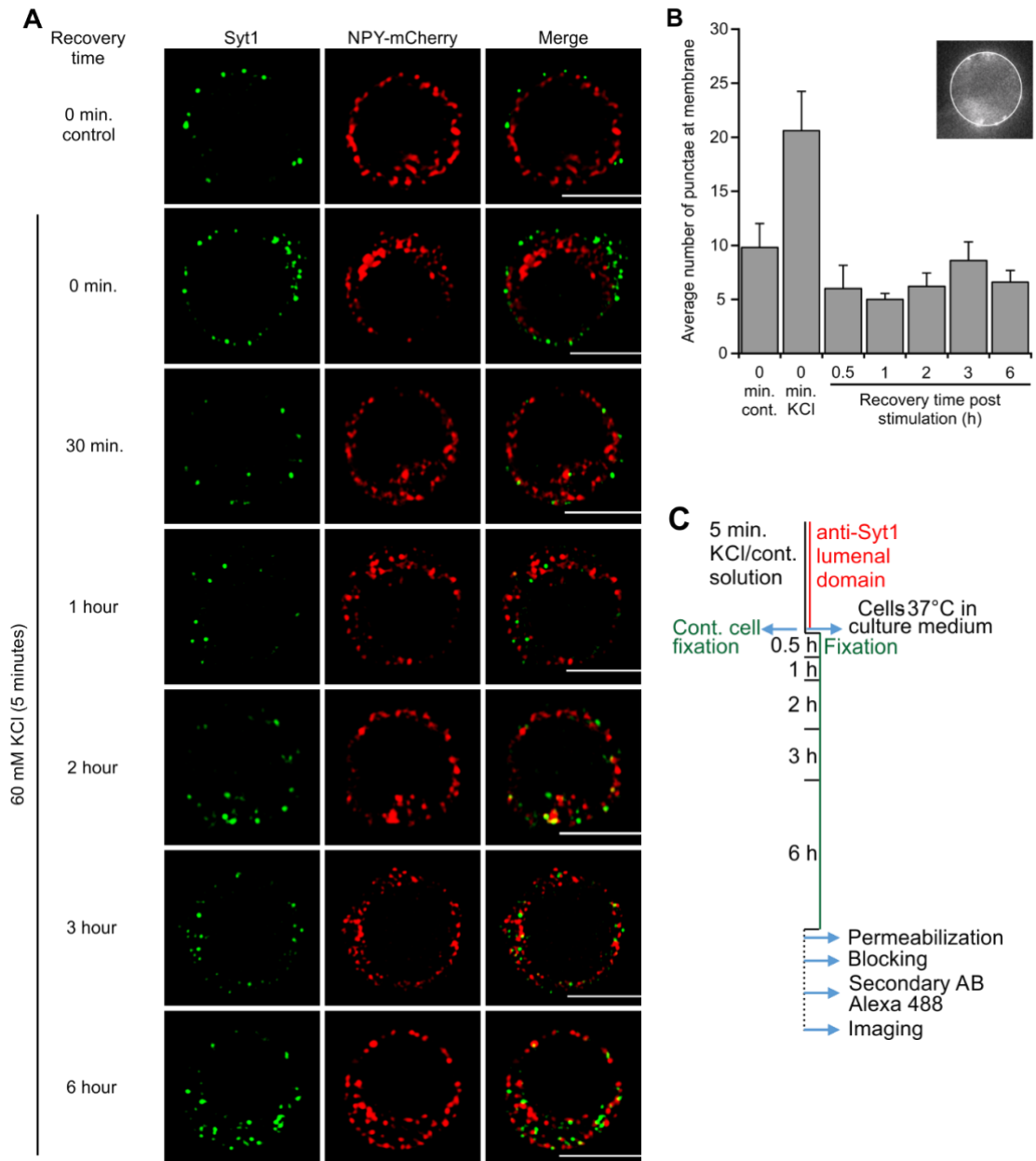


**Figure 22: Endocytosis of Syt1.** (A) Endocytosis of Syt1 (Syt1, green) was studied in NPY-mCherry (red) overexpressing chromaffin cells. Cells were stimulated with 60 mM KCl or normal extracellular solution (control) for 5 minutes in presence of the anti-Syt1 luminal domain antibody. Cells were then maintained at rest in order to recover for various times as indicated on the left of the images. Represented are single plane images acquired by SIM. (B) Analysis of the number of Syt1 punctae localized at the cell periphery at varying recovery time post stimulation. Counted were Syt1 punctae touching the border of the region of interest delimiting the PM. (C) Schematic representation of the protocol used for labelling of recycling Syt1. Cells were incubated in 60 mM KCl/control solution for 5 minutes together with anti-Syt1 luminal domain antibody. Control cells were fixed after 5 minutes and the remaining cells were allowed to recover at 37°C with 13% CO<sub>2</sub> for various times before fixation. N = 5 cells for each time point. Plotted are average colocalization coefficients ± s.e.m. Scale bars: 5 µm.

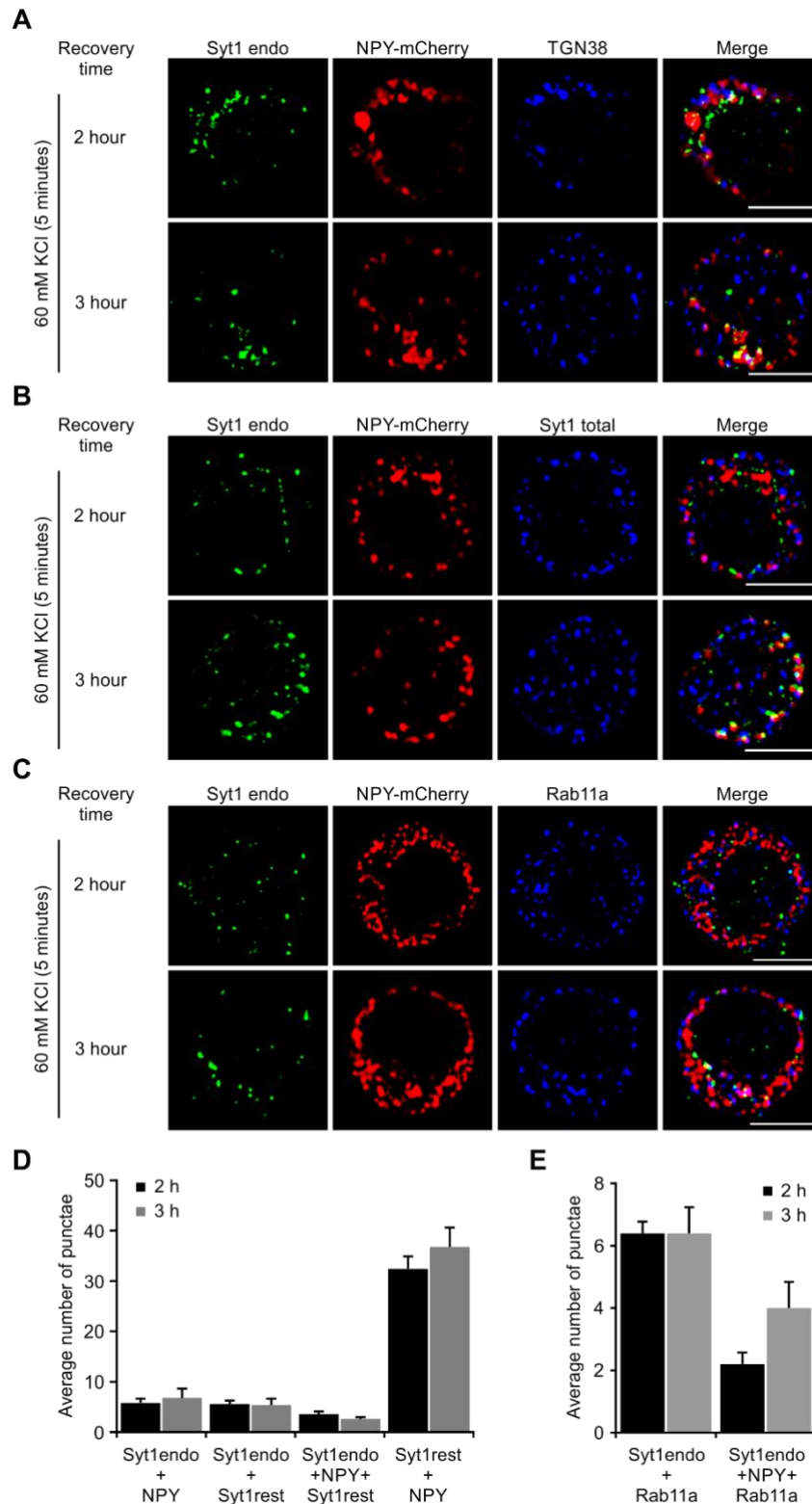


**Figure 23: Recycled Syt1 is found on LDCVs and merges with reserve pool of Syt1.** Endocytosis of Syt1 (green) observed in NPY-mCherry (red) overexpressing chromaffin cells that were stimulated with 60 mM KCl for 5 minutes in presence of anti-Syt1 luminal domain antibody, co-immunolabeled with anti-TGN38 antibody (A), anti-Syt1 (B), and anti-Rab11A (C). Cells were maintained at rest to recover for 2 h and 3 h. Displayed are single plane images acquired by SIM. (D) Analysis of the number of endocytosed Syt1 (Syt1 endo) punctae that were also stained by NPY-mCherry only, or that contained only reserve pool of Syt1 (Syt1 rest), or both. (E) Analysis of the number of endocytosed Syt1 punctae that overlapped with vesicles containing only Rab11A, and vesicles containing Rab11A and NPY-mCherry both. N = 5 cells for each time point. Displayed are average  $\pm$  s. e. m. Scale bars: 5  $\mu$ m.

## 4.2 Molecular mechanisms of “dead-end docking” in mouse chromaffin cells

### 4.2.1 Dead-end vesicles exist in mouse chromaffin cells

Our group successfully identified a new pool of vesicles called “dead-end” vesicles by using TIRFM and patch clamp method simultaneously in bovine chromaffin cells. We defined dead-end vesicles as those vesicles that stay close to the PM and that do not fuse even after long stimulation (5 min) with high  $\text{Ca}^{2+}$ . We found that 15% of LDCVs at the cell’s footprint, were dead-end vesicles in bovine chromaffin cells. Furthermore, we could show that in bovine chromaffin cells the 2:1 unproductive t-SNARE acceptor complex exists and that it is functional *in vivo* to induce dead-end anchoring (Hugo et al., 2013; Kreutzberger et al., 2016). To fully understand the molecular mechanism of dead-end anchoring we wanted to find out which vesicular protein interacts with this 2:1 unproductive t-SNARE acceptor complex inducing dead-end anchoring. For this purpose, we decided to study the effect of deleting specific proteins located on LDCVs membrane. Since gene knock out is done in mouse, it was necessary to confirm the existence of dead-end vesicles in mouse chromaffin cells. For this purpose, I used wild type mouse chromaffin cells prepared from newborn pups (p3), and I standardized the electroporation of NPY-mCherry in mouse chromaffin cells to label the LDCVs. Then I carried out the experiments, in which cells were perfused with a solution containing  $6 \mu\text{M}$  intracellular free  $\text{Ca}^{2+}$  for 5 min to induce steady secretion.

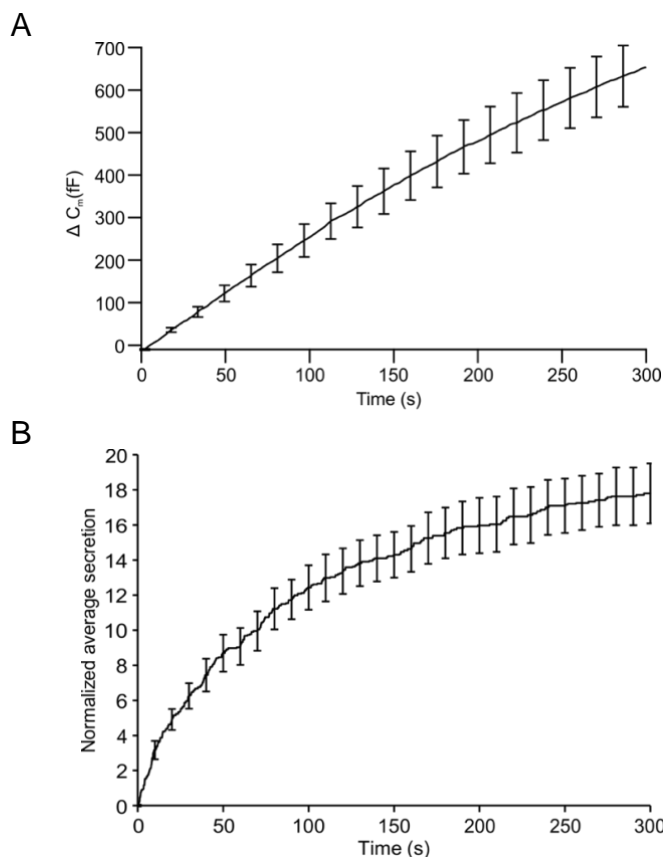


**Figure 24: Exocytosis of LDCVs induced by long-lasting and strong stimulus.** Cells were patched with intracellular solution containing  $6 \mu\text{M}$   $\text{Ca}^{2+}$ . Displayed is the average capacitance increase (A) and the cumulative number of LDCVs exocytosed as monitored by TIRFM normalized to the footprint area of the cell (B).  $N_{\text{cells}} = 15$ .

Simultaneously, I measured the membrane capacitance by patch-clamp technique and monitored individual vesicle fusion by TIRFM (Becherer et al., 2007). The high  $[Ca^{2+}]_i$  stimulation produced a nearly linear increase in the membrane capacitance up to  $654.2 \pm 1.3$  fF and at the same time  $17.8 \pm 1.7$  LDCVs were secreted at the foot of the cells visualized with TIRFM (fig. 24). There was a difference in the time course of secretion between membrane capacitance increase and the number of vesicles secreted in TIRF. However, our group showed previously (Becherer et al., 2007; Hugo et al., 2013) that in bovine chromaffin cells the time course of secretion was identical between membrane capacitance increase and the number of vesicles secreted in TIRF. One possible explanation for this discrepancy is that NPY-mCherry label a subset of young LDCVs that would be secreted first and unlabeled old LDCVs are secreted afterwards. To address this possibility, I used FFN511 that labels all the vesicles in NPY-mCherry transfected cells and analyzed secretion as mentioned earlier. Results showed that there was no difference between the number of FFN511 labeled vesicles or NPY-mCherry labeled vesicles (see annexure fig. 48A). I also tested the effect of collagen coating on the cell's footprint by transfecting NPY-mCherry electroporated cells with semliki forest virus Lifeact-GFP to quantify the amount of actin near the PM using TIRFM. Purpose of this experiment was to know if the collagen coating was creating more stress fibers at the PM which in turn was affecting the number of secreting vesicles in TIRFM. Result showed that there was no change in the amount of actin at the PM in coated or uncoated coverslips (see annexure fig. 48B). I also used NPY-venus transfected chromaffin cells for similar experiment in order to know if there were more kiss-and-run events instead of full fusion which can lead to an underestimate of the number of vesicles secreted in TIRFM (Becherer et al., 2007). However, it was not the case because there were only few kiss-and-run events (data not shown).

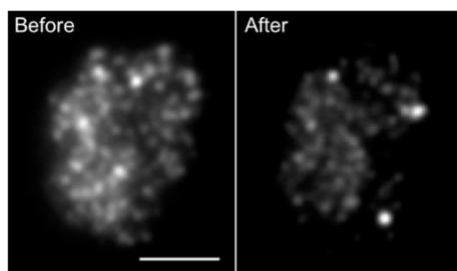


**Figure 25: TIRFM images of WT mouse chromaffin cells.** Images show the footprint of exemplary cells in TIRFM taken immediately before reaching whole-cell configuration (left) and after 5 min of perfusion with intracellular solution containing  $6 \mu\text{M } Ca^{2+}$ . Scale bar is  $5 \mu\text{m}$ .

As revealed from TIRF imaging, some vesicles remained at the foot-print of the cell until the end of the recording (fig. 25). These vesicles were mainly of two types: first, “newcomers”, which correspond to vesicles that approached the PM during the recording, and second, “dead-end vesicles” that were present at the footprint from the beginning of the recording, stayed at the PM throughout. If those LDCVs, which stayed at the PM for very long time, belong to a separate pool of vesicles, then they will appear as a separate component in a survival plot. I analyzed how long the LDCVs, which were visible in the first image of the experiment, stayed at the PM before leaving either by exocytosis or through undocking. Then I plotted their number as a function of time (fig. 26). Fitting this curve revealed that the data was best described with a double

exponential decay; suggesting that two kinetic components were present. The time constant of first component was  $42.1 \pm 0.3$  s. The second component was  $\approx 10$  times slower, with a time constant of  $477 \pm 3$  s, demonstrating the existence of an apparently unreleasable pool of vesicles. According to the second time constant, the total recording time of the experiment should be around 7.95 min to totally deplete this pool of vesicles. However, curve fitting showed that the number of unreleasable vesicles remaining relatively unchanged from 4.5 to 5 min (fig. 25). Hence, I recorded the cells for 5 min.

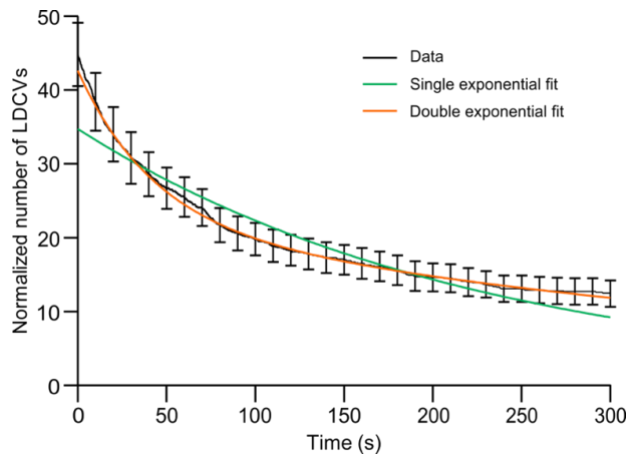


**Figure 26: Survival plot of LDCVs at the cell's footprint.** Graph represents the survival plot of all LDCVs visible in the first image of the cells perfused with a solution containing  $6 \mu\text{M Ca}^{2+}$  (black line). The data was best fit by double exponential decay (orange line) as compared to a mono exponential decay (green line).  $N_{\text{cells}} = 15$ .

There was a lot of movement of vesicles at the cell's footprint revealing the dynamic behavior of vesicles that continuously commute to the PM for fusion. I analyzed different parameters from the TIRFM movies, namely the number of vesicles at PM before stimulation, the total number of secreted vesicles, the number of vesicles moving away from the PM during the acquisition of the movie, and the number of vesicles left at the PM after stimulation. Then I backtracked LDCVs from the last image of the movie to the first image and divided them in two categories, "dead-end vesicles" and "newcomer vesicles". All the values for the number of vesicles in different categories, were normalized to the average size of the footprint (fig. 27) and values are given in table 5. For normalization procedure see materials and methods section.

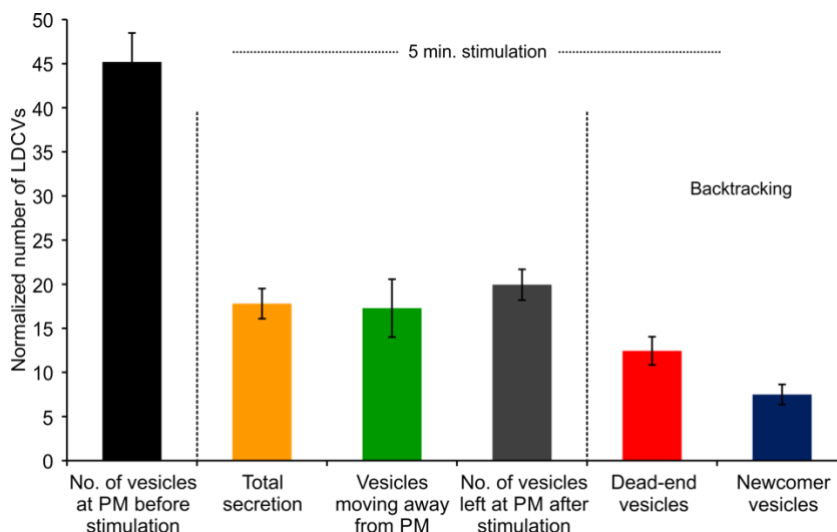


**Figure 27: Analysis of different LDCV parameters in TIRFM.** Represented are the average density of LDCVs near the PM at the beginning and the end of the experiment and the average total secretion. LDCVs visible at the end of the experiment were separated between newcomer and dead-end vesicles.  $N_{\text{cells}} = 15$ .

**Table 5: Number of vesicles at the footprint of the cell in WT cells.**

	Vesicles before stimulation	Total secretion	Vesicles moving away from PM	Vesicles left after stimulation	Dead-end vesicles	Newcomer vesicles
WT	45.2 ± 3.3	17.8 ± 1.7	17.3 ± 3.3	19.9 ± 1.7	12.4 ± 1.6	7.5 ± 1.1

Out of the  $45 \pm 3$  LDCVs present at the beginning,  $12 \pm 1$  were dead-end vesicles. This indicated that 27.52% of vesicles visible at the cell's footprint before stimulation, were dead-end vesicles (fig. 27). After confirming the existence of dead-end vesicles in mouse chromaffin cells, next step was to identify the vesicular protein that interacts with the 2:1 unproductive SNARE acceptor complex to generate dead-end vesicles.

#### 4.2.2 v-SNAREs are not involved in dead-end docking

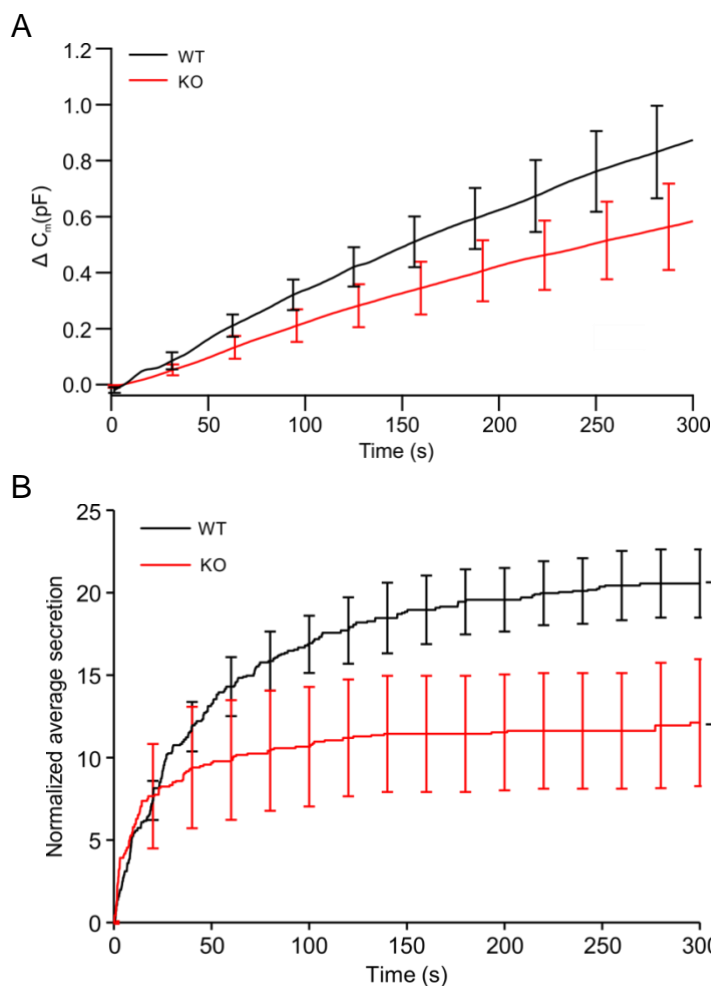


**Figure 28: Exocytosis of LDCVs in WT and Syb-2 KO cells.** Cells were patched with intracellular solution containing  $6 \mu\text{M Ca}^{2+}$ . Displayed is the average capacitance increase for (A) and the cumulative number of LDCVs secreted as monitored by TIRFM normalized to the footprint area (B) for WT and Syb-2 KO cells.  $N_{\text{cells}} = 10$  (WT and Syb-2 KO cells).  $p$  value \*  $<0.05$ .

It is known that vesicular protein Syb-2 interacts with the t-SNARE complex to mediate fusion of vesicles. It has also been shown that Syb-2 and Ceb are functionally redundant in mouse chromaffin cells (Borisovska et al., 2005). Also, Syb-2 and Ceb are localized to LDCVs (fig. 20). So, it is possible that these proteins might be involved in dead-end docking as well. I started by studying the role of Syb-2 in this process using the same technique described above comparing Syb-2 KO cells with WT cells from littermate controls. Stimulation with intracellular solution containing  $6 \mu\text{M Ca}^{2+}$  resulted

in a linear capacitance increase upto  $873.4 \pm 1.9$  fF in WT and  $534.5 \pm 2.1$  fF in Syb-2 KO cells. This reduction in global secretion was not significant.

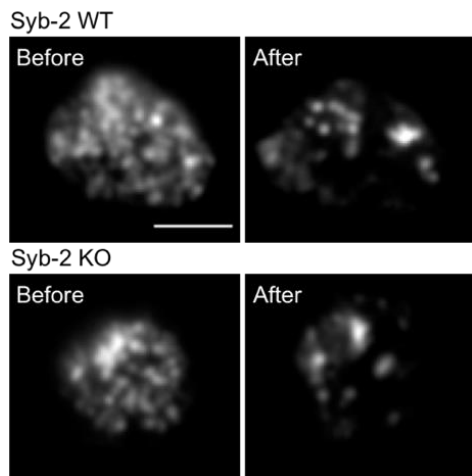


**Figure 29: TIRFM images of WT and Syb-2 KO mouse chromaffin cells.** Images show the footprint of exemplary cells in TIRFM taken immediately before reaching whole-cell configuration (left) and after 5 min of perfusion with solution containing  $6 \mu\text{M Ca}^{2+}$ . Scale bar is  $5 \mu\text{m}$ .

In contrast, the simultaneous measurement of LDCV exocytosis via TIRFM was significantly decreased by a factor of nearly 2 between WT and Syb-2 KO cells (fig. 28). As can be seen from fig. 29, some vesicles remained at the PM at the end of stimulation in WT and KO cells. This indicated that dead-end vesicles might be present in KO cells.

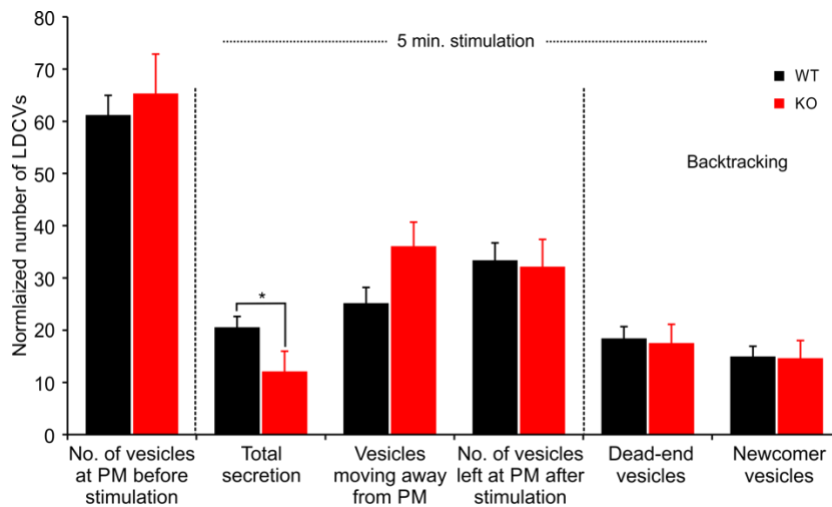


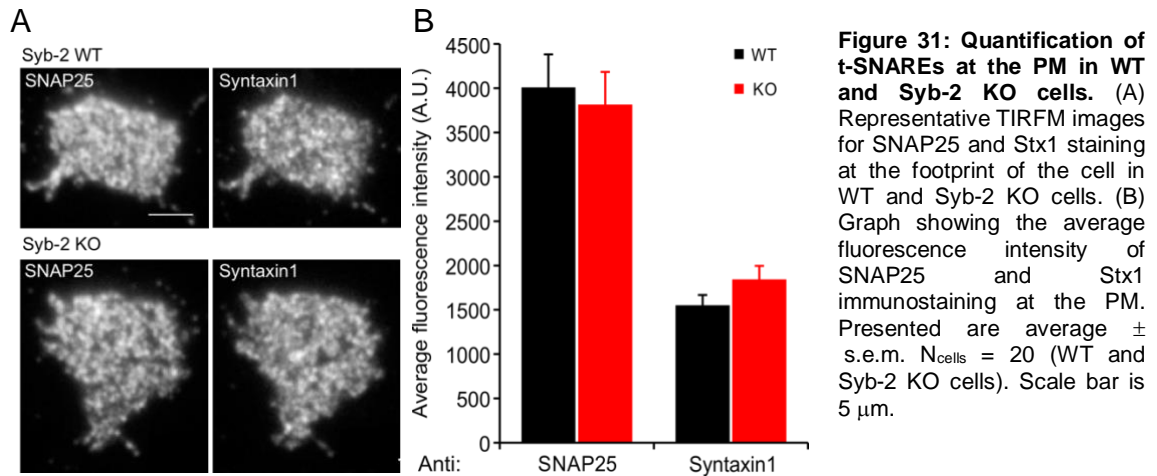
**Figure 30: Analysis of different parameters in TIRFM.** Represented are the average density of LDCVs near the PM at the beginning and the end of experiments and the average total secretion in WT and Syb-2 KO cells. LDCVs visible at the end of the experiment were separated between newcomer and dead-end vesicles.  $N_{\text{cells}} = 10$  (WT and Syb-2 KO cells).  $p$  value \*  $<0.05$ .

**Table 6: Number of vesicles at the footprint of the cell in WT and Syb-2 KO cells.**

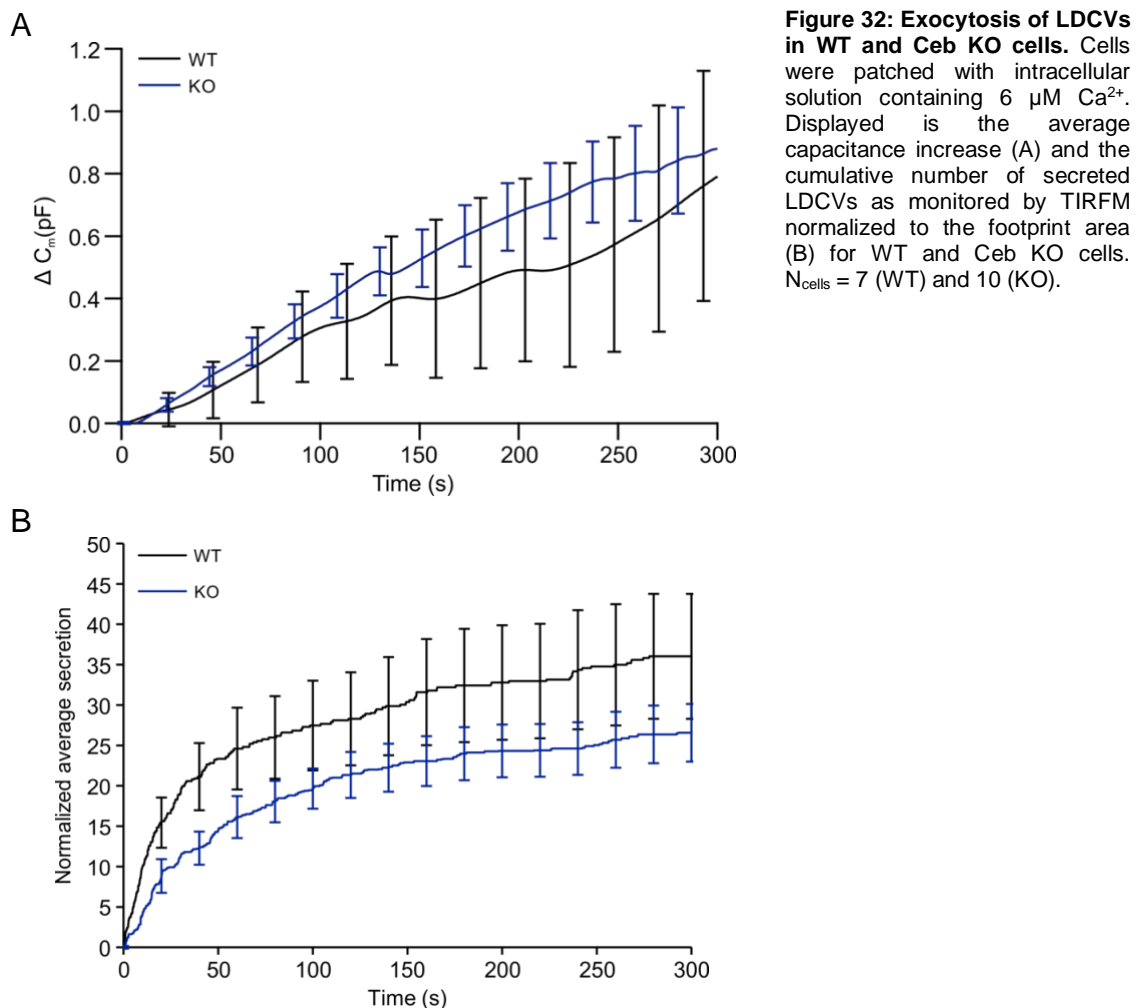
Syb-2	Vesicles before stimulation	Total secretion	Vesicles moving away from PM	Vesicles left after stimulation	Dead-end vesicles	Newcomer vesicles
WT	$61.2 \pm 3.7$	$21.0 \pm 2.1$	$25.2 \pm 3.0$	$33.4 \pm 3.3$	$18.4 \pm 2.2$	$15.0 \pm 2.0$
KO	$65.3 \pm 7.5$	$12.1 \pm 3.9$	$36.1 \pm 4.6$	$32.2 \pm 5.2$	$17.5 \pm 3.6$	$14.6 \pm 3.4$

There was no difference in the number of vesicles present at the PM before stimulation in WT and Syb-2 KO cells. Also, number of dead-end vesicles was unchanged (fig. 30, table 6). Hugo et. al., (2013) showed that t-SNAREs are the main interacting partners

mediating dead-end docking, hence I quantified t-SNAREs, by immunolabeling with antibodies against Stx1 and SNAP25 in WT and Syb-2 KO cells using TIRFM (fig. 31).



There was no change in the concentration of t-SNAREs in the PM of WT and Syb-2 KO cells. This led to the conclusion that Syb-2 does not play a role in dead-end docking. Thus, I investigated the other v-SNARE present on LDCVs, Ceb.



Long stimulation with 6  $\mu\text{M}$   $\text{Ca}^{2+}$  showed a straight increase in capacitance reaching upto  $858.1 \pm 3.8$  fF in WT and  $880.3 \pm 2.0$  fF in Ceb KO cells, whereas  $36.0 \pm 7.7$

vesicles and  $26.6 \pm 3.5$  vesicles were secreted in WT and KO cells respectively (fig. 32). There was a lot of variability in the responses of WT cells that was reflected in the error bars. Nevertheless, there was no difference in the amount of exocytosis in WT and KO cells, neither in membrane capacitance recording by patching nor in individual vesicle secretion measured by TIRFM.

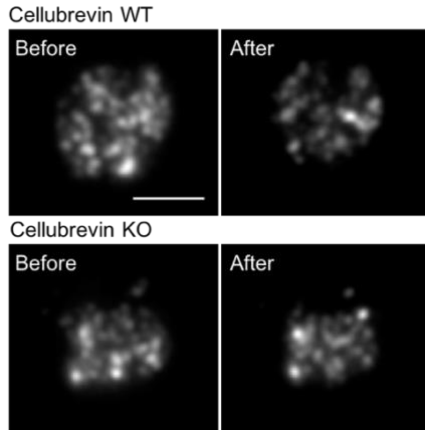


**Figure 33: TIRFM images of WT and Ceb KO mouse chromaffin cells.** Images show the footprint of exemplary cells taken in TIRFM immediately before reaching the whole-cell configuration (left) and after 5 min of perfusion with intracellular solution containing  $6 \mu\text{M Ca}^{2+}$ . Scale bar is  $5 \mu\text{m}$ .

Similarly, to Syb-2 WT and KO cells, vesicles were still present at the PM after 5 min stimulation with intracellular solution containing high  $\text{Ca}^{2+}$  in Ceb WT and KO cells (fig. 33).

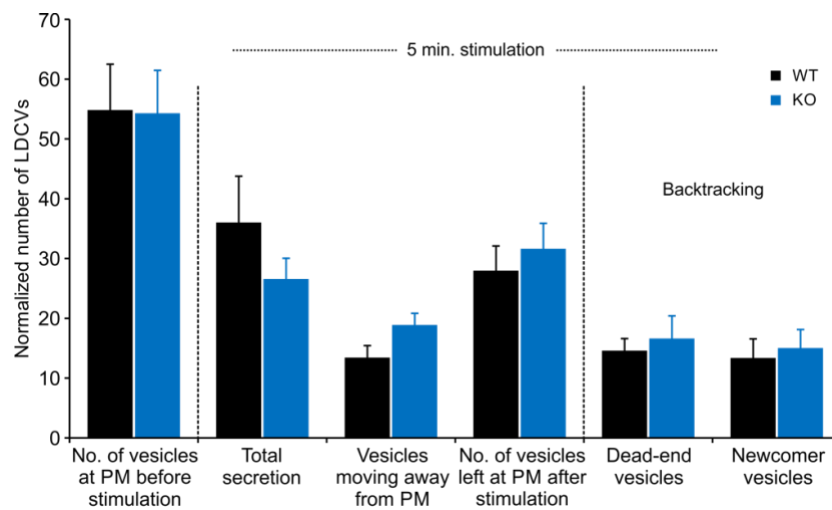
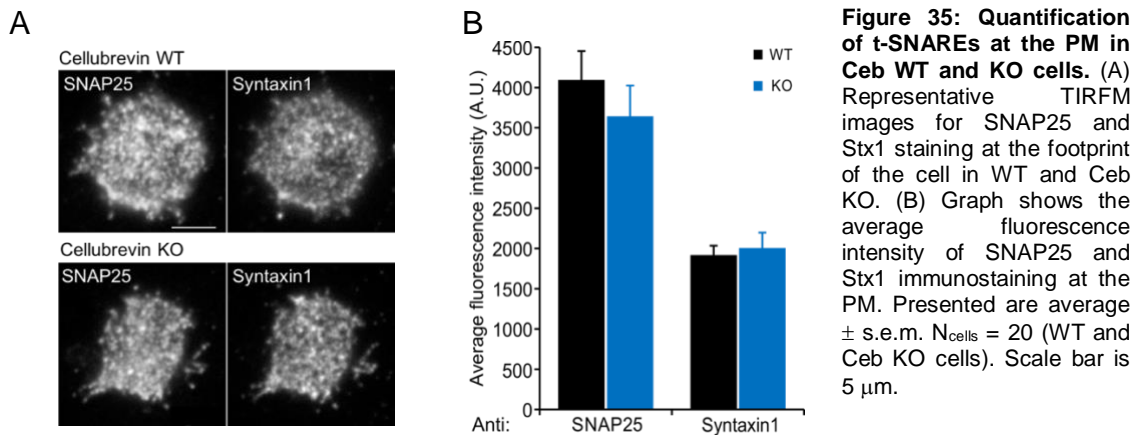


**Figure 34: Analysis of different parameters in TIRFM.** Represented are the average density of LDCVs near the PM at the beginning and the end of the experiment and the average total secretion in WT and Ceb KO cells. LDCVs visible at the end of the experiment were separated between newcomer and dead-end vesicles.  $N_{\text{cells}} = 7$  (WT) and 10 (KO).

**Table 7: Number of vesicles at the footprint of the cell in WT and Ceb KO.**

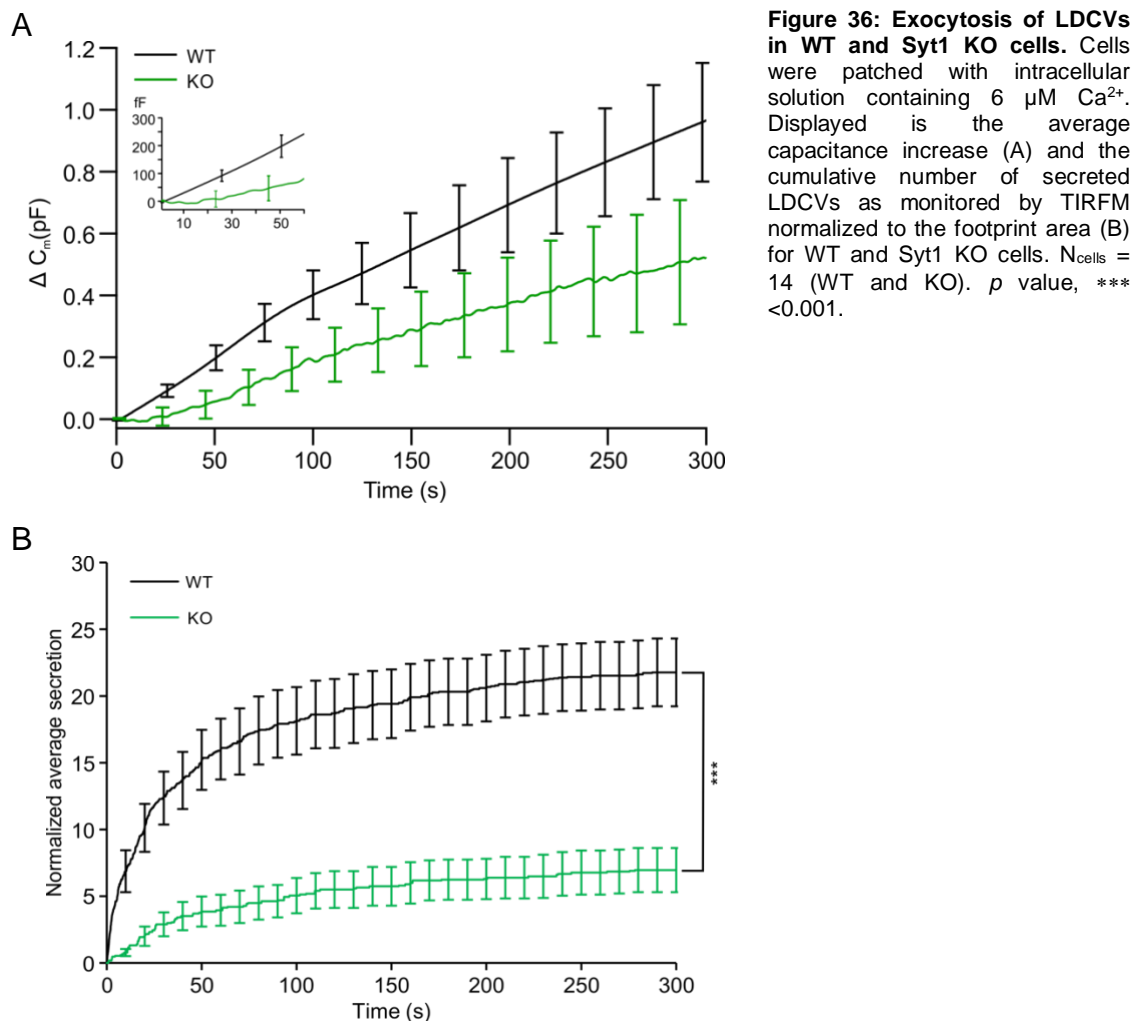
Ceb	Vesicles before stimulation	Total secretion	Vesicles moving away from PM	Vesicles left after stimulation	Dead-end vesicles	Newcomer vesicles
WT	$54.8 \pm 7.7$	$36.0 \pm 7.7$	$13.4 \pm 2.0$	$28.0 \pm 4.1$	$14.6 \pm 2.0$	$13.4 \pm 3.2$
KO	$54.3 \pm 7.2$	$26.6 \pm 3.5$	$18.9 \pm 1.9$	$31.7 \pm 4.2$	$16.6 \pm 3.8$	$15.0 \pm 3.1$

None of the TIRFM parameters in WT and KO cells was changed upon deletion of Ceb (fig. 34, table 7). Further quantification of t-SNAREs in TIRFM indicated that there was no change in the concentration of SNAP25 and Stx1 in Ceb KO cells as compared to WT (fig. 35).



Confirming previous studies, these results suggested that absence of Syb-2 or Ceb has no major effect on the vesicle secretion because both proteins are functionally redundant in mouse chromaffin cells (Borisovska et al., 2005). They had no influence on the number of dead-end vesicles, and also no effect on the concentration of SNAP25 and Stx1 at the PM. Therefore, I concluded that v-SNAREs do not contribute to dead-end docking.

#### 4.2.3 Syt1 has a role in functional docking but not dead-end docking



Previously, de Wit et al., (2009) have shown a clear docking defect upon deletion of Syt1 proposing that Syt1 is the vesicular protein that docks the secretory vesicles to the 1:1 Stx1:SNAP-25 productive SNARE. Henceforth, I investigated Syt1.

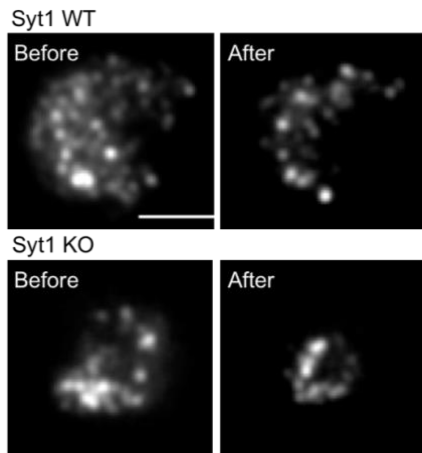


**Figure 37: TIRFM images of WT and Syt1 KO mouse chromaffin cells.** Images show the footprint of exemplary cells in TIRFM taken immediately before reaching whole-cell configuration (left) and after 5 min of perfusion with 6  $\mu\text{M}$   $\text{Ca}^{2+}$ . Scale bar is 5  $\mu\text{m}$ .

Membrane capacitance measurement showed that deletion of Syt1 did not change global secretion in comparison to WT. Although, there was no significant reduction in amount of exocytosis, the initial phase of secretion was delayed in Syt1 KO cells (fig. 36, inset) reproducing previous studies (Schonn et al., 2008). In contrast to capacitance recording, the individual secretion of vesicles measured by TIRFM was highly reduced by 32% in the KO cells (fig. 36, table 8). TIRFM recording also revealed that there were vesicles still remaining close to the PM even after long stimulation with high  $\text{Ca}^{2+}$  in WT and Syt1 KO cells (fig. 37).

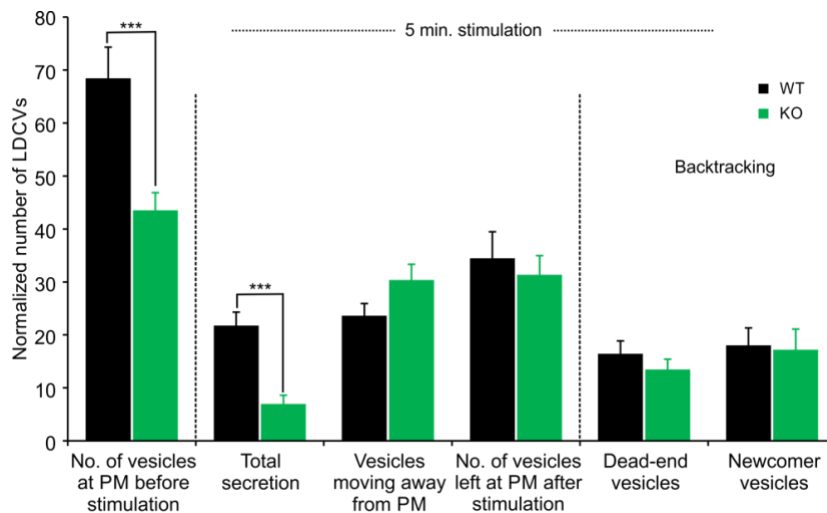
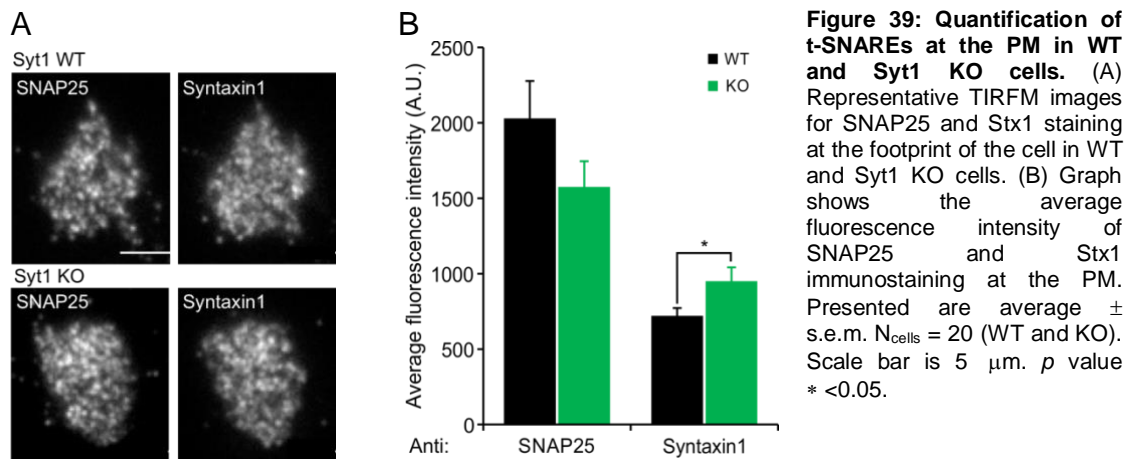


**Figure 38: Analysis of different parameters in TIRFM.** Represented are the average density of LDCVs near the PM at the beginning and the end of the experiment and the average total secretion in WT and Syt1 KO cells. LDCVs visible at the end of the experiment were separated between newcomer and dead-end vesicles.  $N_{\text{cells}} = 14$  (WT and KO).  $p$  value, \*\*\*  $< 0.001$ .

**Table 8: Number of vesicles at the footprint of the cell in WT and Syt1 KO cells.**

Syt1	Vesicles before stimulation	Total secretion	Vesicles moving away from PM	Vesicles left after stimulation	Dead-end vesicles	Newcomer vesicles
WT	68.4 ± 5.9	21.8 ± 2.5	23.6 ± 2.3	34.5 ± 5.0	16.4 ± 2.4	18.0 ± 3.3
KO	44.0 ± 3.3	7.0 ± 1.7	30.0 ± 3.0	31.0 ± 3.6	13.0 ± 2.0	17.0 ± 3.9

In KO cells the number of LDCVs visible at the footprint of the cells before stimulation was reduced by 64% in comparison to WT control. However, after stimulation their number was similar (fig. 38, table 8). Additionally, the number of dead-end vesicles and the newcomers was unchanged in KO cells as compared to WT control. Because Syt1 KO caused a strong docking defect that can be appreciated by the large reduction of LDCVs at the PM prior to stimulation, we decided to analyze the number of dead-end LDCVs in relation to the number of predocked LDCVs. The percentage of dead-end LDCVs from all predocked LDCVs was increased from 24% in WT to 30% in KO cells ( $p=0.154$ ,  $N_{\text{cells}} = 14$  for WT and KO), indicating a proportional increase in dead-end docking. This result was also supported by analysis of t-SNAREs at the PM, which revealed that there was a slight but not significant decrease in SNAP25, conversely Stx1 was significantly increased in Syt1 KO (fig. 39), a situation in which dead-end docking is favored.



Taking together, all these results suggested that loss of Syt1 had no direct influence on the dead-end vesicle number, but indirectly affects dead-end docking by changing the relative amounts of t-SNAREs in the PM. Nevertheless, we confirmed previous studies showing that Syt1 plays an important role in functional docking (de Wit et al., 2009) because absence of Syt1 resulted in significantly reduced number of vesicles at the PM before stimulation. On the other hand, Syt7 is co-expressed in chromaffin cells with Syt1 and both appear to have a functional redundancy for triggering exocytosis (Schonn et al., 2008). However, the role of Syt7 in docking remain elusive. Therefore, Syt7 was my next candidate that could be responsible for dead-end docking.

#### 4.2.4 Syt7 is involved in unproductive or dead-end docking

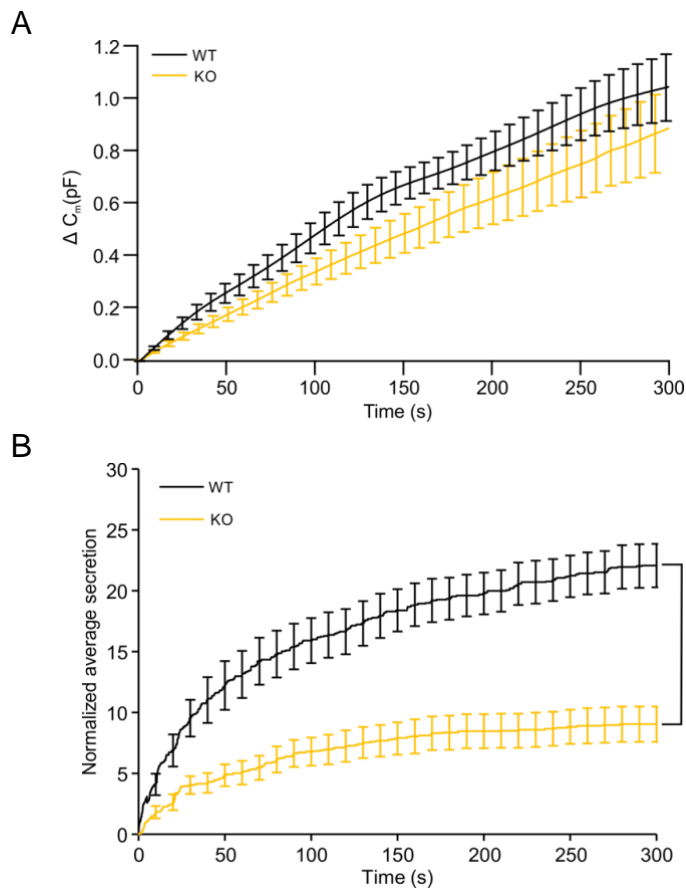


**Figure 40: Exocytosis of LDCVs in WT and Syt7 KO cells.** Cells were patched with solution containing  $6 \mu\text{M Ca}^{2+}$ . Displayed is the average capacitance increase (A) and the cumulative number of LDCVs secreted as monitored by TIRFM normalized to the footprint area (B) for WT and Syt7 KO cells.  $N_{\text{cells}} = 14$  (WT) and 15 (KO).  $p$  value \*\*\*  $<0.001$ .

Measurement of global secretion resulted in a linear increase of the membrane capacitance reaching  $1.0 \pm 0.1$  pF in WT and  $0.9 \pm 0.2$  pF in KO cells. Like in Syt1 KO, secretion measured in TIRFM was reduced by a factor of 2 in Syt7 KO cells in comparison to WT control. Counting the number of LDCVs in the first image of TIRFM movie revealed a small but significant decrease in Syt7 KO as compared to WT (fig. 40).

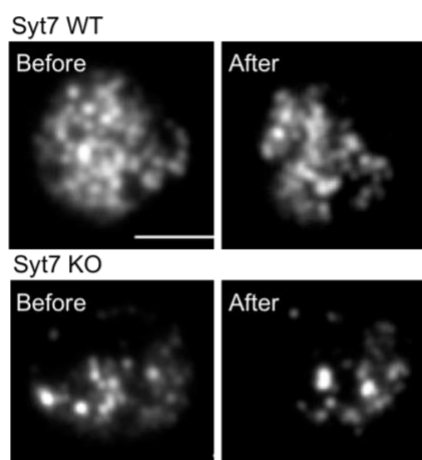


**Figure 41: TIRFM images of WT and Syt7 KO mouse chromaffin cells.** Images show the footprint of exemplary cells in TIRFM taken immediately before reaching whole-cell configuration (left) and after 5 min of perfusion with intracellular solution containing  $6 \mu\text{M Ca}^{2+}$ . Scale bar is  $5 \mu\text{m}$ .

As for the other knockout cells studied earlier in this work, there were vesicles remaining at cell's footprint after 5 min stimulation with  $6 \mu\text{M Ca}^{2+}$  (fig. 41). This indicated that dead-end vesicles might also be present in Syt7 KO. Differentiating

between dead-end and newcomer LDCVs revealed a surprising large decrease in the number of dead-end vesicle in KO cells as compared to WT cells (fig. 42, table 9). Not only their average number was decreased by a factor of 2 but also in proportion to predocked LDCVs they were significantly reduced from 34% in WT to 20% in KO cells ( $p=0.005$ ,  $N_{\text{cells}} = 14$  and  $15$  in WT and KO respectively). Simultaneously, the newcomers were significantly increased (fig. 42, table 9).

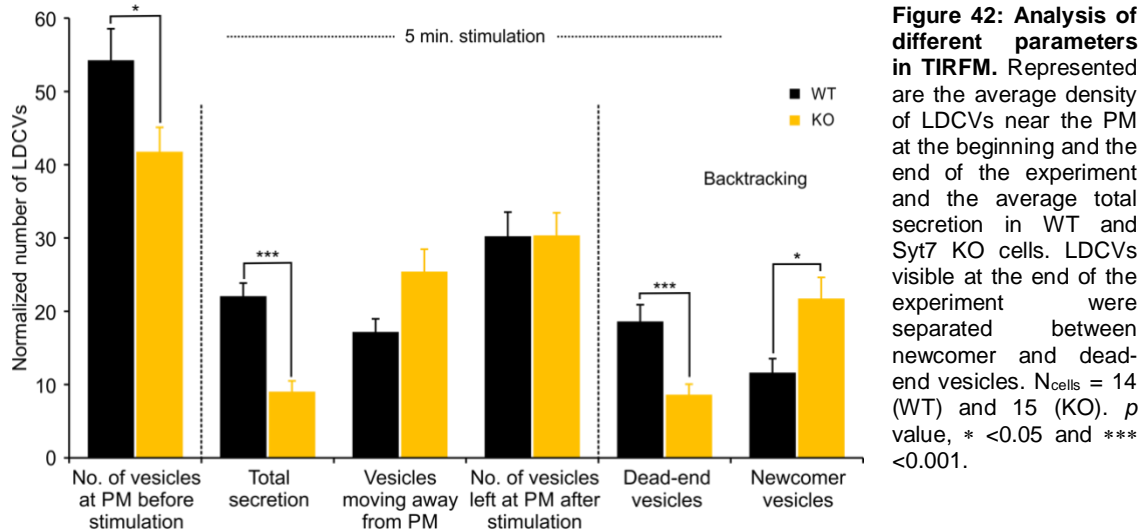


**Figure 42: Analysis of different parameters in TIRFM.** Represented are the average density of LDCVs near the PM at the beginning and the end of the experiment and the average total secretion in WT and Syt7 KO cells. LDCVs visible at the end of the experiment were separated between newcomer and dead-end vesicles.  $N_{\text{cells}} = 14$  (WT) and  $15$  (KO).  $p$  value, \*  $<0.05$  and \*\*\*  $<0.001$ .

**Table 9: Number of vesicles at the footprint of the cell in Syt7 WT and KO.**

Syt7	Vesicles before stimulation	Total secretion	Vesicles moving away from PM	Vesicles left after stimulation	Dead-end vesicles	Newcomer vesicles
WT	54.3 ± 4.3	22.1 ± 1.8	17.2 ± 1.8	30.2 ± 3.3	18.6 ± 2.3	11.6 ± 1.9
KO	41.8 ± 3.3	9.0 ± 1.5	25.4 ± 3.0	30.4 ± 3.1	8.6 ± 1.4	21.7 ± 2.9

Not only the newcomers were increased by a factor of 2 in KO as compared to WT cells but also in proportion to predocked LDCVs they were increased from 21% in WT to 52% in KO cells ( $p<0.001$ ,  $N_{\text{cells}} = 14$  and  $15$  in WT and KO respectively) (fig. 42, table 9). Additionally, the quantification of t-SNAREs in the punctae revealed that there was no difference between WT and KO cells (fig. 43). These results clearly showed that absence of Syt7 had a very strong effect on dead-end docking, suggesting a clear role of Syt7 in the interaction with 2:1 unproductive SNARE acceptor complex.

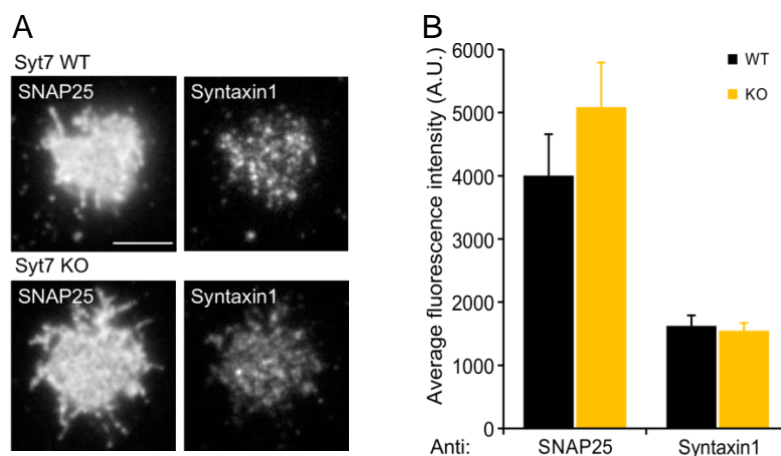


**Figure 43: Quantification of t-SNAREs at the PM in WT and Syt7 KO cells.** (A) Representative TIRFM images for SNAP25 and Stx1 staining at the footprint of the cell in WT and Syt7 KO cells. (B) Graph shows the average fluorescence intensity of SNAP25 and Stx1 staining at the PM. Presented are average  $\pm$  s.e.m.  $N_{\text{cells}} = 20$  (WT and KO). Scale bar is  $5 \mu\text{m}$ .

In order to confirm the role of Syt7 in dead-end docking, Syt7 was reintroduced in Syt7 KO cells via co-transfection with NPY-mCherry in Syt7 KO cells. The efficiency of double transfection was very low, nevertheless I performed the membrane capacitance measurements and TIRFM measurements simultaneously on 8 to 9 transfected cells. As it was difficult to hold the gigaseal in the Syt7 overexpressing cells for long time during patching, I analyzed the capacitance measurements and TIRFM secretion for 4 min and 20 s.

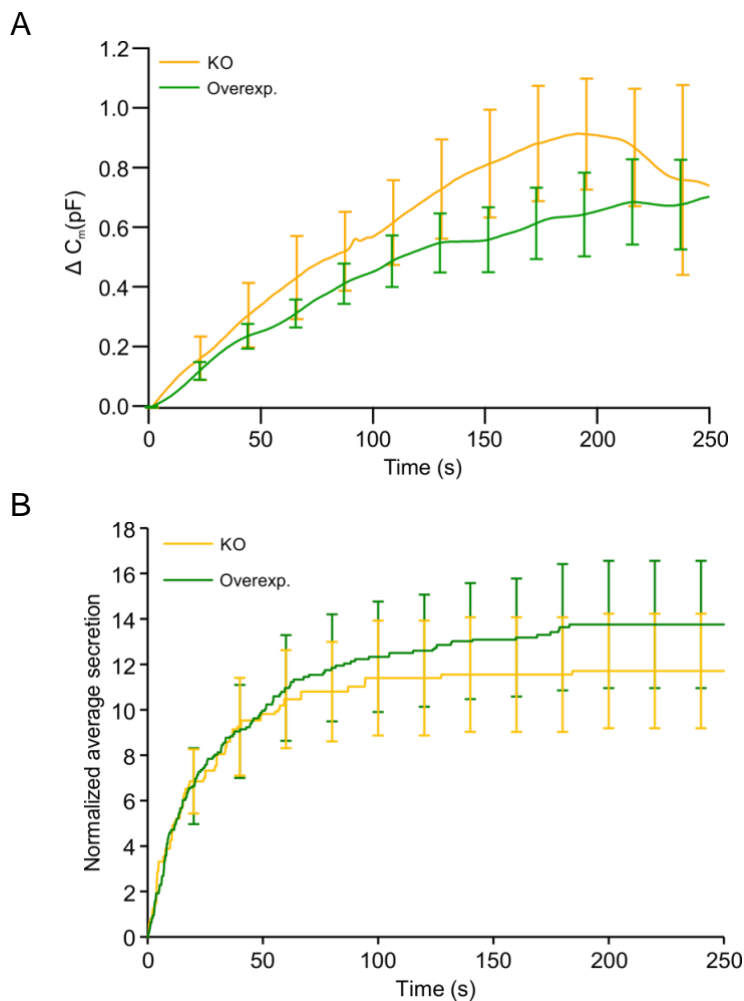
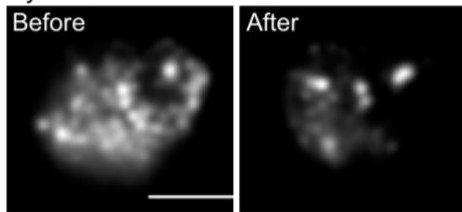


**Figure 44: Exocytosis of LDCVs in Syt7 KO and Syt7 overexpressing cells.** Cells were patched with intracellular solution containing 6  $\mu\text{M}$   $\text{Ca}^{2+}$ . Displayed is the average capacitance increase (A) and the cumulative number of LDCVs secreted as monitored by TIRFM normalized to the footprint area (B) for Syt7 KO and cells overexpressing Syt7.  $N_{\text{cells}} = 8$  (Syt7 KO) and 9 (Syt7 overexpressing cells).

Membrane capacitance measurement displayed a global increase reaching up to  $740.5 \pm 1.4$  fF in Syt7 KO and  $702.4 \pm 0.9$  fF in Syt7 overexpressing cells (fig. 44A). Also, the number of individual vesicle secreted in TIRFM was not rescued as  $11.8 \pm 2.5$  vesicles secreted in Syt7 KO cells and  $13.9 \pm 2.9$  vesicles secreted in cells transfected with Syt7 (fig. 44B). Similarly, to previous findings there were vesicles present at the cell's footprint after long stimulation with intracellular solution containing 6  $\mu\text{M}$   $\text{Ca}^{2+}$  in Syt7 KO cells overexpressing Syt7 (fig. 45). The number of vesicles present at the PM before stimulation as well as the number of vesicles moving away from the PM during the recording, and the number of vesicles left at the PM after stimulation was not different between Syt7 KO and Syt7 overexpressing cells (fig. 46, table 10). This

indicated that the docking defect due to Syt7 KO cannot be rescued by Syt7 overexpression.

Syt7 KO



Syt7 overexpression

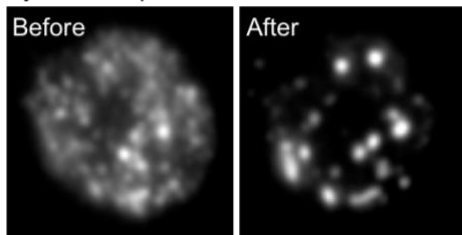


**Figure 45: TIRFM images of Syt7 KO and Syt7 overexpressing mouse chromaffin cells.** Images show the footprint of exemplary cells in TIRFM taken immediately before reaching whole-cell configuration (left) and after 4 min and 20 s of perfusion with intracellular solution containing 6  $\mu\text{M}$   $\text{Ca}^{2+}$ . Scale bar is 5  $\mu\text{m}$ .

Amazingly, the number of dead-end vesicles and newcomer vesicles were significantly changed. Dead-end vesicles were increased by a factor of 2 and newcomer vesicles were reduced in Syt7 transfected KO cells as compared to Syt7 KO (fig. 46, table 10).

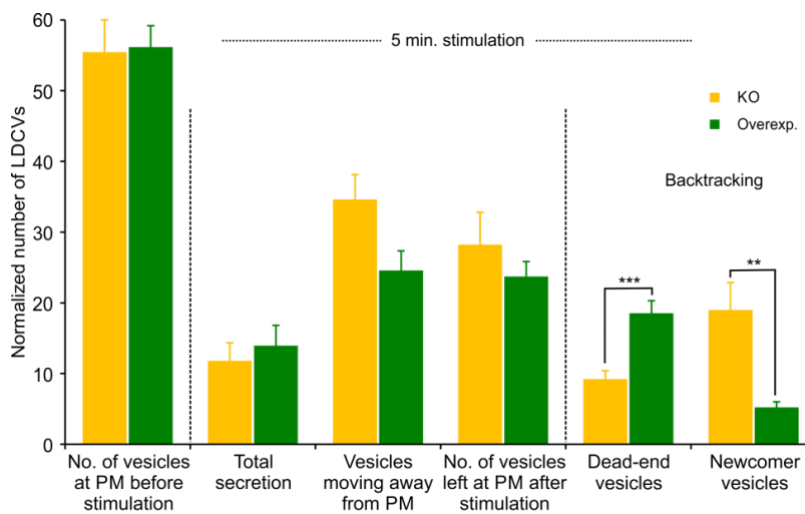


**Figure 46: Analysis of different parameters in TIRFM.** Represented are the average density of LDCVs near the PM at the beginning and the end of the experiment and the average total secretion in Syt7 KO and Syt7 overexpressing cells. LDCVs visible at the end of the experiment were separated between newcomer and dead-end vesicles.  $N_{\text{cells}} = 8$  (KO) and 9 (Syt7 overexpressing cells).  $p$  value, \*\* <0.01 and \*\*\* <0.001.

**Table 10: Number of vesicles at the footprint of the cell in Syt7 KO and Syt7 overexpressing cells.**

Syt7	Vesicles before stimulation	Total secretion	Vesicles moving away from PM	Vesicles left after stimulation	Dead-end vesicles	Newcomer vesicles
KO	55.4 ± 4.6	11.8 ± 2.5	34.6 ± 3.5	28.2 ± 4.6	9.2 ± 1.2	19.0 ± 3.9
Ov.	56.2 ± 3.0	13.9 ± 2.9	24.6 ± 2.8	23.7 ± 2.1	18.5 ± 1.8	5.2 ± 0.8

Taking together all the results from different knock out mouse models, I concluded that Syt7 is the only vesicular protein which induce non-functional dead-end docking by interacting with the 2:1 unproductive t-SNARE complex formed by two Stx1 molecules and one SNAP25 molecule.

## 5. Discussion

### 5.1 Biogenesis of LDCVs in adrenal chromaffin cells of newborn mice

In the present study, I studied the biogenesis and trafficking of LDCVs in mouse chromaffin cells using the overexpression of NPY-mCherry as a marker for LDCVs. We favored the method of electroporation over virus transfection because we needed to follow the biogenesis of the vesicles for upto 24 h, which is impossible with semiliki forest virus transfection because it is lethal for chromaffin cells within 5 to 6 h. We used high resolution SIM in our study because it improves the resolution by a factor of 2 in all three dimensions and therefore allows a detailed analysis of colocalization between proteins (Rego et al., 2012, Bost et al., 2013). From the colocalization experiments with CgA and LAMP1, we knew that NPY-mCherry truly labeled the LDCVs (fig. 13). This was further confirmed with our CLEM experiment because we could clearly observe an overlap between the electron dense granules in the electron micrograph and the NPY-mCherry containing LDCVs in SIM images (fig. 16E). I tracked the newly generated LDCVs over time after transfection, performed immunocytochemistry by co-labeling NPY-mCherry transfected cells with cis-Golgi marker together with Phalloidin-Alexa 488 labeling the cortical actin network to visualize the cell boundary, and analyzed the distribution of LDCVs from their first appearance at 2 h upto 24 h (fig. 14, 15). At the initial time point stained vesicles were mostly present near the cis-Golgi compartment and moved towards PM over time (fig. 16A-G). Accumulation of vesicles in the cortical actin ring in the vicinity of PM over time (fig. 16H) indicate the movement and accretion of newly formed vesicles which was in agreement with the model proposed by Rudolf et al., (2001) where they have shown that immature vesicles accumulate in the cortical actin network in PC12 cells. Similarly, Solimena and Gerdes (2003) proposed a model for age-dependent distribution of vesicles in bovine chromaffin cells, suggesting that youngest granules are found in close proximity to the PM whereas older granules are located towards the cell interior. It is possible that vesicles further away from the PM corresponds to older granules that are displaced back in the cytoplasm by new vesicles that are released first upon secretagogue treatment (Duncan et al., 2003).

Park et al., in 2011 showed that in PC12 cells CgA-RFP did not colocalize with cis- and medial-Golgi region but colocalize with Golgin97 trans-Golgi compartment. Similarly, our result revealed that NPY-mCherry only partially colocalize with the cis-Golgi, indicating that NPY-mCherry might be also localized to the trans-Golgi network. Accordingly, the co-immunolabeling of cis- and trans-Golgi network in NPY-mCherry transfected cells revealed that there was a partial overlap of NPY with both the Golgi markers suggesting that there was a transport of NPY from cis- to trans-Golgi compartment to get packed in the newly formed LDCVs (fig. 16A, B, C, and 17). Nevertheless, the localization of NPY 2 h after transfection to a relatively large

compartment that was neither the cis nor the trans-Golgi indicated that there is an additional compartment at/near the Golgi where NPY-mCherry accumulates. The CLEM experiment suggested that the extra-cis/trans-Golgi compartment that contained NPY-mCherry was indeed located near to the Golgi (fig. 16E). This NPY-mCherry containing extra-cis/trans-Golgi compartment needs to be characterized but it could be the Golgin97 or Stx6 positive compartment as proposed by Park et al., (2011) and Walter et al., (2014).

Transport of vesicular membrane proteins onto the newly generated vesicles is thought to occur at the trans-Golgi compartment as the vesicles are formed. However, our findings from co-immunolabeling of endogenous vesicular membrane proteins like Syb-2, Ceb, and Syt1 in NPY-mCherry transfected chromaffin cells suggests otherwise. We found no apparent colocalization between NPY and either of the three vesicular proteins at 2h (fig. 18, 19, 21, A first lane, B, C), indicating no association of these proteins with the newly formed vesicles. On later time points the colocalization increased and at 24 h it was highest for all three tested proteins (fig. 18, 19, 21, A fourth lane, B, C). Moreover, the double immunolabeling of the two v-SNAREs in NPY-mCherry transfected cells showed that not all NPY positive vesicles contained the v-SNAREs (fig. 9). Sequential increase of colocalization indicates that the vesicular membrane proteins are getting associated with the NPY-mCherry positive vesicles at a late stage in the trafficking pathway and not directly from the Golgi. Urbé et al., (1998) and Tooze SA (2001) described a possible fusion of immature secretory granule with a carrier vesicle. Also, Walter et al., (2014) have proposed that Syb-2 and Syt1 are associated to LDCVs via transport vesicle in a last step of biogenesis because they are needed only for fusion. This type of fusion of immature secretory granule with a transport vesicle was also demonstrated in PC12 cells by Wendler et al., (2001). According to our findings, this carrier vesicle or transport vesicle could be a precursor vesicle or a recycling vesicle carrying the vesicular membrane proteins to fuse with NPY-mCherry containing vesicle when it approaches the PM.

Furthermore, we also demonstrated with our Syt1 endocytosis experiment that the vesicular membrane proteins might originate from recycling after a round of exo- and endocytosis (fig. 22A). Number of endocytosed Syt1 punctae increased with time after stimulation together with a decrease of the number of Syt1 punctae at the PM due to endocytosis (fig. 22B). However, some Syt1 punctae remained continuously visible at the cell periphery, which indicate that after being endocytosed some Syt1 might go directly back to PM for next round of exocytosis or all the molecules of Syt1 are not endocytosed from the PM at the same time. This would agree with the theory that a pool of vesicular membrane protein remain in the PM ready for fast endocytosis (Hua et al., 2011). Additionally, similar number of LDCVs positive for NPY-mCherry were also positive for endocytosed Syt1, reserved Syt1 or both. This indicates that fusion of recycling vesicles including endocytosed Syt1 with the precursor vesicles containing newly synthesized Syt1 is not essential for generation of mature LDCVs because these proteins can be derived from recycling or de novo synthesis. In conclusion,

endocytosed Syt1 needed at least 2 h to associate with NPY-mCherry positive vesicles (fig. 22, 23D). This timing agrees well with the recycling of LDCV membrane protein Glycoprotein III/clusterin which is recycled to electron dense vesicles within 45 min but required 6 h to passage through classical LDCVs in bovine chromaffin cells (Patzak and Winkler, 1986). We also showed that the endocytosed Syt1 is not recycled through the vesicles containing Rab11A (fig. 23C, E). We know that the recycling pathway involves numerous specialized compartments like Rab5(early endosome), Rab7 (late endosome), Rab11 (recycling endosome), etc. (Le Roy and Wrana, 2005; Scott et al., 2014). Hence, next step would be to find out the endosomal pathway through which the endocytosed vesicular membrane proteins travels. Finally, for vesicular membrane proteins it still remains unclear when these recycled proteins are ready for the next round of exocytosis. Our experiments support previous findings showing that 1 h is not sufficient recycling time to generate a releasable LDCV with recycled Syt1 (Walter et al., 2014).

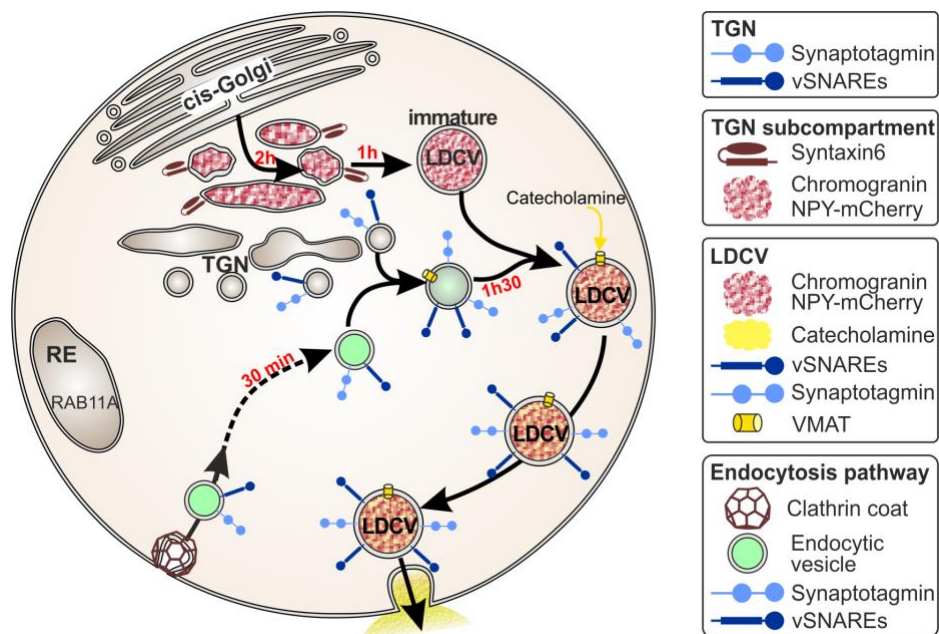


**Figure 47: Schematic model for biogenesis and recycling of LDCVs in mouse chromaffin cells.** NPY is processed within 3 h of synthesis to fully functional LDCV. The transport pathway involves a Stx6 positive subcompartment of the TGN. LDCV membrane proteins are added to LDCVs at a late stage after NPY has already been packed in immature vesicles. The exocytosis machinery (v-SNAREs and Syt1) is presumably taken by clathrin-mediated endocytosis and then recycled within 2 h to LDCVs. These freshly endocytosed membrane proteins can mix with proteins from a reserve pool.

In conclusion (fig. 47), our study shows that newly generated LDCVs do not contain vesicular membrane proteins as they leave the Golgi apparatus. Their association with freshly generated LDCVs occurs within 1 h of budding from the Golgi because some NPY-mCherry positive vesicles clearly contain vesicular membrane proteins making them possibly fusion competent. This also confirms previous findings by Nofal et al., (2007) that in bovine chromaffin cells exocytosis of NPY-mRFP labeled vesicles occurs at 12 h post transfection. However, this contradicts the hypothesis by Pinheiro et al., (2014) and Walter et al., (2014) that vesicles require one day of maturation to become fully fusion competent. Also, we showed that the association of vesicular membrane proteins with the newly made immature LDCVs occurs through the fusion with

precursor vesicles. Immature LDCVs are generated at the Golgi where they get filled with NPY, Cgs, other peptides. The fusion with a precursor vesicle happens at a late stage of biogenesis where the vesicular membrane proteins are transferred to the LDCV. This process of LDCV biogenesis is very similar to LDCV biogenesis in PC12 demonstrated by Tooze et al., (1991) where they have shown that it happens at a very slow time scale. In this study I analyzed the association of already three vesicular membrane proteins with LDCVs but there are many other known vesicular proteins and it needs to be determined whether they also follow the same route.

## **5.2 Molecular mechanisms of “dead-end docking” in mouse chromaffin cells**

The existence of unproductive t-SNARE acceptor complex formed in 2:1 ratio between 2 Stx1 and 1 SNAP25 molecule was demonstrated in *in vitro* experiments by Bajohrs et al., (2004) and it was hypothesized that vesicles binding to this complex could undergo dead-end docking (Verhage and Sørensen, 2008). We successfully identified this new pool of vesicles which we called “dead-end” vesicles using TIRFM and patch clamp method simultaneously in bovine chromaffin cells (Hugo et al., 2013). They represent 15% of LDCVs at the cell’s footprint in bovine chromaffin cells and their pool size was affected by the overexpression of Munc18-2, SNAP25, and Stx1. This indicated the presence of unproductive t-SNARE acceptor complex *in vivo* and that it is responsible for the generation of dead-end vesicles (Hugo et al., 2013). What remained unclear was the nature of the vesicular protein that interacts with the unproductive t-SNARE acceptor complex. To identify it we investigated dead-end docking in chromaffin cells originating from genetically modified mice in which genes for vesicular proteins that have been shown to interact with t-SNAREs have been deleted. However, first it was important to demonstrate the presence of dead-end vesicles in mouse chromaffin cells. We measured the overall exocytosis of cells through membrane capacitance recording using the patch clamp technique and we monitored simultaneously single vesicle fusion at the footprint of the cell with TIRFM in WT mouse chromaffin cells. We could show that 27.5% of vesicles visible at the cell’s footprint were dead-end vesicles (fig. 27) which is substantially more than in bovine chromaffin cells (Hugo et al., 2013). We used knock out mouse models for v-SNAREs Syb-2 and Ceb and the Ca<sup>2+</sup> sensors Syt1 and Syt7.

In WT cells the capacitance change upon perfusion with 6 μM Ca<sup>2+</sup> showed a linear increase over time whereas secretion in TIRFM was best described as a monoexponential rise. This contradicts the studies in bovine chromaffin cells (Becherer et al., 2007; Hugo et al., 2013) where they have shown a correlation between the time course of capacitance change and individual vesicle secretion in TIRFM. It is possible that LDCVs generated before the NPY-mCherry transfection were released later in comparison to the NPY-mCherry transfected vesicles at the footprint of the cell. But experiment with FFN511 that label all vesicles in contrast to NPY-mCherry that label

vesicle only after the transfection, which was done 48 h before the experiment, showed no difference in the number of vesicles secreted in TIRFM (Annex fig. 48A). Second possibility is that there are more kiss-and-run events than full fusion in mouse chromaffin cells. When LDCVs are stained with NPY-mCherry, exocytosis is detected by the very fast (200 ms) disappearance of the vesicle. However, when kiss-and-run occurs, the narrow fusion pore allows only partial and slow release of the cargo resulting in slow or no disappearance of the LDCV. Thus, these type of fusion events would not be counted as exocytosis inducing an underestimate of exocytosis measured by TIRFM. To address this problem we used NPY-venus that is a pH dependent fluorescent tag, with which kiss-and-run events can easily be detected in the form of a sudden increase in the fluorescence of LDCV when the fusion pore opens followed by some dispersion of the cargo. Unfortunately, we couldn't detect high amount of kiss-and-run events with NPY-venus transfection (data not shown). It is also possible that the collagen coating on the coverslips is resulting in the formation of stress fibers that in turn is influencing the secretion in TIRFM by trapping the LDCVs at the interface of coverslip and the cell. If this is the case then analyzing the concentration of actin at the PM can provide a possible explanation. However, there was no difference in the amount of actin at the PM in cells plated on coated or uncoated coverslips (Annex fig. 48B). Other possibility is that the docking or priming of vesicles is low at the cell's footprint in comparison to the rest of the cell, which would result in the faster depletion of releasable pool of vesicles at the footprint of the cell. Different factors could be responsible for the later possibility. Presence of different actin network could be one of the reason. Lang et al., (2000) showed that in PC12 cells actin filaments are arranged in a criss-cross fashion resembling stress fibers that form thick or dense pad at the coverslip interface whereas they are thinner in the rest of the cell where PM was facing the culture medium. These dense actin fibers could result in low mobility of vesicles towards the PM reducing the pool size of docked/primed LDCV at the PM in comparison to the rest of the cell, which would result in the rapid depletion of releasable vesicles in the TIRFM. If that were true than the dichotomy between the overall exocytosis ( $\Delta C_m$ ) and exocytosis at the footprint (TIRFM) should be stronger in cells showing a docking/priming defect. We and others showed that docking was strongly reduced in Syt1 KO cells (de Wit et al., 2009; fig. 38) while Syt7 deletion induced a milder docking phenotype (fig. 42). Syb-2 and Ceb KO did not induce a docking defect (Borisovska et al., 2005; fig. 30, 34). However, Syb-2 KO has been shown to induce a stronger priming defect than Ceb KO. If our hypothesis is correct than the difference between global exocytosis and exocytosis at the footprint should decrease in the following order: Syt1>Syt7>Syb-2>Ceb. This is exactly what we found. The various KOs did not changed global secretion but decreased exocytosis at the footprint of the cells by a factor of 3.2, 2.5, and 2 in Syt1, Syt7, and Syb-2 KO in comparison to WT respectively. In Ceb KO no change was observed in global secretion as well as in exocytosis at the footprint. Thus, our data suggest that in mouse chromaffin cells a barrier probably made out of actin stress fibers reduces docking of LDCVs at the footprint of the cells (fig. 28, 32, 36, 40).

Syb-2 has been shown to be involved in priming of LDCVs in mouse chromaffin cells (Borisovska et al., 2005; Walter et al., 2010; Borisovska et al., 2012), and in docking of synaptic vesicle at mouse hippocampal synapses (Imig et al., 2014). The number of vesicles before and after stimulation remained unchanged between WT and KO cells. The same was true for newcomer and dead-end vesicles (fig. 29, 30). We know that concentration of t-SNAREs, SNAP25 and Stx1 play a major role in mediating dead-end docking. Our quantification of SNAP25 and Stx1 in Syb-2 KO cells using TIRFM showed that their concentration was similar as in WT cells (fig. 31). It has also been shown that Syb-2 and Ceb have a functional redundancy in regulated exocytosis of chromaffin cells (Borisovska et al., 2005). The phenotype of Ceb KO chromaffin cells was very similar to that of Syb-2 KO cells. The vesicular parameters measured with TIRFM were unchanged in Ceb KO cells in comparison to WT control. Similarly to Syb-2 KO, the amount of t-SNAREs in the PM was not affected by deletion of Ceb. Therefore, our results confirm and complement the findings from Borisovska et al., (2005). Furthermore, we show that like Syb-2, Ceb is not involved in dead-end docking. Hence, we conclude that none of the v-SNAREs present on chromaffin cell LDCVs play a role in this phenomenon.

de Wit et al., (2009) demonstrated by electron microscopy that deletion of Syt1 results in a clear docking defect in mouse chromaffin cells. They proposed that Syt1 is the vesicular protein that docks the secretory vesicles to the 1:1 Stx1:SNAP25 productive SNARE complex. We confirmed this finding because the number of vesicles at the cell's footprint before stimulation were reduced by 64% (fig. 38). Furthermore, as expected the absence of the fast  $Ca^{2+}$  sensor induced a delay in the initial phase of secretion indicating a reduced pool of ready releasable vesicles (Voets et al., 2001; Schonn et al., 2008). Newcomers and dead-end vesicles were not changed in Syt1 KO. If anything, their number was proportionally increased from 24% in WT to 30% in KO. In parallel t-SNAREs quantification at the PM showed that the concentration of Stx1 in the PM was significantly increased in Syt1 KO cells (fig. 39). In bovine chromaffin cells increasing the concentration of Stx1 resulted in a significant rise in the number of dead-end vesicles because it increases the amount of unproductive t-SNARE acceptor complex (Hugo et al., 2013). Thus, Syt1 increases dead-end docking by increasing the availability of unproductive t-SNARE complexes, but not through its putative interaction with the t-SNAREs. In conclusion, Syt1 has an important role in functional docking reaction because our results clearly showed that number of vesicles before stimulation were significantly reduced but loss of Syt1 did not directly affect the number of dead-end vesicles, indicating no direct role of Syt1 in dead-end docking reaction.

Schonn et al., (2008) showed that Syt1 and Syt7 possess a functional redundancy in mouse chromaffin cells. They identified Syt7 as a major  $Ca^{2+}$  sensor for regulated exocytosis in mouse chromaffin cells because loss of Syt7 resulted in a dramatic decrease of  $Ca^{2+}$  mediated exocytosis. In our study, the loss of Syt7 resulted in significant decrease in the number of vesicles before stimulation like for Syt1 KO

phenotype albeit to a lesser extent (fig. 42). This shows that Syt7 is also involved in docking mechanism in mouse chromaffin cells. Interestingly, the number of dead-end vesicles were hugely decreased from 34% in Syt7 WT to 20% in Syt7 KO cells and concurrently the newcomer vesicles were significantly increased from 21% in Syt7 WT to 52% in Syt7 KO cells (fig. 42). Furthermore, the t-SNAREs quantification analysis did not show any change between Syt7 WT and KO cells (fig. 43), indicating that absence of Syt7 does not affect the formation of unproductive t-SNARE acceptor complex. Hence, Syt7 loss had a dramatic effect on dead-end docking, suggesting a new role for Syt7 as an interaction partner with the 2:1 unproductive t-SNARE acceptor complex.

The function of Syt7 in dead-end docking was also further demonstrated by rescue experiments. We expressed Syt7 together with NPY-mCherry in Syt7 KO cells. There was no change in the overall secretion examined by capacitance measurements as well as in the number of single vesicle secreted in TIRF between Syt7 KO and the overexpressing cells (fig. 44, 46). Similarly, there was no difference in the number of vesicles before stimulation, vesicles moving away from PM, and number of vesicles after stimulation between Syt7 KO and overexpressing cells (fig. 46). This clearly showed that Syt 7 expression in Syt7 KO did not rescue the docking defect. However, there was a dramatic increase in the number of dead-end vesicles by a factor of 2 and a simultaneous decrease in the number of newcomer vesicles in Syt7 overexpressing cells (fig. 46). These results indicate that Syt7 is not able to rescue the secretion which is puzzling. In bovine chromaffin cells, F-actin has a major role in the organization of the secretory proteins at the PM (Torregrosa-Hetland et al., 2011). L- and P-Q-type  $Ca^{2+}$  channels, Stx1, Syt1 are localized at the edges of cytoskeletal polygonal cages formed by F-actin, which are the preferred sites of vesicle exocytosis (Torregrosa-Hetland et al., 2011). Syt7 has been shown to accumulate in the PM (Rao et al., 2014). If overexpression of Syt7 results in very high amount of Syt7 in the PM then there is a possibility that it affects the localization of  $Ca^{2+}$  channels and SNARE proteins at the edges of the F-actin network. This might affect the fusion of vesicles and as a result secretion is not rescued.

In addition to the functional redundancy between Syt1 and Syt7 (Schonn et al., 2008), our experiments indicate that both proteins also possess some distinct functions. This is supported by recent findings. Both proteins are localized on different population of LDCVs rendering Syt7 positive LDCVs more prone for dead-end docking. Furthermore, the pattern of fusion is more dispersed with Syt1 granules than for Syt7 containing granules which fuse in clusters (Rao et al., 2014), and fusion kinetics of Syt1 granules are faster than Syt7 positive granules, finally their requirements for  $Ca^{2+}$  dependent activation are different (Rao et al., 2017).

Taking together all our findings from different knock out mouse systems, I reached the conclusion that Syt7 is the unique vesicular protein, which is interacting with the unproductive 2:1 t-SNARE acceptor complex formed between 2 molecules of Stx1 and one molecule of SNAP25. However, further study is needed to know if this dead-end

vesicle pool can be regulated. NSF and SNAP are known to disassemble the functional SNARE complexes after exocytosis (Block et al., 1988; Clary et al., 1990). By overexpressing NSF/SNAP in chromaffin cells, one can study if the overexpression of NSF also disassembles the unproductive SNARE complexes and thereby renders dead-end vesicles release competent. It is also possible that dead-end vesicles make a distinct pool (Hugo et al., 2013) that is functional under special conditions that are not known yet. Studying Syt7 KO in further detail can shed a light on such conditions and can provide more insights into the docking mechanisms in chromaffin cells but also other cell types. In pancreatic islet  $\beta$ -cells, Syt7 is also a major  $\text{Ca}^{2+}$  sensor for exocytosis of insulin granules (Gao et al., 2000; Gauthier et al., 2008; Gustavsson et al., 2008). Wu et al., (2015) showed that Syt7 is phosphorylated by PKA at a single serine residue located in the linker region between the Syt7 transmembrane region and its C-terminal  $\text{Ca}^{2+}$  binding C2 domain. This phosphorylation enhances the secretion of insulin from pancreatic islet  $\beta$ -cells. This indicate that PKA might also modulate dead-end docking by its effect on Syt7 activity and thereby may confer release capability to dead-end vesicles.

## **6. REFERENCES**

1. Allen JM, Adrian TE, Polak JM, Bloom SR. (1983) Neuropeptide Y (NPY) in the adrenal gland. *J Auton Nerv Syst.* Nov;9(2-3):559-63.
2. Ashery U, Varoqueaux F, Voets T, Betz A, Thanku P, Koch H, Neher E, Brose N, Rettig J. (2000) Munc13-1 acts as a priming factor for large dense-core vesicles in bovine chromaffin cells. *EMBO J.* Jul 17;19(14):3586-96.
3. Ashery U, Bielpolski N, Barak B, Yizhar O. (2009) Friends and foes in synaptic transmission: the role of tomosyn in vesicle priming. *Trends Neurosci.* May;32(5):275-82.
4. Aunis D, Langley K. (1999) Physiological aspects of exocytosis in chromaffin cells of the adrenal medulla. *Acta Physiol Scand.* Oct;167(2):89-97.
5. Axelrod D. (2001) Total internal reflection fluorescence microscopy in cell biology. *Traffic.* 2:764-774.
6. Bajohrs M, Rickman C, Binz T, Davletov B. (2004) A molecular basis underlying differences in the toxicity of botulinum serotypes A and E. *EMBO REP.* NOV;5(11):1090-5.
7. Becherer U, Pasche M, Nofal S, Hof D, Matti U, Rettig J. (2007) Quantifying exocytosis by combination of membrane capacitance measurements and total internal reflection fluorescence microscopy in chromaffin cells. *PLoS One.* Jun 6;2(6):e505.
8. Becherer U, Medart MR, Schirra C, Krause E, Stevens D, Rettig J. (2012) Regulated exocytosis in chromaffin cells and cytotoxic T lymphocytes: how similar are they? *Cell Calcium.* Sep-Oct;52(3-4):303-12.
9. Berridge MJ. (2012) *Cell Signalling Biology. Module 7. Cellular Processes.* Portland press limited.
10. Bittner MA, Aikman RL, Holz RW. (2013) A nibbling mechanism for clathrin-mediated retrieval of secretory granule membrane after exocytosis. *J Biol Chem.* Mar 29;288(13):9177-88.

11. Blaschko H, Welch AD. (1953) Localization of adrenaline in cytoplasmic particles of the bovine adrenal medulla. *Naunyn Schmiedeberg's Arch Exp Pathol Pharmacol.* 219(1-2):17-22.
12. Block MR, Glick BS, Wilcox CA, Wieland FT, Rothman JE. (1988) Purification of an N-ethylmaleimide-sensitive protein catalyzing vesicular transport. *Proc Natl Acad Sci U S A.* Nov;85(21):7852-6.
13. Bolte S, Cordelières FP. (2006) A guided tour into subcellular colocalization analysis in light microscopy. *J Microsc.* Dec;224(Pt 3):213-32.
14. Bonnemaïson ML, Eipper BA, Mains RE. (2013) Role of adaptor proteins in secretory granule biogenesis and maturation. *Front Endocrinol (Lausanne).* Aug 14;4:101.
15. Borgonovo B, Ouwendijk J, Solimena M. (2006) Biogenesis of secretory granules. *Curr Opin Cell Biol.* Aug; 18(4):365-70.
16. Borisovska M, Zhao Y, Tsytsyura Y, Glyvuk N, Takamori S, Matti U, Rettig J, Südhof T, Bruns D. (2005) v-SNAREs control exocytosis of vesicles from priming to fusion. *EMBO J.* Jun 15;24(12):2114-26.
17. Borisovska M, Schwarz YN, Dhara M, Yarzagaray A, Hugo S, Narzi D, Siu SW, Kesavan J, Mohrmann R, Böchmann RA, Bruns D. (2012) Membrane-proximal tryptophans of synaptobrevin II stabilize priming of secretory vesicles. *J Neurosci.* Nov 7;32(45):15983-97.
18. Bost A, Pasche M, Schirra C, Becherer U. (2013) Super-resolution microscopy in studying neuroendocrine cell function. *Front Neurosci.* Nov 25;7:222.
19. Bowman GR, Cowan At, Turkewitz AP. (2009) Biogenesis of dense-core secretory granules. *Trafficking inside cells* chapter 10. Pp.183-209.
20. Burgoyne RD, Morgan A. (2003) Secretory granule exocytosis. *Physiol rev.* Apr;83(2):581-632.
21. Ceccarelli B, Hurlbut W, Mauro A. (1972) Depletion of vesicles from frog neuromuscular junctions by prolonged tetanic stimulation. *J Cell Biol.* 54:30-38.

22. Chan SA, Smith C. (2001) Physiological stimuli evoke two forms of endocytosis in bovine chromaffin cells. *J Physiol.* Dec 15;537(Pt 3):871-85.
23. Chen YA, Scales SJ, Scheller RH. (2001) Sequential SNARE assembly underlies priming and triggering of exocytosis. *Neuron.* Apr;30(1):161-70.
24. Clary DO, Griff IC, Rothman JE. (1990) SNAPs, a family of NSF attachment proteins involved in intracellular membrane fusion in animals and yeast. *Cell.* May 18;61(4):709-21.
25. Colmers WF, Wahlestedt C. (1993) The biology of neuropeptide Y and related peptides. Book: *Contemporary Neuroscience*. ISBN: 978-1-59259-465-8.
26. Crivellato E, Nico B, Ribatti D. (2008) the chromaffin vesicle: advances in understanding the composition of a versatile, multifunctional secretory organelle. *The Anatomical record.* 291:1587-1602.
27. Coupland RE. (1965) Electron microscopic observations on the structure of the rat adrenal medulla. I. The ultrastructure and organization of chromaffin cells in the normal adrenal medulla. *J Anat.* Apr;99:231-54.
28. Coupland RE. (1965) Electron microscopic observations on the structure of the rat adrenal medulla: II. Normal innervation. *J Anat.* Apr;99(Pt 2):255-72.
29. de Wit H, Cornelisse LN, Toonen RF, Verhage M. (2006) Docking of secretory vesicle is Syntaxin dependent. *PLoS One.* Dec 27;1:e126.
30. de Wit H, Walter AM, Milosevic I, Gulyás-Kovács A, Riedel D, Sørensen JB, Verhage M. (2009) Synaptotagmin-1 docks secretory vesicles to Syntaxin-1/SNAP-25 acceptor complexes. *Cell.* Sep 4;138(5):935-46.
31. de Wit H. (2010) Morphological docking of secretory vesicles. *Histochem Cell Biol.* Aug;134(2):103-13.
32. de Wit H. (2010) Molecular mechanism of secretory vesicle docking. *Biochem Soc Trans.* Feb;38(Pt 1):192-8.
33. Dhara M, Yarzagaray A, Schwarz Y, Dutta S, Grabner C, Moghadam PK, Bost A, Schirra C, Rettig J, Reim K, Brose N, Mohrmann R, Bruns D. (2014) Complexin

synchronizes primed vesicle exocytosis and regulates fusion pore dynamics. *J Cell Biol.* Mar 31;204(7):1123-40.

34. Dulubova I, Sugita S, Hill S, Hosaka M, Fernandez I, Südhof TC, Rizo J. (1999) A conformational switch in syntaxin during exocytosis: role of munc18. *EMBO J.* Aug 16;18(16):4372-82.

35. Duncan RR, Greaves J, Wiegand UK, Matskevich I, Bodammer G, Apps DK, Shipston MJ, Chow RH. (2003) Functional and spatial segregation of secretory vesicle pools according to vesicle age. *Nature.* Mar 13;422(6928):176-80.

36. Dunn KW, Kamocka MM, McDonald JH. (2011) A practical guide to evaluating colocalization in biological microscopy. *Am J Physiol Cell Physiol.* Apr;300(4):C723-42.

37. Engisch KL, Nowycky MC. (1998) Compensatory and excess retrieval: two types of endocytosis following single step depolarizations in bovine adrenal chromaffin cells. *J Physiol.* Feb 1;506(Pt 3):591-608.

38. Fasshauer D, Eliason WK, Brünger AT, Jahn R. (1998) Identification of a minimal core of the synaptic SNARE complex sufficient for reversible assembly and disassembly. *Biochemistry.* Jul 21;37(29):10354-62.

39. Fernandez I, Araç D, Ubach J, Gerber SH, Shin O, Gao Y, Anderson RG, Südhof TC, Rizo J. (2001) Three-dimensional structure of the synaptotagmin 1 C2B-domain: synaptotagmin 1 as a phospholipid binding machine. *Neuron.* Dec 20;32(6):1057-69.

40. Fernández-Chacón R, Königstorfer A, Gerber SH, García J, Matos MF, Stevens CF, Brose N, Rizo J, Rosenmund C, Südhof TC. (2001) Synaptotagmin I functions as a calcium regulator of release probability. *Nature.* Mar 1;410(6824):41-9.

41. Gad H, Löw P, Zotova E, Brodin L, Shupliakov O. (1998) Dissociation between Ca<sup>2+</sup>-triggered synaptic vesicle exocytosis and clathrin-mediated endocytosis at a central synapse. *Neuron.* Sep;21(3):607-16.

42. Gao Z, Reavey-Cantwell J, Young RA, Jegier P, Wolf BA. (2000) Synaptotagmin III/VII isoforms mediate Ca<sup>2+</sup>-induced insulin secretion in pancreatic islet beta-cells. *J Biol Chem.* Nov 17;275(46):36079-85.

43. García AG, García-De-Diego AM, Gandía L, Borges R, García-Sancho J. (2006) Calcium signaling and exocytosis in adrenal chromaffin cells. *Physiol rev.* Oct;86(4):1093-131.
44. Gauthier BR, Duhamel DL, Iezzi M, Theander S, Saltel F, Fukuda M, Wehrle-Haller B, Wollheim CB. (2008) Synaptotagmin VII splice variants alpha, beta, and delta are expressed in pancreatic beta-cells and regulate insulin exocytosis. *FASEB J.* Jan;22(1):194-206.
45. Gillis KD, Mossner R, Neher E. (1996) Protein Kinase C enhances exocytosis from chromaffin cells by increasing the size of the readily releasable pool of secretory granules. *Neuron.* Jun;16(6):1209-20.
46. Glombik MM, Gerdes HH. (2000) Signal-mediated sorting of neuropeptides and prohormones: secretory granule biogenesis revisited. *Biochemie.* Apr;82(4):315-26.
47. Gustavsson N, Lao Y, Maximov A, Chuang JC, Kostromina E, Repa JJ, Li C, Radda GK, Südhof TC, Han W. (2008) Impaired insulin secretion and glucose tolerance in synaptotagmin-7 null mutant mice.
48. He E, Wierda K, van Westen R, Broeke JH, Toonen RF, Cornelisse LN, Verhage M. (2017) Munc13-1 and Munc18-1 together prevent NSF-dependent de-priming of synaptic vesicles. *Nat Commun.* Jun 21;8:15915.
49. Heuser JE, Reese TS. (1973) Evidence for recycling of synaptic vesicle membrane during transmitter release at the frog neuromuscular junction. *J Cell Biol.* May;57(2):315-44.
50. Hillarp NA, Lagerstedt S, Nilson B. (1953) The isolation of a granular fraction from the suprarenal medulla, containing the sympathomimetic catecholamines. *Acta Physiol Scand.* Oct 6;29(2-3):251-63.
51. Hillarp NA, Hokfelt B, Nilson B. (1954) The cytology of the adrenal medullary cells with special reference to the storage and secretion of the sympathomimetic amines. *Acta Anat (Basel).* 21(2):155-67.
52. <http://www.andor.com/learning-academy/super-resolution-imaging-structured-illumination-microscopy-application-note>.

53. <http://www.leica-microsystems.com/science-lab/total-internal-reflection-fluorescence-tirf-microscopy>.
54. <https://www.microscopyu.com/techniques/fluorescence/total-internal-reflection-fluorescence-tirf-microscopy>.
55. <http://www.leica-microsystems.com/science-lab/the-patch-clamp-technique/>
56. Hua Y, Sinha R, Thiel CS, Schmidt R, Hüve J, Martens H, Hell SW, Egnér A, Klingauf J. (2011) A readily retrievable pool of synaptic vesicles. *Nat Neurosci.* Jun 12;14(7):833-9.
57. Hugo S, Dembla E, Halimani M, Matti U, Rettig J, Becherer U. (2013) Deciphering dead-end docking of large dense core vesicles in bovine chromaffin cells. *J Neurosci.* Oct 23;33(43):17123-37.
58. Husten EJ, Eipper BA. (1994) Purification and characterization of PAM-1, an integral membrane protein involved in peptide processing. *Arch Biochem Biophys.* Aug 1;312(2):487-92.
59. Imig C, Min SW, Krinner S, Arancillo M, Rosenmund C, Südhof TC, Rhee J, Brose N, Cooper BH. (2014) The morphological and molecular nature of synaptic vesicle priming at presynaptic active zones. *Neuron.* Oct 22;84(2):416-31.
60. Jahn R, Fasshauer D. (2012) Molecular machines governing exocytosis of synaptic vesicles. *Nature.* Oct 11;490(7419):201-7.
61. James DJ, Martin TF. (2013) CAPS and Munc13: CATCHRs that SNARE Vesicles. *Front Endocrinol (Lausanne).* Dec 4;4:187.
62. Kienzle C, von Blume J. (2014) Secretory cargo sorting at the trans-Golgi network. *Trends Cell Biol.* Oct;24(10):584-93.
63. Kilic G. (2002) Exocytosis in bovine chromaffin cells: studies with patch-clamp capacitance and FM1-43 fluorescence. *Biophys J.* Aug;83(2):849-57.
64. Kim T, Tao-Cheng JH, Eiden LE, Loh YP. (2001) Chromogranin A, an "on/off" switch controlling dense-core secretory granule biogenesis. *Cell.* Aug 24;106(4):499-509.

65. Kim T, Zhang CF, Sun Z, Wu H, Loh YP. (2005) Chromogranin A deficiency in transgenic mice leads to aberrant chromaffin granule biogenesis. *J Neurosci*. Jul 27;25(30):6958-61.
66. Kim T, Gondré-Lewis MC, Arnaoutova I, Loh YP. (2006) Dense-core secretory granule biogenesis. *Physiology (Bethesda)*. Apr;21-124-33.
67. Klumperman J, Kuliawat R, Griffith JM, Geuze HJ, Arvan P. (1998) Mannose 6-phosphate receptors are sorted from immature secretory granules via adaptor protein Ap-1, clathrin, and Syntaxin 6-positive vesicles. *J Cell Biol*. Apr 20;141(2):359-71.
68. Kreuzberger AJ, Liang B, Kiessling V, Tamm LK. (2016) Assembly and comparison of plasma membrane SNARE acceptor complexes. *Biophys J*. May 24;110(10):2147-50.
69. Kryvi H, Flatmark T, Terland O. (1979). Comparison of the ultrastructure of adrenaline and noradrenaline storage granules of bovine adrenal medulla. *Eur J Cell Biol*. Oct;20(1):76-82.
70. Kukulski W, Schorb M, Welsch S, Picco A, Kaksonen M, Briggs JA. (2012) Precise, correlated fluorescence microscopy and electron tomography of lowicryl sections using fluorescent fiducial markers. *Methods Cell Biol*. 111:235-57.
71. Ladinsky MS, Mastrorade DN, McIntosh JR, Howell KE, Staehelin LA. (1999) Golgi structure in three dimensions: functional insights from the normal rat kidney cell. *J Cell Biol*. Mar 22;144(6):1135-49.
72. Lang T, Wacker I, Wunderlich I, Rohrbach A, Giese G, Soldati T, Almers W. (2000) Role of actin cortex in the subplasmalemmal transport of secretory granules in PC-12 cells. *Biophys J*. Jun;78(6):2863-77.
73. Le Roy C, Wrana JL. (2005) Clathrin- and non-clathrin-mediated endocytic regulation of cell signaling. *Nat Rev Mol Cell Biol*. Feb;6(2):112-26.
74. Lindau M, Neher E. (1988) Patch-clamp techniques for time-resolved capacitance measurements in single cells. *Pflugers Arch*. Feb;411(2):137-46.
75. Lin WJ, Salton SR. (2013) The regulated secretory pathway and human disease: insights from gene variants and single nucleotide polymorphisms. *Front Endocrinol (Lausanne)*. Aug 6;4:96.

76. Liu Y, Schirra C, Edelmann L, Matti U, Rhee J, Hof D, Bruns D, Brose N, Rieger H, Stevens DR, Rettig J. (2010) Two distinct secretory vesicle-priming steps in adrenal chromaffin cells. *J Cell Biol.* Sep 20;190(6):1067-77.
77. Mahapatra NR, Mahata M, Hazra PP, McDonough PM, O'Connor DT, Mahata SK. (2004) A dynamic pool of calcium in catecholamine storage vesicles. Exploration in living cells by a novel vesicle-targeted chromogranin A-aequorin chimeric photoprotein. *J Biol Chem.* Dec 3;279(49):51107-21.
78. Mahapatra S, Calorio C, Vandael DH, Marcantoni A, Carabelli V, Carbone E. (2012) Calcium channel types contributing to chromaffin cell excitability, exocytosis and endocytosis. *Cell Calcium.* Mar-Apr;51(3-4):321-30.
79. Majane EA, Alho H, Kataoka Y, Lee CH, Yang HY. (1985) Neuropeptide Y in bovine adrenal glands: distribution and characterization. *Endocrinology.* Sep;117(3):1162-8.
80. Martin TF, Kowalchuk JA. (1997) Docked secretory vesicles undergo  $Ca^{2+}$ -activated exocytosis in a cell-free system. *J Biol Chem.* May 30;272(22):14447-53.
81. Martínez-Menárguez JA. (2013) Intra-Golgi transport: Roles for vesicles, tubules, and cisternae. *ISRN Cell Biology*, Article ID 126731, 15 pages, 2013.
82. Martínez-Alonso E, Tomás M, Martínez-Menárguez JA. (2013) Golgi tubules: their structure, formation and role in intra-Golgi transport. *Histochem Cell Biol.* Sep;140(3): 327-39.
83. Matti U, Pattu V, Halimani M, Schirra C, Krause E, Liu Y, Weins L, Fang Chang H, Guzman R, Olausson J, Freichel M, Schmitz F, Pasche M, Becherer U, Bruns D, Rettig J. (2013) Synaptobrevin2 is the v-SNARE required for cytotoxic T-lymphocyte lytic granule fusion. *Nat Commun.* 4:1439.
84. Murthy VN, De Camilli P. (2003) Cell biology of the presynaptic terminal. *Annu Rev Neurosci.* 26:701-28.
85. Nagy G, Reim K, Matti U, Brose N, Binz T, Rettig J, Neher E, Sørensen JB. (2004) Regulation of releasable vesicle pool sizes by protein kinase A-dependent phosphorylation of SNAP-25. *Neuron.* Feb 5;41(3):417-29.

86. Nofal S, Becherer U, Hof D, Matti U, Rettig J. (2007) Primed vesicles can be distinguished from docked vesicles by analyzing their mobility. *J Neurosci.* Feb 7;27(6):1386-95.
87. Nussdorfer GG, Gottardo G. (1998) Neuropeptide-Y family of peptides in the autocrine-paracrine regulation of adrenocortical function. *Horm Metab Res.* Jun-Jul;30(6-7):368-73.
88. Palade G. (1975) Intracellular aspects of the process of protein synthesis. *Science.* Sep 12; 189(4206):867.
89. Palfrey HC, Artalejo CR. (1998) Vesicle cycling revisited: rapid endocytosis may be the first step. *Neuroscience.* Apr;83(4):969-89.
90. Park JJ, Gondré-Lewis MC, Eiden LE, Loh YP. (2011) A distinct trans-Golgi network subcompartment for sorting of synaptic and granule proteins in neurons and neuroendocrine cells. *J Cell Sci.* Mar 1;124(Pt 5):735-44.
91. Pasche M, Matti U, Hof D, Rettig J, Becherer U. (2012) Docking of LDCVs is modulated by lower intracellular  $[Ca^{2+}]$  than priming. *PLoS One.* 7(5):e36416.
92. Patzak A, Winkler H. (1986) Exocytotic exposure and recycling of membrane antigens of chromaffin granules: ultrastructural evaluation after immunolabeling. *J Cell Biol.* Feb;102(2):510-5.
93. Penner R, Neher E. (1989) The patch-clamp technique in the study of secretion. *Trends Neurosci.* Apr;12(4):159-63.
94. Phillips JH, Burridge K, Wilson SP, Kirshner N. (1983) Visualization of the exocytosis/endocytosis secretory cycle in cultured adrenal chromaffin cells. *J Cell Biol.* Dec;97(6):1906-17.
95. Pinheiro PS, Jansen AM, de Wit H, Tawfik B, Madsen KL, Verhage M, Gether U, Sørensen JB. (2014) The BAR domain protein PICK1 controls vesicle number and size in adrenal chromaffin cells. *J Neurosci.* Aug 6;34(32):10688-700.
96. Plattner H, Artalejo AR, Neher E. (1997) Ultrastructural organization of bovine chromaffin cell cortex-analysis by cryofixation and morphometry of aspects pertinent to exocytosis. *J Cell Biol.* Dec 29;139(7):1709-17.

97. Rajappa R, Gauthier-Kemper A, Böning D, Hüve J, Klingauf J. (2016) Synaptophysin 1 clears Synaptobrevin 2 from the presynaptic active zone to prevent shorty-term depression. *Cell Rep.* Feb 16;14(6):1369-81.
98. Ramakrishnan NA, Drescher MJ, Drescher DG. (2012) The SNARE complex in neuronal and sensory cells. *Mol Cell Neurosci.* May;50(1):58-69.
99. Rao TC, Passmore DR, Peleman AR, Das M, Chapman ER, Anantharam A. (2014) Distinct fusion properties of synaptotagmin-1 and synaptotagmin-7 bearing dense core granules. *Mol Biol Cell.* Aug 15;25(16):2416-27.
100. Rao TC, Santana Rodriguez Z, Bradberry MM, Ranski AH, Dahl PJ, Schmidtke MW, Jenkins PM, Axelrod D, Chapman ER, Giovannucci DR, Anantharam A. (2017) Synaptotagmin isoforms confer distinct activation kinetics and dynamics to chromaffin cell granules. *J Gen Physiol.* Jul 7. pii:jgp.201711757.
101. Rego EH, Shao L, Macklin JJ, Winoto L, Johansson GA, Kamps-Hughes N, Davidson MW, Gustafsson MG. (2012) Nonlinear structured-illumination microscopy with a photoswitchable protein reveals cellular structures at 50-nm resolution. *Proc Natl Acad Sci U S A.* Jan 17;109(3):E135-43.
102. Rhee JS, Li LY, Shin OH, Rah JC, Rizo J, Südhof TC, Rosenmund C. (2005) Augmenting neurotransmitter release by enhancing the apparent  $Ca^{2+}$  affinity of synaptotagmin 1. *Proc Natl Acad Sci U S A.* Dec 20;102(51):18664-9.
103. Rizo J, Südhof TC. (2002) Snares and Mun18 in synaptic vesicle fusion. *Nat Rev Neurosci.* Aug;3(8):641-53.
104. Rizo J, Südhof TC. (2012) The membrane fusion enigma: SNAREs, Sec1/Munc18 proteins, and their accomplices—guilty as charged? *Annu Rev Cell Dev Biol.* 28;279-308.
105. Robinson LJ, Martin TF. (1998) Docking and fusion in neurosecretion. *Curr Opin Cell Biol.* Aug;10(4):483-92.
106. Rudolf R, Salm T, Rustom A, Gerdes HH. (2001) Dynamics of immature secretory granules: role of cytoskeletal elements during transport, cortical restriction, and F-actin-dependent tethering. *Mol Biol Cell.* May;12(5):1353065.

107. Rosa JM, Nanclares C, Orozco A, Colmena I, de Pascual R, García AG, Gandía L. (2012) Regulation by L-type calcium channels of endocytosis: an overview. *J Mol Neurosci.* Oct;48(2):360-7.
108. Schalling M, Dagerlind A, Brené S, Hallman H, Djurfeldt M, Persson H, Terenius L, Goldstein M, Schlesinger D, Hökfelt T. (1988) Coexistence and gene expression of phenylethanolamine N-methyltransferase, tyrosine hydroxylase, and neuropeptide tyrosine in the rat and bovine adrenal gland: effects of reserpine. *Proc Natl Acad Sci U S A.* Nov;85(21):8306-10.
109. Schollmeier Y, Krause JM, Kreye S, Malsam J, Söllner TH. (2011) Resolving the function of distinct Munc18-1/SNARE protein interaction modes in a reconstituted membrane fusion assay. *J Biol Chem.* Sep 2;286(35):30582-90.
110. Schonh JS, Maximov A, Lao Y, Südhof TC, Sørensen JB. (2008) Synaptotagmin-1 and -7 are functionally overlapping  $Ca^{2+}$  sensors for exocytosis in adrenal chromaffin cells. *Proc Natl Acad Sci U S A.* Mar 11;105(10):3998-4003.
111. Scott CC, Vacca F, Gruenberg J. (2014) Endosome maturation, transport and functions. *Semin Cell Dev Biol.* Jul;31:2-10.
112. Smith C, Neher E. (1997) Multiple forms of endocytosis in bovine adrenal chromaffin cells. *J Cell Biol.* Nov 17;139(4):885-94.
113. Smith C, Moser T, Xu T, Neher E. (1998) Cytosolic  $Ca^{2+}$  acts by two separate pathways to modulate the supply of release-competent vesicles in chromaffin cells. *Neuron.* Jun;20(6):1243-53.
114. Smyth AM, Duncan RR, Rickman C. (2010) Munc18-1 and syntaxin1: unraveling the interactions between the dynamic duo. *Cell Mol Neurobiol.* Nov;30(8):1309-13.
115. Solimena M, Gerdes HH. (2003) Secretory granules: and the last shall be first. *Trends Cell Biol.* Aug;13(8):399-402.
116. Speese S, Petrie M, Schuske K, Ailion M, Ann K, Iwasaki K, Jorgensen EM, Martin TF. (2007) UNC-31 (CAPS) is required for dense-core vesicle but not synaptic vesicle exocytosis in *Caenorhabditis elegans*. *J Neurosci.* Jun 6;27(23):6150-62.

117. Steinberg BE, Huynh KK, Brodovitch A, Jabs S, Stauber T, Jentsch TJ, Grinstein S. (2010) A cation counterflux supports lysosomal acidification. *J Cell Biol.* Jun 28;189(7):1171-86.
118. Steyer JA, Horstmann H, Almers W. (1997) Transport, docking and exocytosis of single secretory granules in live chromaffin cells. *Nature.* Jul 31;388(6641):474-8.
119. Sutton RB, Davletov BA, Berghius AM, Südhof TC, Sprang SR. (1995) Structure of the first C2 domain of synaptotagmin I: a novel  $Ca^{2+}$ /phospholipid-binding fold. *Cell.* Mar 24;80(6):929-38.
120. Sutton RB, Fasshauer D, Jahn R, Brunger AT. (1998) Crustal structure of a SNARE complex involved in synaptic exocytosis at 2.4 Å resolution. *Nature.* Sep 24;395(6700):347-53.
121. Südhof TC, De Camilli P, Niemann H, Jahn R. (1993) Membrane fusion machinery: insights from synaptic proteins. *Cell.* Oct 8;75(1):1-4.
122. Südhof TC, Rizo J. (2011) Synaptic vesicle exocytosis. *Cold Spring Harb Perspect Biol.* Dec 1;3(12). pii: a005637.
123. Tatemoto K. (1982) Neuropeptide Y: complete amino acid sequence of the brain peptide. *Proc Natl Acad Sci U S A.* Sep;79(18):5485-9.
124. Taupenot L, Harper KL, O'Connor DT. (2003) The chromogranin-secretogranin family. *N Engl J Med.* Mar 20;348(12):1134-49.
125. Teng H, Wilkinson RS. (2005) Clathrin-mediated endocytosis in snake motor terminals is directly facilitated by intracellular  $Ca^{2+}$ . *J Physiol.* Jun 15;565(Pt 3):743-50.
126. Tooze SA, Flatmark T, Tooze J, Huttner WB. (1991) Characterization of the immature secretory granule, an intermediate in granule biogenesis. *J Cell Biol.* Dec;115(6):1491-503.
127. Tooze SA, Martens GJ, Huttner WB. (2001) Secretory granule biogenesis: rafting to the SNARE. *Trends Cell Biol.* Mar;11(3):116-22.
128. Torregrosa-Hetland CJ, Villanueva J, Giner D, Lopez-Font I, Nadal A, Quesada I, Viniegra S, Expósito-Romero G, Gil A, Gonzalez-Velez V, Segura J, Gutiérrez LM.

(2011) The F-actin cortical network is a major factor influencing the organization of the secretory machinery in chromaffin cells. *J Cell Sci.* Mar 1;124(Pt 5):727-34.

129. Trudeau LE, Emery DG, Haydon PG. (1996) Direct modulation of the secretory machinery underlies PKA-dependent synaptic facilitation in hippocampal neurons. *Neuron.* Oct;17(4):789-97.

130. Urbé S, Page LJ, Tooze SA. (1998) Homotypic fusion of immature secretory granules during maturation in a cell-free assay. *J Cell Biol.* Dec 28;143(7):1831-44.

131. van Weering JR, Toonen RF, Verhage M. (2007) The role of Rab3a in secretory vesicle docking requires association/dissociation of guanidine phosphates and Munc13-1. *PLoS One.* Jul 18;2(7):e616.

132. Verhage M, Maia AS, Plomp JJ, Brussaard AB, Heeroma JH, Vermeer H, Yoonen RF, Hammer RE, van der Berg TK, Missler M, Geuze HJ, Südhof TC. (2000) Synaptic assembly of the brain in the absence of neurotransmitter secretion. *Science.* Feb 4;287(5454):864-9.

133. Verhage M, Sørensen JB. (2008) Vesicle docking in regulated exocytosis. *Traffic.* Sep;9(9):1414-24.

134. Voets T. (2000) Dissection of three Ca<sup>2+</sup>-dependent steps leading to secretion in chromaffin cells from adrenal slices. *Neuron.* Nov;28(2):537-45.

135. Voets T, Moser T, Lund PE, Chow RH, Geppert M, Südhof TC, Neher E. (2001) Intracellular calcium dependence of large dense-core vesicle exocytosis in the absence of synaptotagmin I. *Proc Natl Acad Sci U S A.* Sep 25;98(20):11680-5.

136. Voets T, Toonen RF, Brian EC, de Wit H, Moser T, Rettig J, Südhof TC, Neher E, Verhage M. (2001) Munc18-1 promotes large dense-core vesicle docking. *Neuron.* Aug 30;31(4):581-91.

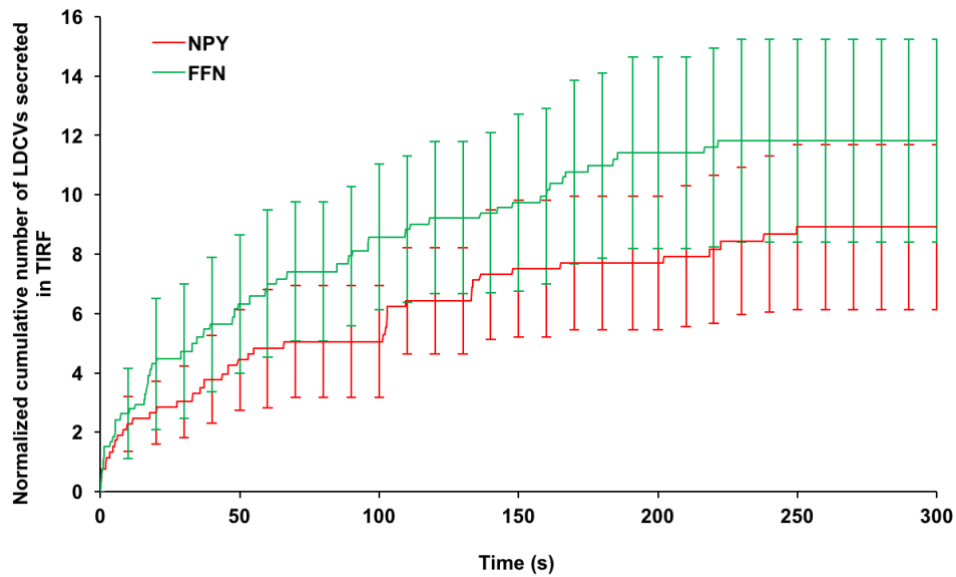
137. Walter AM, Wiederhold K, Bruns D, Fasshauer D, Sørensen JB. (2010) Synaptobrevin N-terminally bound to Syntaxin-SNAP-25 defines the primed vesicle state in regulated exocytosis. *J Cell Biol.* Feb 8;188(3):401-13.

138. Walter AM, Kurps J, de Wit H, Schöning S, Toft-Bertelsen TL, Lauks J, Ziomkiewicz I, Weiss AN, Schulz A, Fischer von Mollard G, Verhage M, Sørensen JB.

- (2014) The SNARE protein vti1a functions in dense-core vesicle biogenesis. *EMBO J.* Aug 1;33(15):1681-97.
139. Watanabe S. (2015) Slow or fast? A tale of synaptic vesicle recycling. *Science.* Oct 2;350(6256):46-7.
140. Wendler F, Page L, Urbé S, Tooze SA. (2001) Homotypic fusion of immature secretory granules during maturation requires Syntaxin 6. *Mol Biol Cell.* Jun;12(6):1699-709.
141. Weninger K, Bowen ME, Choi UB, Chu S, Brunger AT. (2008) Accessory proteins stabilize the acceptor complex for synaptobrevin, the 1:1 syntaxin/SNAP-25 complex. *Structure.* Feb;16(2):308-20.
142. Whyte JR, Munro S. (2002) Vesicle tethering complexes in membrane traffic. *J Cell Sci.* Jul 1;115 (Pt 13):2627-37.
143. Wu B, Wei S, Petersen N, Ali Y, Wang X, Bacaj T, Rorsman P, Hong W, Südhof TC, Han W. (2015) Synaptotagmin-7 phosphorylation mediates GLP-1-dependent potentiation of insulin secretion from  $\beta$ -cells. *Proc Natl Acad Sci U S A.* Aug 11;112(32):9996-10001.
144. Wu LG, Hamid E, Shin W, Chiang HC. (2014) Exocytosis and endocytosis: modes, functions, and coupling mechanisms. *Annu Rev Physiol.* 76:301-31.
145. Wu MM, Grabe M, Adams S, Tsien RY, Moore HP, Machen TE. (2001) Mechanisms of pH regulation in the regulated secretory pathway. *J Biol Chem.* Aug 31;276(35):33027-35.
146. Wu XS, Zhang Z, Zhao WD, Wang D, Luo F, Wu LG. (2014) Calcineurin is universally involved in vesicle endocytosis at neuronal and nonneuronal secretory cells. *Cell Rep.* May 22;7(4):982-8.
147. Wu Y, Gu Y, Morphew MK, Yao J, Yeh FL, Dong M, Chapman ER. (2012) All three components of the neuronal SNARE complex contribute to secretory vesicle docking. *J Cell Biol.* Aug 6;198(3):323-30.

## 7. ANNEX

A



B

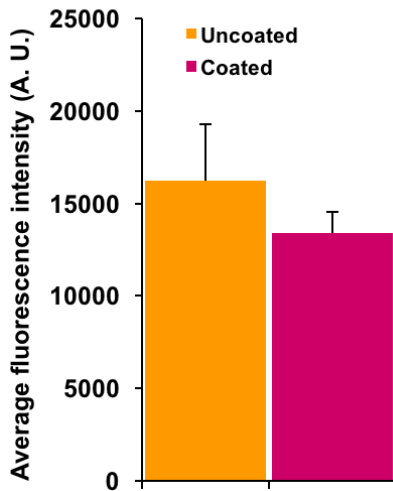


**Figure 48: (A) Same number of old and newly generated LDCVs were secreted in TIRFM.** Graph represents normalized average number of LDCVs secreted in TIRF in NPY-mCherry transfected WT mouse chromaffin cells that were loaded with FFN511. Presented are average  $\pm$  s.e.m.  $N_{\text{cells}} = 5$ . **(B) There was no effect of collagen coating on actin network at PM.** Quantification of actin network at the PM in NPY-mCherry transfected WT mouse chromaffin cells plated on collagen coated and uncoated coverslips. Presented are average  $\pm$  s.e.m.  $N_{\text{cells}} = 10$ .

## 8. ABBREVIATIONS

ATP	Adenosine Tri Phosphate
CaM	Calmodulin
CaN	Calcineurin
Ceb	Cellubrevin
CgA	Chromogranin A
CgB	Chromogranin B
CLEM	Correlative fluorescence Electron Microscopy
DCV	Dense Core Vesicle
DMEM	Dulbecco's Modified Eagle Medium
DMSO	Dimethyl Sulfoxide
DPBS	Dulbecco's Phosphate Buffered Saline
EDTA	Ethylenediaminetetraacetic acid
E18	Embryonic stage 18
ER	Endoplasmic Reticulum
EtBr	Ethidium Bromide
Fig.	Figure
FCS	Fetal Calf Serum
GTPase	Guanosinetriphosphatase
HCl	Hydrochloric acid
HEPES	N-2-Hydroxyethylpiperazine-N'-2- Ethanesulfonic Acid
HZ	Heterozygous
HPLC	High Pressure Liquid Chromatography
ITS-X	Insulin T
ISGs	Immature Secretory Granules
JACoP	Just Another Colocalization Plugin
KCl	Potassium Chloride
KO	Knock Out
LAMP1	Lysosomal Associated Protein 1
LDCV	Large Dense Core Vesicle
NGS	Neural Goat Serum
NPY	Neuropeptide Y
Overexp.	Overexpression
PFA	Paraformaldehyde
PBS	Phosphate Buffered Saline
PC12	Pheochromocytoma cells 12
PM	Plasma membrane
PCR	Polymerase Chain Reaction
p3	Postnatal day 3
Sgs	Secretogranins
Syb-2	Synaptobrevin-2
Syt1	Synaptotagmin1
Syt7	Synaptotagmin7

SIM	Structured Illumination Microscopy
SNARE	Soluble NSF Attachment Protein Receptor
SNAP25	Synaptosome associated protein of 25 kDa
Stx1	Syntaxin1
Syp1	Synaptophysin1
TAE	Tris Acetate EDTA
TGN38	Trans-Golgi Network 38
TIRFM	Total Internal Reflection Fluorescence Microscopy
t-SNARE	target-SNARE
Tris	Trishydroxymethylaminomethane
v-SNARE	vesicle-SNARE
WT	Wild Type

## UNITS

bp	Base Pair
°C	Degree Celsius
fF	Femto Farad
g	Gram
h	Hour
Hz	Hertz
kHz	Kilohertz
mg	Milligram
mL	Milliliter
ms	Millisecond
mM	Milli Molar
mOsm.	Milliosmole
mV	Millivolt
μL	Microliter
μm	Micrometer
μM	Micro Molar
Min.	Minutes
Nm	Nanometer
nM	Nano molar
N	Normal
pF	Pico farad
rpm	Revolutions Per Minute
s	Second
U/mL	Units/Milliliter
V	Volt

## **9. LIST OF FIGURES**

<b>Title</b>	<b>Page No.</b>
<b>Figure: 1 Steps involved in LDCV biogenesis.</b>	<b>15</b>
<b>Figure: 2 Adrenal gland structure and function.</b>	<b>16</b>
<b>Figure: 3 Structural organization of the chromaffin cells.</b>	<b>17</b>
<b>Figure: 4 Steps in synaptic vesicle fusion.</b>	<b>18</b>
<b>Figure: 5 Structures of synaptic SNARE and SM proteins.</b>	<b>19</b>
<b>Figure: 6 Docking proteins and their interaction steps leading to priming and fusion.</b>	<b>20</b>
<b>Figure: 7 Model for dead-end docking.</b>	<b>21</b>
<b>Figure: 8 Models of synaptic vesicle recycling.</b>	<b>21</b>
<b>Figure: 9 Method of analysis.</b>	<b>30</b>
<b>Figure: 10 General principle of patch-clamp recordings.</b>	<b>31</b>
<b>Figure: 11 Principle of TIRFM.</b>	<b>32</b>
<b>Figure: 12 Illustration of genotyping results.</b>	<b>35</b>
<b>Figure: 13 NPY-mCherry containing vesicles are LDCVs.</b>	<b>36</b>
<b>Figure: 14 First expression of NPY-mCherry is visible at 2 h post transfection.</b>	<b>37</b>
<b>Figure: 15 LDCVs exit the Golgi only one hour after first expression of NPY-mCherry.</b>	<b>39</b>
<b>Figure: 16 NPY-mCherry expression partially overlaps with cis- and trans-Golgi network recognizing a discrete cellular compartment.</b>	<b>41</b>
<b>Figure: 17 Colocalization analysis between NPY, TGN38, and GM130 over the entire cell.</b>	<b>42</b>
<b>Figure: 18 Syb-2 is associated with LDCVs at later stage in biogenesis.</b>	<b>43</b>
<b>Figure: 19 Ceb is localized to a relatively small population of LDCVs.</b>	<b>45</b>
<b>Figure: 20 Co-immunolabelling of Syb-2 and Ceb.</b>	<b>46</b>
<b>Figure: 21 Like v-SNAREs, Syt1 is sorted to LDCVs at a late stage of their biogenesis.</b>	<b>46</b>
<b>Figure: 22 Endocytosis of Syt1.</b>	<b>48</b>
<b>Figure: 23 Recycled Syt1 is found on LDCVs and merges with reserve pool of Syt1.</b>	<b>49</b>
<b>Figure: 24 Exocytosis of LDCVs induced by long-lasting and strong stimulus.</b>	<b>50</b>
<b>Figure: 25 TIRFM images of WT mouse chromaffin cells.</b>	<b>51</b>
<b>Figure: 26 Survival plot of LDCVs at the cell's footprint.</b>	<b>51</b>

<b>Figure: 27 Analysis of different LDCV parameters in TIRFM.</b>	<b>52</b>
<b>Figure: 28 Exocytosis of LDCVs in WT and Syb-2 KO.</b>	<b>53</b>
<b>Figure: 29 TIRFM images of WT and Syb-2 KO mouse chromaffin cells.</b>	<b>53</b>
<b>Figure: 30 Analysis of different parameters in TIRFM.</b>	<b>54</b>
<b>Figure: 31 Quantification of t-SNAREs at the PM in WT and Syb-2 KO cells.</b>	<b>54</b>
<b>Figure: 32 Exocytosis of LDCVs in WT and Ceb KO.</b>	<b>55</b>
<b>Figure: 33 TIRFM images of WT and Ceb KO mouse chromaffin cells.</b>	<b>55</b>
<b>Figure: 34 Analysis of different parameters in TIRFM.</b>	<b>56</b>
<b>Figure: 35 Quantification of t-SNAREs at the PM in WT and Ceb KO cells.</b>	<b>56</b>
<b>Figure: 36 Exocytosis of LDCVs in WT and Syt1 KO.</b>	<b>57</b>
<b>Figure: 37 TIRFM images of WT and Syt1 KO mouse chromaffin cells.</b>	<b>57</b>
<b>Figure: 38 Analysis of different parameters in TIRFM.</b>	<b>58</b>
<b>Figure: 39 Quantification of t-SNAREs at the PM in WT and Syt1 KO cells.</b>	<b>58</b>
<b>Figure: 40 Exocytosis of LDCVs in WT and Syt7 KO.</b>	<b>59</b>
<b>Figure: 41 TIRFM images of WT and Syt7 KO mouse chromaffin cells.</b>	<b>59</b>
<b>Figure: 42 Analysis of different parameters in TIRFM.</b>	<b>60</b>
<b>Figure: 43 Quantification of t-SNAREs at the PM in WT and Syt7 KO cells.</b>	<b>60</b>
<b>Figure: 44 Exocytosis of LDCVs in Syt7 KO and Syt7 overexpressing cells.</b>	<b>61</b>
<b>Figure: 45 TIRFM images of Syt7 KO and Syt7 overexpressing mouse chromaffin cells.</b>	<b>61</b>
<b>Figure: 46 Analysis of different parameters in TIRFM.</b>	<b>62</b>
<b>Figure: 47 Schematic model for biogenesis and recycling of LDCVs in mouse chromaffin cells</b>	<b>68</b>
<b>Figure 48: (A) Same number of old and newly generated LDCVs were secreted in TIRFM.</b>	<b>88</b>
<b>Figure 48: (B) There was no effect of collagen coating on actin network at PM.</b>	<b>88</b>

## 10. LIST OF TABLES

<b>Title</b>	<b>Page No.</b>
<b>Table: 1 Pearson's correlation coefficients between NPY, GM130, and TGN38.</b>	<b>40</b>
<b>Table: 2 Mander's correlation coefficients between NPY, GM130, and TGN38.</b>	<b>42</b>
<b>Table: 3 Pearson's correlation coefficients between NPY and vesicular proteins.</b>	<b>44</b>
<b>Table: 4 Mander's correlation coefficients between NPY and vesicular proteins.</b>	<b>44</b>
<b>Table: 5 Number of vesicles at the footprint of the cell in WT cells.</b>	<b>52</b>
<b>Table: 6 Number of vesicles at the footprint of the cell in Syb-2 WT and KO.</b>	<b>54</b>
<b>Table: 7 Number of vesicles at the footprint of the cell in Syb-2 WT and KO.</b>	<b>56</b>
<b>Table: 8 Number of vesicles at the footprint of the cell in Syt1 WT and KO.</b>	<b>58</b>
<b>Table: 9 Number of vesicles at the footprint of the cell in Syt7 WT and KO.</b>	<b>60</b>
<b>Table: 10 Number of vesicles at the footprint of the cell in Syt7 KO and Syt7 overexpressing cells.</b>	<b>62</b>